Quill
RADAR

KP-II
PROGRAM REPORT

☐ RT DATA ENTERED
DATE _____
☐ MICROFICHED
DATE _____

AKP-II-596 / UCL II

1 APRIL 1965

SSF-II-1018-2

~~SECRET~~
SPECIAL HANDLING

HANDLE VIA BYEMAN
CONTROL SYSTEM ONLY

COPY NO. 17

KP-II
PROGRAM REPORT

KP-II ORBITAL DOPPLER RADAR
THOR/AGENA SATELLITE PROGRAM

VOLUME II - TESTING

AKP-II-596

1 APRIL 1965
S

GOODYEAR AEROSPACE CORPORATION
ARIZONA DIVISION LITCHFIELD PARK, ARIZONA

This page intentionally left blank.

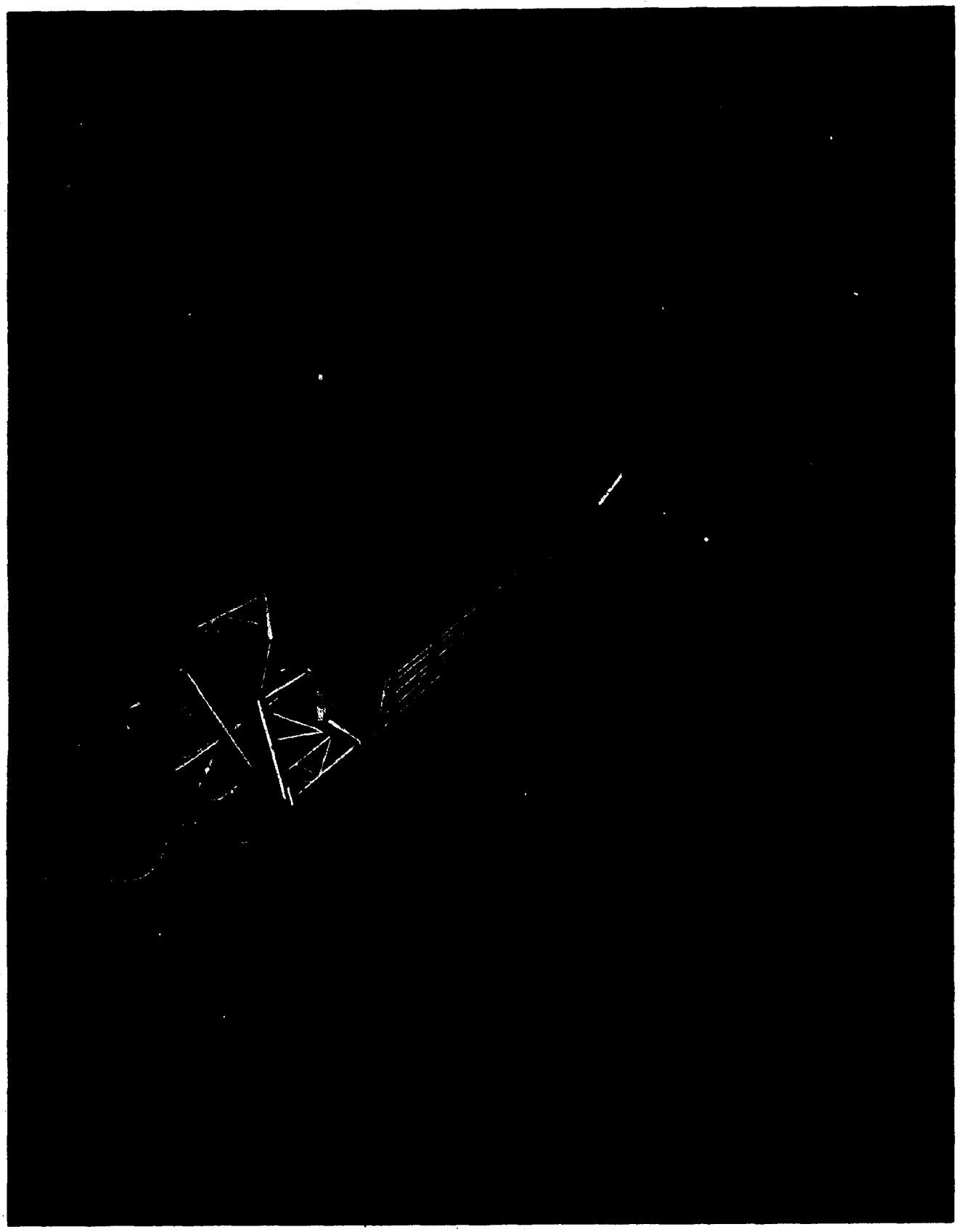

This page intentionally left blank.

TABLE OF CONTENTS

LIST OF ILLUSTRATIONS

This page intentionally left blank.

LIST OF TABLES

SECTION I - INTRODUCTION

The initial design and development phase of the KP-II doppler radar is documented in Volume I of this report. This volume – Volume II – documents the ground test and flight test phases.

The sections on ground testing include a description of the specialized test equipment which was used, the tests that were performed on the equipment, the problems encountered, and the corrective actions that were taken.

The sections on flight testing describe the operations which were carried out during the mission and present a detailed analysis of the radar system performance.

A summary of testing events on a monthly basis is included as Appendix I.

Estimates based on flight data of the radar back-scattering coefficient, σ_o, are presented in Appendix II.

This page intentionally left blank.

SECTION II - GROUND SUPPORT EQUIPMENT

1. GENERAL

The KP-II radar ground support equipment is composed of a system tester and five maintenance testers (one for each radar unit). The system tester is capable of detecting a malfunction in the system and locating the malfunction to one of the unit maintenance testers. The tester is capable of controlling the system and exercising all modes of operation, including radar data recording using simulated targets supplied by the tester. An optical correlator (data film analyzer) is supplied along with the system tester for demonstrating system resolution.

The unit testers are capable of locating malfunctions to within replaceable boards or subassemblies. Each tester supplies power for the unit and controls its mode of operation. Monitoring capabilities for unit alignment are also available.

All system testers and unit testers are one-, two-, or three-bay military cabinets. All cabinets are dark gray with light gray front panels. The front panel nomenclature is black silkscreening.

The testers operate on 115 v ±10 percent, 60-cycle power. The system and Transmitter-Modulator testers require three-phase voltage. All other testers require single-phase primary power. The unit testers supply prime power to each unit but the system tester does not have the capability of supplying the radar set with prime power. All testers control mode switching, simulate inputs as needed, and provide monitoring points for testing. Commercial test equipment is built into each tester to be used in conjunction with the test points.

2. DETAILED DESCRIPTION

a. System Tester

(1) General

The system tester is pictured in Figure 1. The data film analyzer, also a part of the system test equipment, is described in following paragraph (8).

(2) Power Control Chassis

This chassis produces the 28-vdc power for tester operation and controls the 60-cycle power to the various panels and commercial test equipment contained within the tester.

(3) System Control Panel

The system control panel simulates the normal command control function to the radar set. Power control commands of warm-up, pre-operate, and operate can be initiated. In addition, system control functions such as prf rate, receiver attenuation, built-in-test, clutterlock time constant, clutterlock ground, film drive ON-OFF, and time delay override are provided.

(4) Test Point Panel

The chassis provides access to radar test signals on the front panel of the tester.

(5) Metering Panel

The metering panel provides six meters (M-1 through M-6) for continuous monitoring of selected test points.

(6) Azimuth Target Generator and Transponder Panels

These two panels operate together functionally to simulate the generation of doppler targets as a function of vehicle movement. The

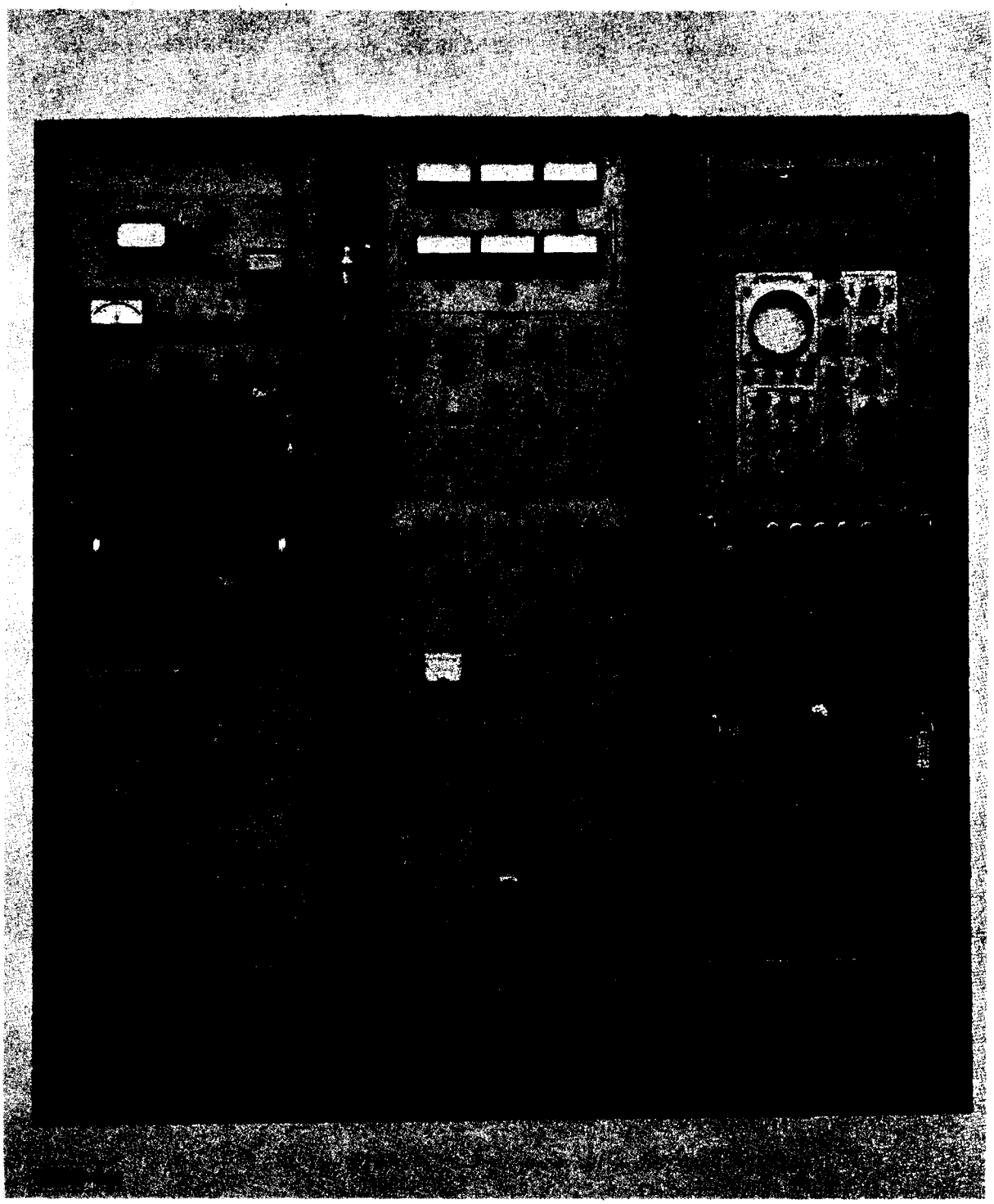

Figure 1 - System Tester

transponder is pictured in Figure 2. The unit is shown removed from the system tester and mounted in its case for portable field use.

(a) Azimuth Target Generator

The azimuth target generator (Figure 3, lower portion) is used to modulate microwave signals in the microwave section of the transponder. The azimuth target generator produces an output simulating the doppler equation

$$f_d = \frac{2v \sin \theta}{\lambda} \qquad (1)$$

where

θ = angle measured from zero doppler

v = velocity of vehicle

λ = wave length of transmitted signal.

As the velocity of the vehicle v and the wave length of the transmitted frequency are constant, the doppler frequency at any point is only a function of the angle or constant doppler line. The rate of change of doppler frequency as the vehicle moves past a given target can be approximated by

$$\frac{df_d}{dt} = \frac{2v^2}{R\lambda} \qquad (2)$$

where R = slant range to target. This doppler signal is produced by mixing the output of two oscillators, one a fixed 5-kc oscillator and the other a voltage-controlled oscillator (vco) which is driven by a ramp through a frequency excursion of 3 kc to 7 kc at a linear rate. The resulting mixer output is a swept frequency 2 kc through 0 to 2 kc simulating a doppler target.

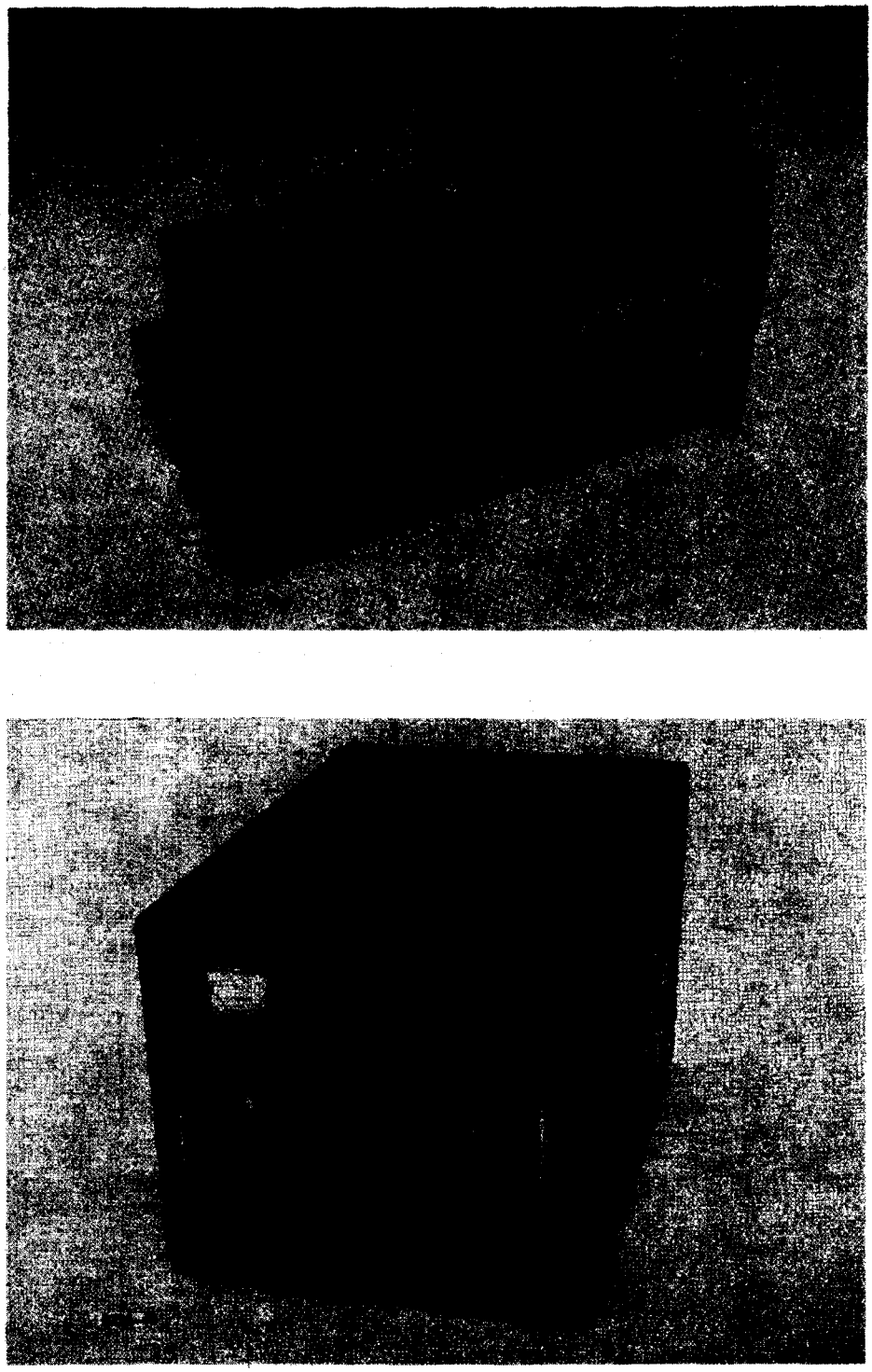

Figure 2 - Transponder

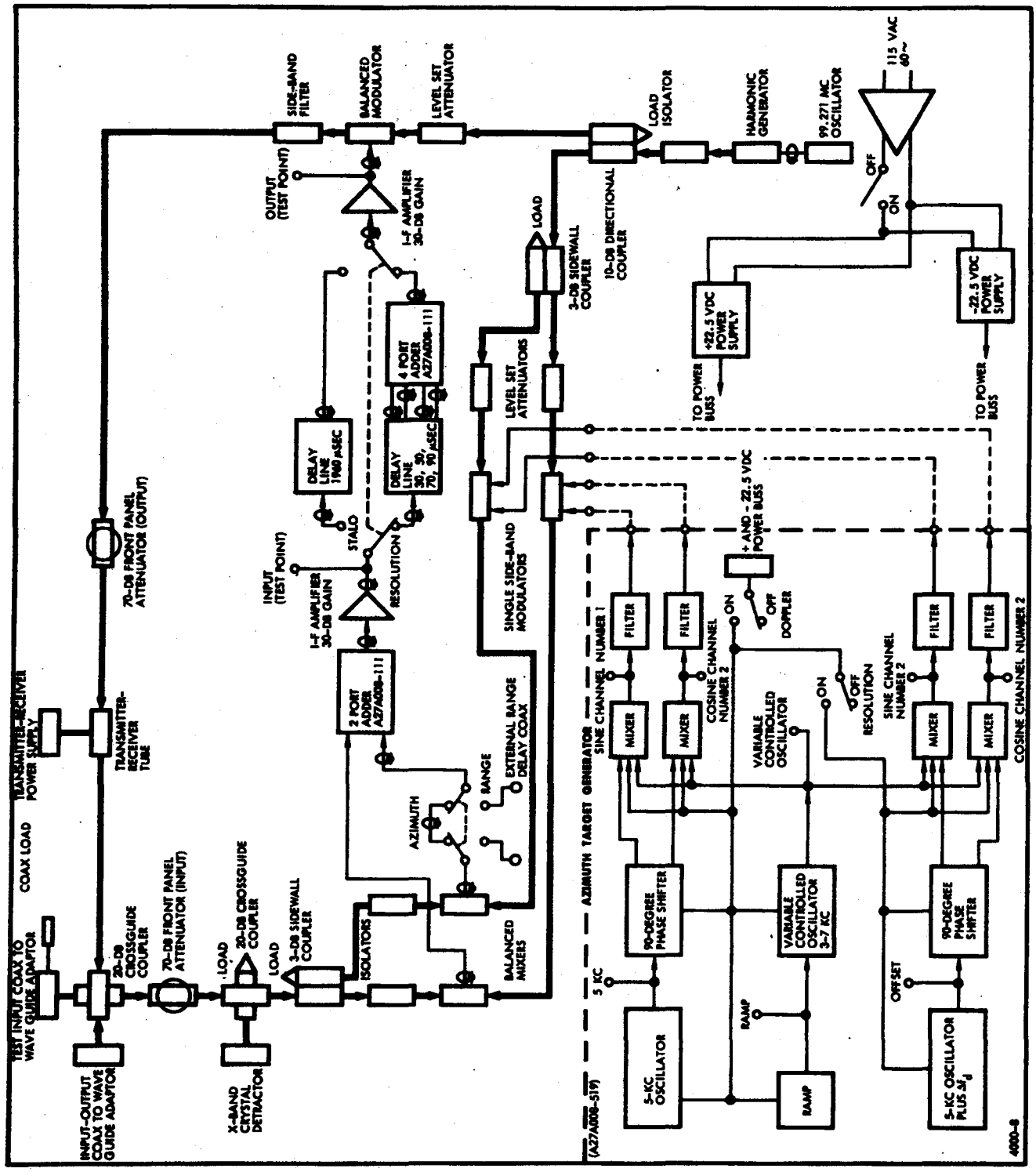

Figure 3 - Azimuth Target Generator

To produce a second doppler target offset from the first target, a second oscillator operating at 5 kc $\pm \Delta f_d$, where Δf_d is the frequency difference between the two oscillators, is mixed with the same vco output as was used for the first doppler target. Δf_d can be calculated from

$$\Delta f_d = \frac{2v}{\lambda} \times \frac{\text{desired azimuth displacement}}{\text{range to target}} \quad . \qquad (3)$$

During operation the DOPPLER ON-OFF switch supplies power to one of the 5-kc oscillators and the ramp and vco to produce one doppler target. Placing the resolution switch to the ON position will supply power to the offset oscillator (5 kc + f_d) which will produce the second doppler target. The frequency of the 5-kc and offset oscillators can be measured from the front-panel test points using the counter. Adjusting the offset control will vary Δf_d and thus provide various azimuth displacements.

For each doppler target two outputs are used, the two differing only in phase. Thus there are four outputs which go to the microwave section. Each doppler target has two outputs, each shifted by 90 degrees so that a single side-band signal can be produced in the microwave section.

(b) Transponder Panel

The transponder panel (Figure 3, upper portion) receives a transmitter pulse from the system under test, modulates the pulse with the doppler wave form received from the azimuth target generator, delays the signal to simulate range, and returns the resulting signal to the system.

The input signal from the system encounters a transmit-receive (t-r) tube which blocks the pulse from entering the receiver channel. The signal, attenuated 20 db by the cross guide coupler,

passes through a front-panel mounted, 70-db variable attenuator. After passing through the attenuator, part of the signal is fed into the crystal detector on the front panel marked POWER DETECTOR. The rest of the signal continues down the wave guide and splits into two parts, Channel No's 1 and 2, where each part or channel encounters an orthomode (balanced) mixer.

At the orthomode mixers each signal is mixed with a local oscillator reference which is generated inside the transponder and modulated in a single side-band modulator by the doppler wave form. The result of mixing the two signals is a third signal whose frequency is 70 mc + f_d (refer to Equation (1)). This signal is fed into the i-f section where it is delayed. A switch in series with the output of the Channel No. 2 orthomode mixer allows the doppler target in Channel No. 2 to appear as displaced in azimuth or range from the doppler target in Channel No. 1. This switch is the AZIMUTH-RANGE switch located on the front panel. (The method whereby the azimuth displacement is varied was discussed in the preceding paragraph (a) on the azimuth target generator.) The range displacement is controlled by the length of a coaxial cable connected to two coaxial connectors marked RANGE on the back of the transponder chassis.

The two channels are added together to form one signal and sent to the delaying portion of the i-f section. Here one of two different delays can be selected by means of the STALO-RESOLUTION switch located on the front panel. The switch is thrown to the STALO-RESOLUTION position when a frequency-stability test is being run and to the RESOLUTION position when a resolution test is being run. The STALO position delays the pulse 1960 microseconds for long-time stability tests. The RESOLUTION position produces four pulses delayed 30, 50, 70 and 90 microseconds. The signal is then applied to a third orthomode mixer (or modulator) where it is mixed with the original continuous-wave local

oscillator signal and filtered to produce a signal identical to the input signal except that it contains the doppler information. This signal then goes through a variable attenuator and the unfired transmit-receive tube to the output.

(c) Derivation of Constants for Transponder

Referring to Figure 4, the azimuth target generator portion of the transponder, it is desired to solve for the ramp period (t), the separation in cycles between the two oscillators (Δf_d) and other similar parameters of the generator.

Starting with the basic equation relating doppler frequency, vehicle velocity, and wave length,

$$f_d = \frac{2v \sin \theta}{\lambda} \quad , \tag{4}$$

differentiating with respect to θ

$$df_d = \left(\frac{2v \cos \theta}{\lambda}\right) d\theta \tag{5}$$

where

$$d\theta = \frac{vdt}{R} \quad .$$

Substituting in Equation (5)

$$df_d = \frac{2v \cos \theta}{\lambda}\left(\frac{vdt}{R}\right) \tag{6}$$

$$\frac{df_d}{dt} = \frac{2v^2}{R\lambda} \cos \theta \cong \frac{2v^2}{R\lambda} \quad \text{(since } \theta \text{ is small).} \tag{7}$$

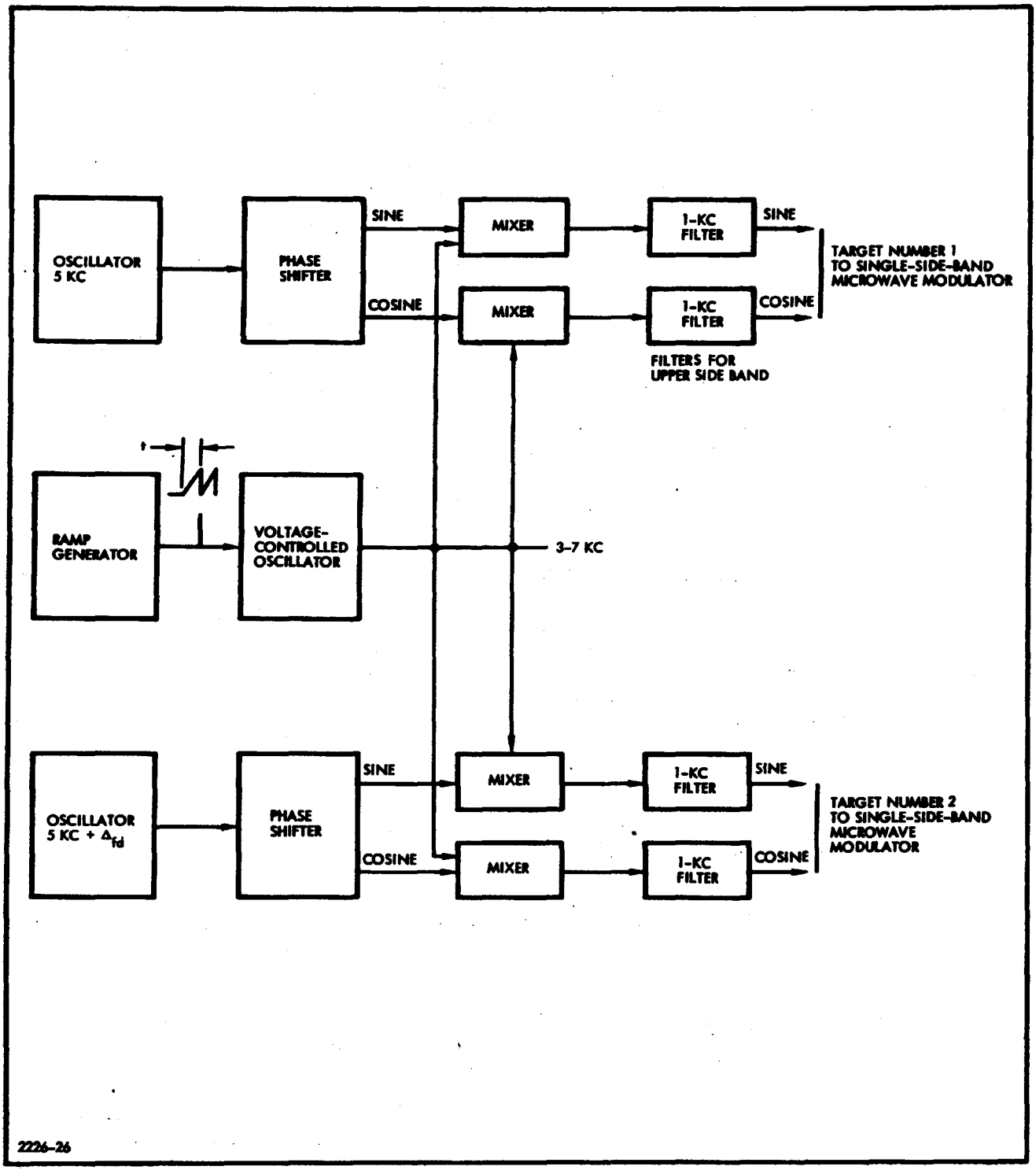

Figure 4 - Block Diagram of Azimuth Target Generator

Assuming a vehicle velocity of 25,500 ft/sec, antenna depression of 55 degrees, and an altitude of 130 nautical miles,

$$\frac{\Delta f_d}{\Delta t} = \frac{2(25.5 \times 10^3)^2 \times 0.82}{130 \times 6076 \times 0.1025}$$

$$= 13,200 \text{ cycles/second.} \qquad (8)$$

Using a total frequency sweep of 2 kc - 0 - 2 kc, or 4 kc, then the ramp period is

$$t = \frac{4000}{13,200} = 0.303 \text{ sec} \quad . \qquad (9)$$

To offset one target 50 feet from the first target, the difference in frequency will be

$$\Delta f_d = \left(\frac{2v \cos \theta}{\lambda}\right) \Delta\theta$$

$$= \left(\frac{2v}{\lambda}\right) \cos \theta \left(\frac{\Delta s}{R}\right) \qquad (10)$$

and, for small values of θ,

$$\Delta f_d = \left(\frac{2v}{\lambda}\right) \frac{\Delta s \sin 55^o}{h} \qquad (\cos \theta \cong 1)$$

$$\Delta f_d = \frac{2 \times 25.5 \times 10^3}{0.1025} \times \frac{50 \times 0.82}{130}$$

$$= 26 \text{ cycles.} \qquad (11)$$

For a beam width of 0.34 degree to the half-power points, from Equation (4),

$$f_d = \frac{2v \sin \theta}{\lambda} = \frac{2v \sin 0.17^o}{\lambda}$$

$$= \frac{2 \times 25.5 \times 10^3 \sin 0.17^o}{0.1025}$$

$$= 1450 \text{ cps} \quad \text{(at half-power points).} \qquad (12)$$

The ramp amplitude is chosen to provide a frequency range of 5 ±2 kc at the output of the vco. The simulated doppler sweep of 2 kc - 0 - 2 kc is processed by a low-pass filter to give a one-half power roll-off at 1500 cps simulating an actual target doppler return.

(7) Commercial Test Equipment

Table I lists the commercial test equipment items which, in addition to the specially designed equipment already described, are housed in the system tester.

TABLE I - SYSTEM TESTER COMMERCIAL EQUIPMENT

Item	Manufacturer	Model no.
VTVM	Hewlett-Packard	410BR
Electronic counter	Hewlett-Packard	523CR
Delay generator	Hewlett-Packard	218AR
X-band test set	Hewlett-Packard	624CRX
Differential voltmeter	John Fluke	803BR
Oscilloscope	Tektronix	585
Spectrum analyzer	Polarad	TSA-W
Scope camera	Tektronix	C19

(8) Data Film Analyzer

The data film analyzer (Figure 5) serves as a simple optical correlator for demonstrating the resolution of the synthetic phase histories of targets provided by the transponder and azimuth target generator. The main optical elements of the data film analyzer are the light source, filter system, condensing system, azimuth lens, data film, range lens, transform plane slit, and microscope. A removable magazine section is provided for insertion of the data film strip to be analyzed.

b. Transmitter-Modulator Maintenance Tester

The Transmitter-Modulator maintenance tester (see Figure 6) consists of specially designed test panels, commercial test equipment, and auxiliary equipment housed in a single-bay test rack. The specially designed equipment includes a microwave equipment chassis, control and monitor chassis, and a high-voltage power supply.

(1) Microwave Equipment Chassis

The microwave chassis contains the wave guide equipment necessary to test the Transmitter-Modulator. The microwave equipment consists of two basic sections: a calibrated continuous-wave r-f source to provide a signal input to the klystron, and a transmitter output power and pulse characteristic monitor.

(2) Control and Monitor Chassis

The control and monitor chassis contains the power switching, interlocks, and indicators necessary for safe operation of the transmitter; a pulse generator to provide the prf trigger to the transmitter; meters and test points for monitoring signal and power voltages and wave forms; and the low-voltage power supplies. The controls and switches for the high-voltage power supply are also included in this chassis.

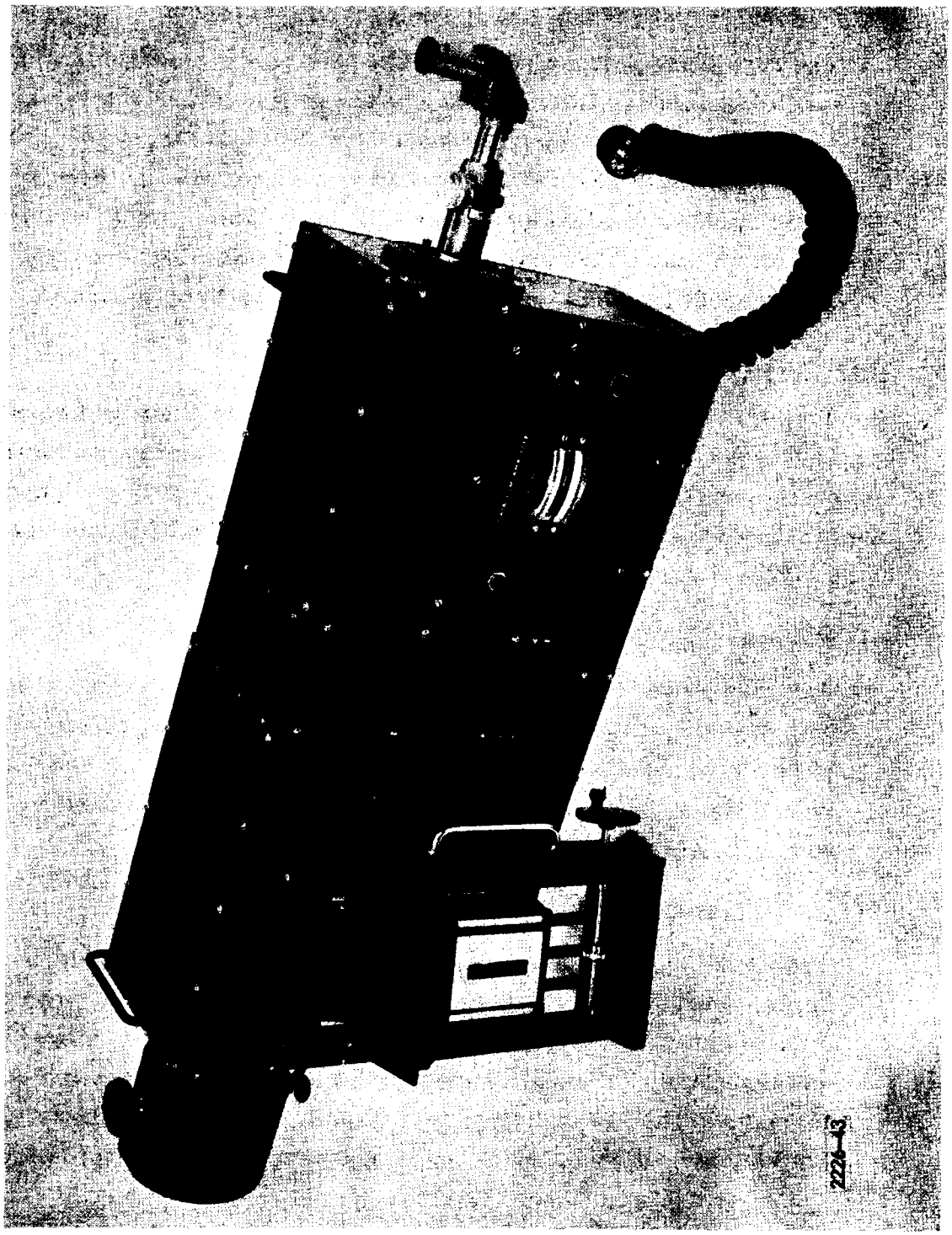

Figure 5 - Data Film Analyzer

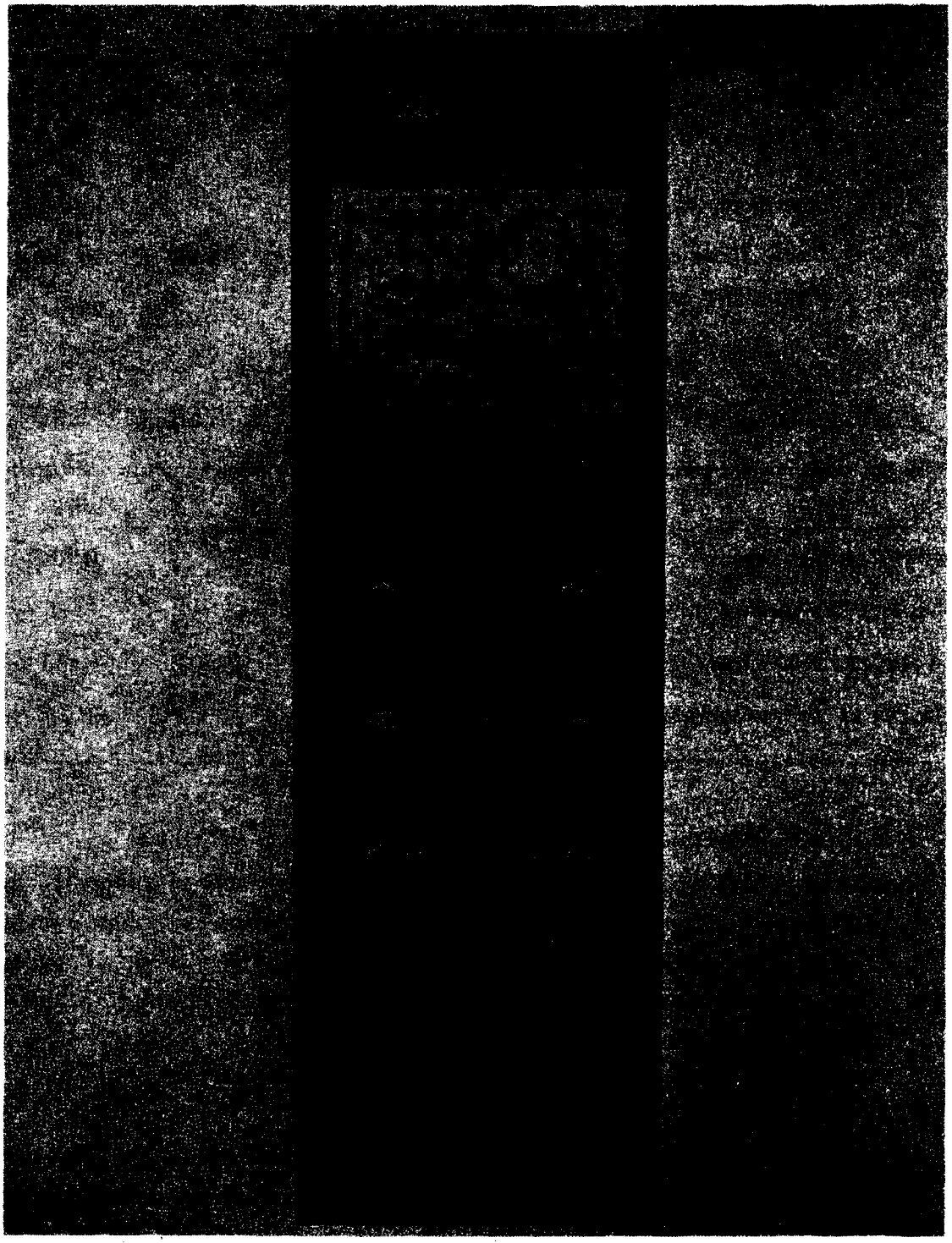

Figure 6 - Transmitter-Modulator Maintenance Tester

(3) High-Voltage Power Supply

The power supply is a standard, three-phase, full-wave, unregulated choke input with a pi-section filter capable of delivering 0 to 5000 vdc at 500 ma with very low ripple.

(4) Commercial Test Equipment

Table II lists the commercial test equipment in the Transmitter-Modulator maintenance tester.

TABLE II - TRANSMITTER-MODULATOR MAINTENANCE TESTER COMMERCIAL EQUIPMENT

Item	Manufacturer	Model no.
Test oscilloscope	Tektronix	RM45A
Microwave power meter	Hewlett-Packard	430CR
Inverter, 2000 cps	Behlman-Invar	R161A
Klystron power supply	Hewlett-Packard	716A

c. R-F/I-F Maintenance Tester

The R-F/I-F maintenance tester (Figure 7) consists of specially designed test panels, commercial test instruments, and auxiliary test equipment housed in a double-bay test rack. The specially designed test panels include a stalo check chassis, controller, noise generator, d-c power supply, and vhf attenuator panel.

(1) Stalo Check Chassis

The stalo check chassis is used to determine the phase stability of the local oscillator in the R-F/I-F unit. The dispersed X-band pulse from the R-F/I-F unit is delayed, then returned to the R-F/I-F unit as a

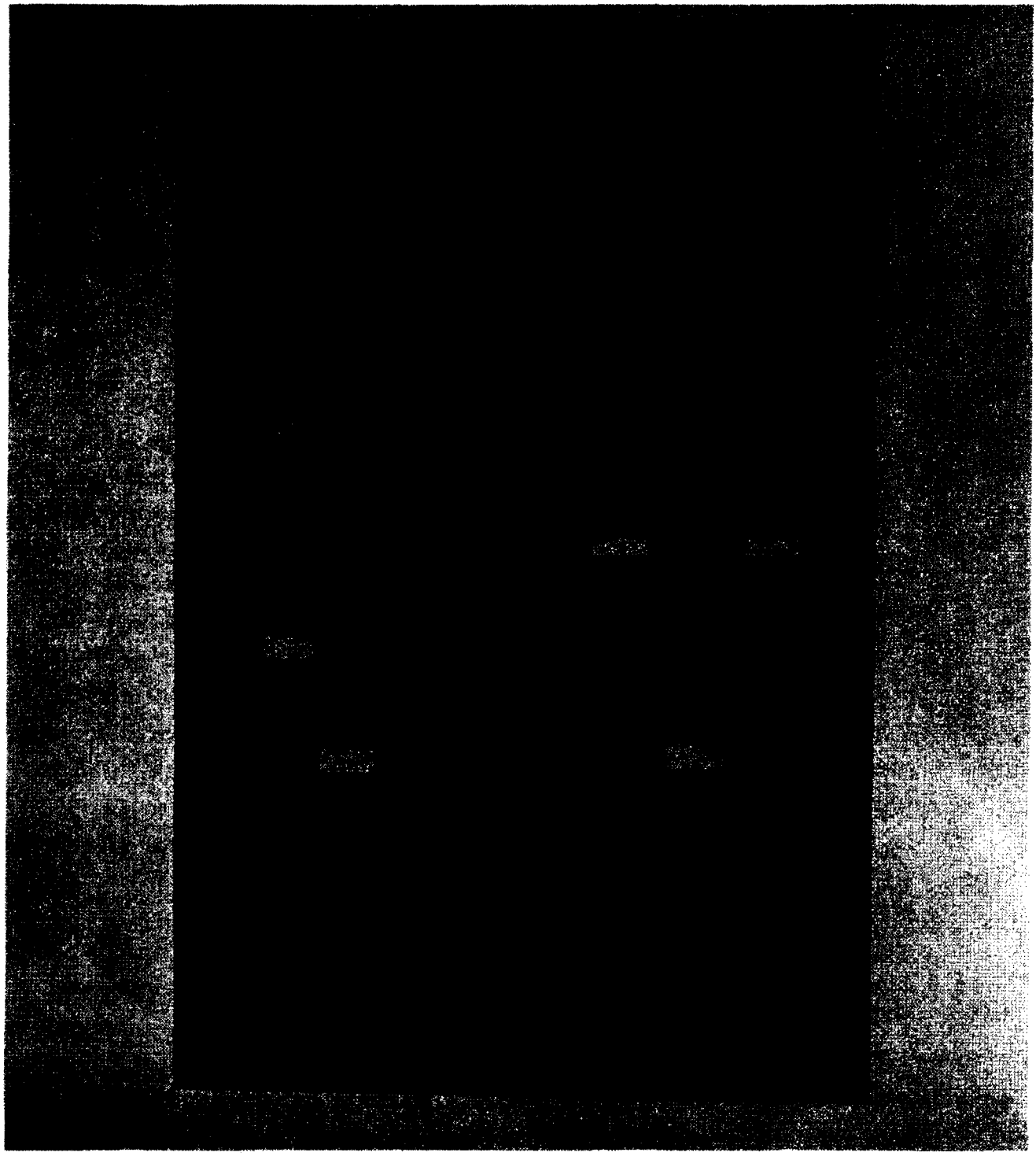

Figure 7 - R-F/I-F Maintenance Tester

target return for detection and compression. When the compressed pulse is synchronously demodulated (phase-detected), the stalo stability can be measured by observing amplitude variations in the detected pulse.

(2) Controller Chassis

The controller chassis contains the power switching and indicators for operation of the R-F/I-F unit, meters and test points for monitoring signals and power voltages, and wave forms and signal-generating circuits required to test the R-F/I-F unit.

(3) Noise Generator Chassis

The noise generator chassis incorporates an X-band noise tube, mount, and power supply with a wave guide attenuator to provide a calibrated variable excess noise source. When making noise figure measurements, the noise generator is connected to the receiver by a coaxial cable and coaxial-to-wave guide adapter. The i-f signal output of the receiver is connected to an r-f voltmeter through an i-f attenuator. With the noise generator off and the receiver on, the i-f attenuator is set for a convenient reference on the r-f voltmeter. The i-f attenuation is increased by 3 db, the noise source turned on, and the noise level attenuator adjusted for the same reference level output on the r-f voltmeter. For this setting the signal noise equals the input noise and the noise figure of the receiver may be calculated.

(4) D-c Power Supply Chassis

Four commercial power supply modules mounted on a common chassis supply d-c power to the tester and to the R-F/I-F unit under test.

d. Reference Computer Maintenance Tester

The Reference Computer maintenance tester (Figure 8) consists of specially designed test panels, auxiliary equipment, and commercial

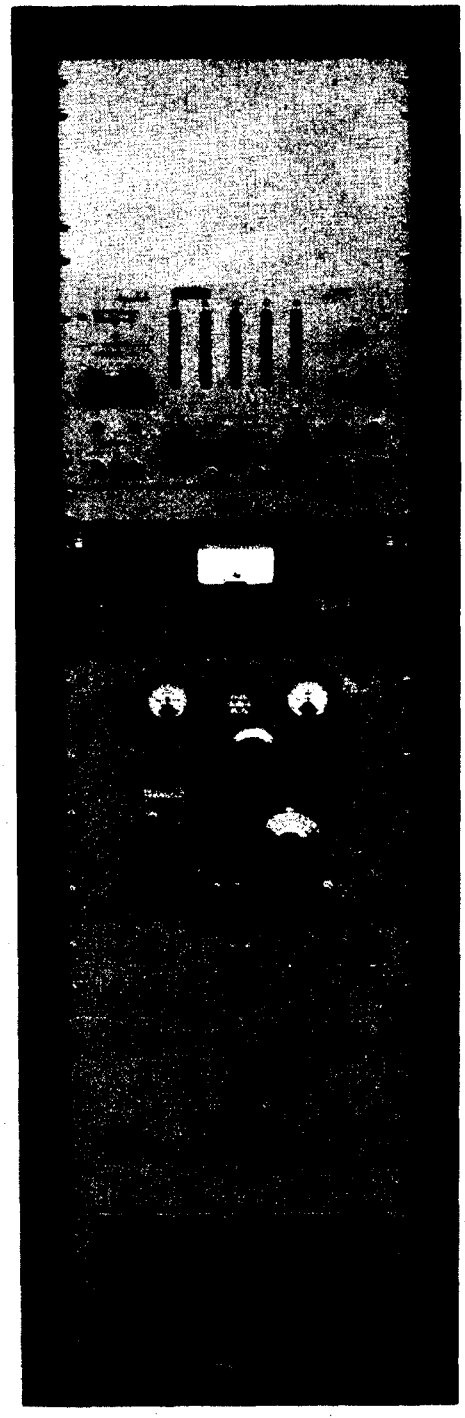

Figure 8 - Reference Computer Maintenance Tester

test equipment housed in a dual-bay test rack. The specially designed panels include a power supply unit, power control unit, and a simulator control unit.

(1) Power Supply Unit

The power supply unit supplies the power for the Reference Computer and for the tester.

(2) Power Control Unit

The power control unit controls the input power to the tester.

(3) Simulator Controller Unit

The simulator controller unit furnishes the following controls and signals for the Reference Computer.

(a) Control of D-c Power

The d-c power is controlled by a d-c power switch which controls power to the Reference Computer.

(b) Mode-Setting

PRF SELECT is accomplished by a four-pole, 16-position rotary switch. The 30-millisecond timer on the timer relay board, when actuated by the C/L RESET switch, generates a 30-millisecond 28.3-vdc pulse for the CLUTTERLOCK ON and CLUTTERLOCK TIME CONSTANT SELECT circuits of the Reference Computer.

The BIT switch energizes the BIT circuit of the Reference Computer.

(c) Conditioned Signals

The conditioned signals from the Reference Computer are monitored by the CONDITIONED SIGNAL SELECT and GROUPING SELECT switches and the CONDITIONED SIGNAL METER.

(d) Reference Computer and Tester Signals

Reference Computer signals and tester signals used to control the Reference Computer are monitored and/or terminated on the front panel.

COUNTER SELECT allows selecting of test signals from the Reference Computer for frequency counting.

(e) Clutterlock Integrator Testing

The integrator linearity and clutterlock response to a step function are tested by the use of a timed variable amplitude test pulse.

The VCO-CAL switch allows testing of the clutterlock operational amplifier as an integrator or as a 1:1 d-c amplifier.

(f) I-f Simulator

The i-f simulator portion of the simulator controller unit provides a simulated i-f output (a chopped, 70-mc single side-band signal) for the closed-loop operation of the clutterlock circuit of the Reference Computer. Figure 9 is a block diagram of the i-f simulator. The 70-mc signal, offset by prf/4 from the Reference Computer, is modulated with a "doppler" frequency (f_d) in a single side band (ssb) modulator and then chopped at a 33-kc rate to provide simulated i-f pulses.

Refering to Figure 9, the output of a vco, whose output frequency can be varied by means of a potentiometer from 40 to 60 kc, is compared in two synchronous demodulators with a 50-kc cosine and a 50-kc sine signal from a fixed 50-kc oscillator. The two outputs of the synchronous demodulators are at the difference frequency and are in quadrature. These two signals serve as a reference in the ssb. The ssb output is 70 mc + prf/4 $\pm f_d$.

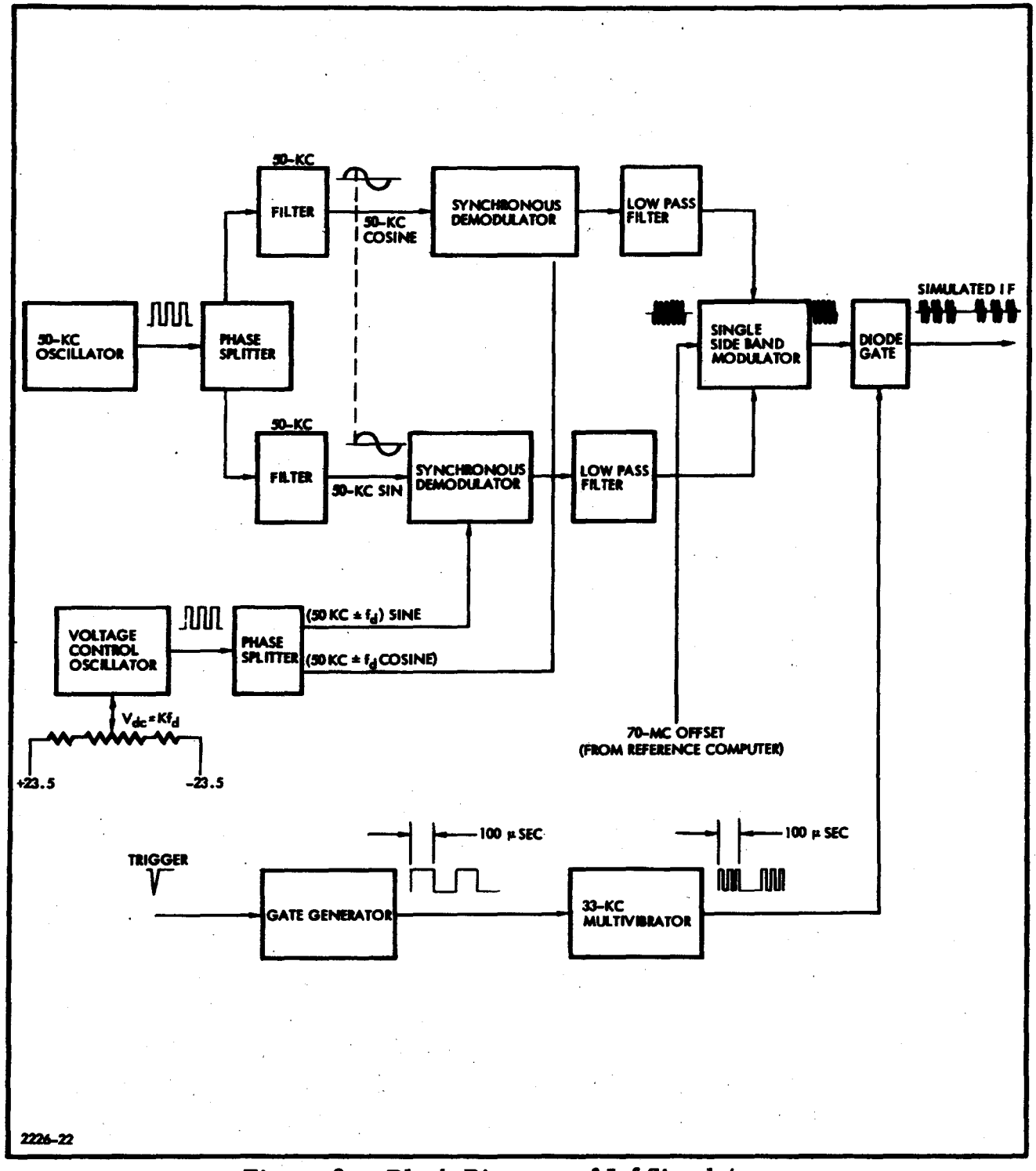

Figure 9 - Block Diagram of I-f Simulator

This output of the ssb modulator is next chopped at a 33-kc rate by gated 33-kc pulses. These pulses are gated on during a 100-μsec pulse which is triggered at prf rate. These gated 33-kc pulses in turn gate the 70 mc + prf/4 $\pm f_d$ output of the ssb modulator in a diode gate. The output of this diode gate is a coherent i-f signal which simulates the i-f return from the radar.

(4) Commercial Test Equipment

Table III lists the commercial test equipment in the Reference Computer maintenance tester.

TABLE III - REFERENCE COMPUTER MAINTENANCE TESTER COMMERCIAL EQUIPMENT

Item	Manufacturer	Model no.
Oscilloscope	Tektronix	585
Counter	Hewlett-Packard	522B
Signal generator	Hewlett-Packard	608C
VTVM	Hewlett-Packard	410B
R-f voltmeter	Boonton Electric	91C
Multimeter	ANPSM-6 (Mil-M-4552C-USAF)	

e. Control Unit Maintenance Tester

The Control unit maintenance tester (Figure 10) consists of specially designed test panels, auxiliary equipment, and commercial test equipment housed in a single-bay test rack. The specially designed panels include a power supply load panel, power control panel, and a-c power oscillator panel.

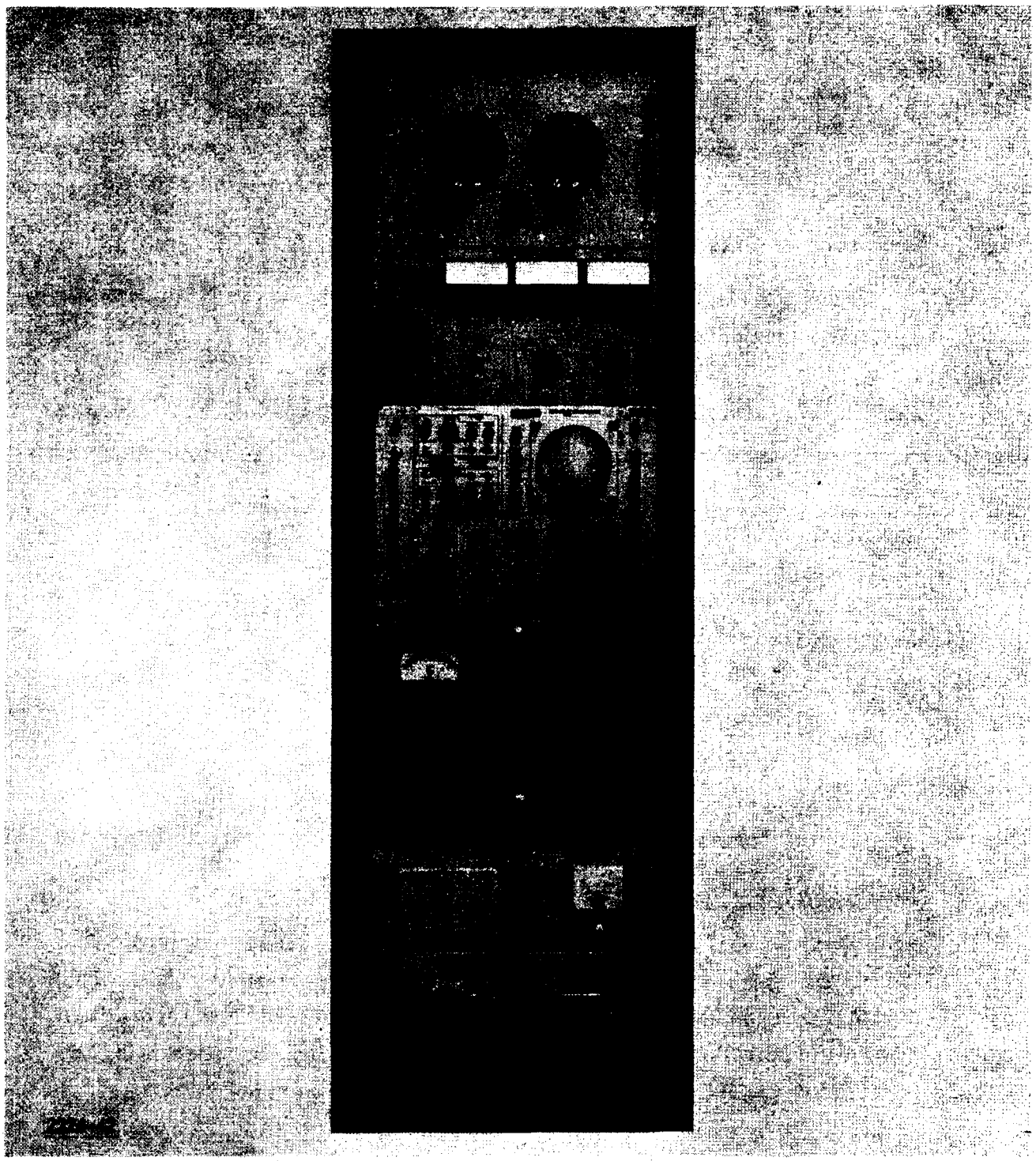

Figure 10 - Control Unit Maintenance Tester

(1) Power Supply Load Panel

This chassis contains three variable power resistors which act as loads for the three power supplies in the Control unit. Provision is made for shorting the outputs of the supplies to ground for overload recovery testing.

(2) Power Control Panel

The power control panel of the tester allows for monitoring, switching and controlling all the input power to the Control unit. It also provides for measurement of the output voltages and currents of the Control unit power supplies. Provision is also made for reading all the monitor voltages from the Control unit.

(3) A-c Power Oscillator Panel

This chassis contains two fixed-frequency power oscillators of 400 and 2000 cycles. The outputs of the oscillators are connected so that either may be switched to drive the Type 351A Invertron power amplifier (refer to Table IV) which supplies the a-c inputs to the Control unit.

(4) Commercial Test Equipment

Table IV lists the commercial test equipment in the Control unit maintenance tester.

TABLE IV - CONTROL UNIT MAINTENANCE TESTER
COMMERCIAL EQUIPMENT

Item	Manufacturer	Model no.
Oscilloscope	Tektronix	RM32
Differential voltmeter	John Fluke	803BR
A-c power supply	Behlman-Invar	Type 351A
D-c power supply	Behlman-Invar	Type 275W-8
Fixed frequency oscillator	Behlman-Invar	Type 1-400 ±0.01 percent
Fixed frequency oscillator	Behlman-Invar	Type 1-2000 ±0.01 percent

f. Recorder Maintenance Tester

The Recorder maintenance tester (Figure 11) consists of specially designed test panels, commercial test equipment, and auxiliary test equipment housed in a commercial single-bay rack. The specially designed equipment consists of a Recorder control and test chassis, d-c power supplies, an auxiliary film take-up cassette, and a recorder service stand.

(1) Recorder Control and Test Chassis

The Recorder control and test chassis provides for Recorder power switching, film drive control and monitor of Recorder d-c voltages, conditioned signals, and wave forms. In addition to these control and monitoring functions the chassis contains a number of test-signal generating circuits and provides a sweep trigger to the Recorder.

(a) Sweep Trigger Generator

The sweep trigger generator provides a pulse for the ramp generator in the Recorder. This circuit consists of a variable frequency multivibrator, blocking oscillator, amplifier, and limiter.

(b) Range Mark Generator

The range mark generator provides a train of pulses that is synchronized with the sweep in the Recorder. These range marks are used to measure crt sweep linearity.

(c) 50-Cps Generator

The output of the 50-cps generator is used to provide pulses which may be recorded on the film to serve as a measure of uniformity of film speed. As the film speed is five inches per second, ten pulses will appear per inch of film.

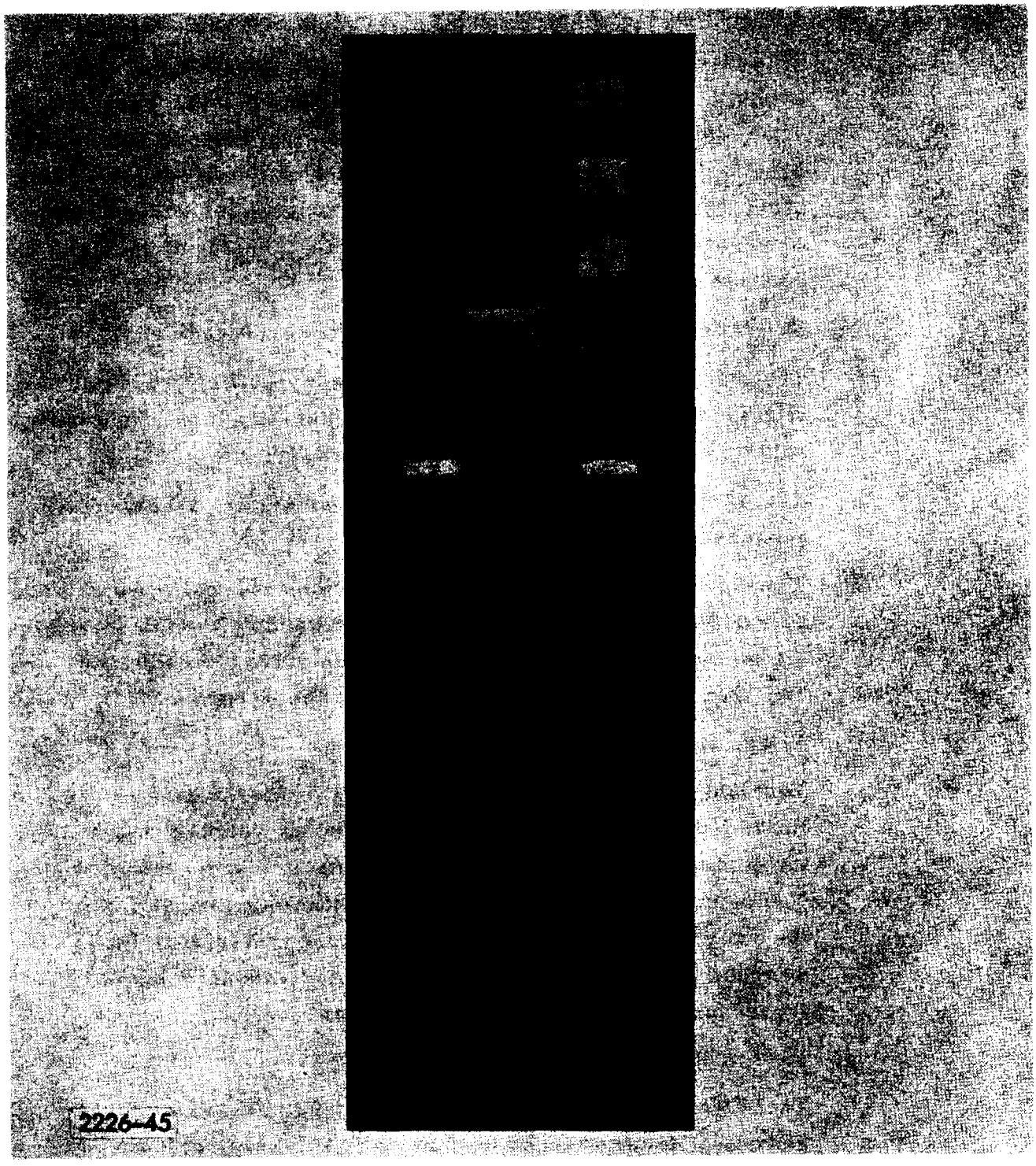

Figure 11 - Recorder Maintenance Tester

(d) 1.6-Kc and 3.2-Kc Generators

This circuit consists of a full-wave bridge rectifier and a pair of synchronized oscillators tuned to 1.6 kc and 3.2 kc, respectively. The outputs, which are sampled by five-microsecond pulses, are used to determine the azimuth resolution of the Recorder. Considering the vehicle velocity to be 25,000 feet per second, these test frequencies correspond to spatial frequencies of 15.6 and 7.8 feet per cycle, respectively.

(e) Prf/2 Generator and Adjustable Video Gate Generator

The prf/2 circuit consists of a bistable multivibrator, which is triggered by the sweep trigger, and a diode limiter. This output is also used to determine azimuth resolution.

The sweep trigger is also used to trigger a delay circuit which produces a delayed video gate.

The video gate is a five-microsecond video test pulse which may be varied to occur from 5 to 80 microseconds after the start of the sweep. A video amplifier is used to drive the cable and 100-ohm input to the video amplifier in the Recorder.

(f) 6-Mc, 10-Mc, and 14-Mc Generators

The unblanking gate from the Recorder is used to gate on a Hartley oscillator to produce, depending on which of three tuned circuits is chosen, one of these three test frequencies. The output is used to check the range resolution capability of the Recorder. Considering the slant range interval to be 73.5 microseconds, these test frequencies correspond to spatial frequencies of 71, 43, and 30 feet respectively.

(g) 10-Cps Generator

This circuit consists of a free-running multivibrator and an emitter follower. The output may be switched to any one of six data lamps in the Recorder.

(2) D-c Power Supplies

This chassis provides the +28.3-vdc, +23.5-vdc, -23.5-vdc, and +300-vdc voltages to the Recorder.

(3) Auxiliary Film Take-Up Cassette

This unit was described in Volume I, page 142.

(4) Recorder Test Stand

A Recorder test stand accompanies each tester and is used to support the Recorder and Auxiliary take-up cassette during test.

(5) Commercial Test Equipment

Table V lists the commercial test equipment in the Recorder maintenance tester.

TABLE V - RECORDER MAINTENANCE TESTER
COMMERCIAL EQUIPMENT

Item	Manufacturer	Model no.
Oscilloscope	Tektronix	RM15
Volt/ohm milliameter	Simpson	270
A-c power supply (3)	Behlman-Invar	161A
Fixed frequency oscillator	Behlman-Invar	Type 400 cps ±0.01 percent
Bridge oscillator	General Radio	Type 1330-A
Photomultiplier microphotometer	American Instrument Co	10-312

This page intentionally left blank.

SECTION III - GROUND-BASED RECORDING EQUIPMENT

1. GENERAL

The ground-based recording equipment located at the tracking station is used to provide a permanent photographic record of the video information telemetered from the vehicle. As this information should match the information recorded in the vehicle, it is only necessary to provide a KP-II Recorder and a means of triggering it to record the telemetered video. The ground-based recording equipment therefore consists of a Recorder and a Recorder maintenance tester which is modified to provide for extracting the video sync-pulse from the composite video. A prf selection simulator is also provided for training tracking-station personnel (refer to paragraph 4 following).

2. GROUND-BASED RECORDER

The Ground-Based Recorder is identical to the flight Recorder described in Volume I, Section VII, paragraph 5. In use it is mounted on the Recorder test stand which is supplied with the Ground-Based Recorder tester.

3. GROUND-BASED RECORDER MAINTENANCE TESTER

This tester is identical to the Recorder maintenance tester described in Section II except that it contains an additional assembly: the synchronizer and test generator chassis.

The synchronizer and test generator chassis contains two circuits: the time-averaging synchronizer and the video sync-pulse generator.

The composite video containing the video sync-pulse and the video signal is fed to the time-averaging synchronizer. The synchronizer detects the video sync-pulse and generates a sweep trigger at the same prf. A manually operated switch is provided for changing the frequency of the synchronizer to the approximate frequency of the video sync-pulse.

The video sync-pulse generator produces a test video sync-pulse that is used to check the synchronizer. A 16-position rotary switch is provided to change the prf of the pulse generator from 8215 to 8735 cps in approximately 35-cps steps.

a. Time-Averaging Synchronizer

The time-averaging synchronizer has the composite video signal as an input, detects when the video sync-pulse occurs, and generates a sweep trigger output that can be more stable than the input. When the synchronizer has no input or is first turned on, automatic search circuits vary the lock-on circuits about the prf number selected on the front panel. After lock-on the search circuits are turned off and the synchronizer can automatically follow small changes in prf.

(1) General Description

The composite video signal (see Figure 12) is fed through a gain-change circuit G-1 which is normally such that the gain, prior to lock-on, is high. The video signal then goes to a diode bridge-sampling circuit S-1 which is gated on by a one-microsecond blocking oscillator BO-1. The output of the sampling circuit is near zero except when the blocking oscillator causes the sampling circuit to sample during the sync pulse. The sync pulse is a one-microsecond positive pulse followed immediately by a one-microsecond negative pulse.

The output sampling circuit drives a vco and helps to set its frequency. The output of the vco in turn is used to trigger BO-1. The trailing edge of BO-1 also triggers a 0.25-microsecond blocking oscillator BO-2 which causes sampling circuit S-2 to sample the sync pulse. After lock-on, S-2 samples only during the negative portion of the sync pulse and causes switching amplifier A-2 to cut off the operation of sawtooth generator ST-1. Before lock-on, ST-1 is sweeping the vco approximately ±50 cycles at an 8 cps rate.

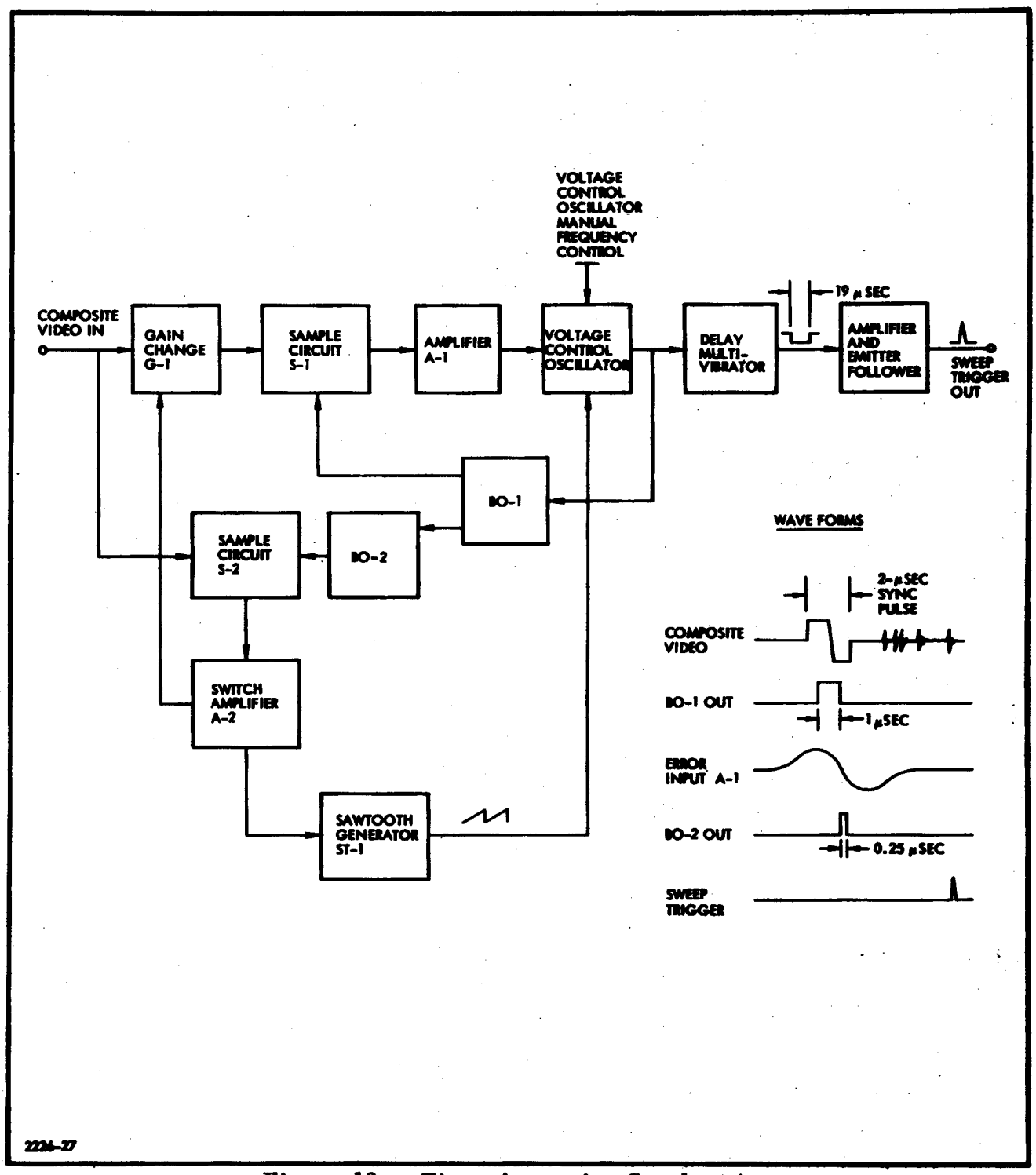

Figure 12 - Time-Averaging Synchronizer

(2) Lock-On

When the synchronizer has an input but is not locked on, and the vco manual frequency control is set approximately correct, lock-on is accomplished in the following manner. The vco is free-running but not at the correct frequency. Blocking oscillator BO-1 is firing and causing the gated bridge sampling circuit S-1 to sample but its filtered output is zero. Therefore, the vco does not receive any bias source from amplifier A-1. The trailing end of BO-1 triggers BO-2 but the filtered output of the gated bridge sampling circuit S-2 is also zero. Switching amplifier A-2 is set in such a manner as to set the gain-change circuit G-1 at high gain, and also to allow the sawtooth generator ST-1 to cause the frequency of the vco to sweep in a sawtooth manner about the frequency of the composite video trigger.

As soon as blocking oscillator BO-1 causes S-1 to sample a portion of the video-sync pulse, the circuit quickly locks on to the sync pulse, the gain-change circuit decreases the gain, the search sawtooth generator is turned off, and the vco operates at the same prf as the input.

(3) Sweep Trigger

The output of the vco is used to trigger a delay multivibrator. The trailing edge of the delay multivibrator is used to develop the sweep trigger pulse in the succeeding amplifier and emitter follower stage.

b. Video Sync-Pulse Generator

A test pulse was needed to check the operation of the synchronizer and, because of the unique shape of the pulse, the video sync-pulse generator was designed to generate this wave form. The frequency is controlled by a 16-position switch circuit that generates prf's from 8215 to 8735 cps in approximately 35-cps steps.

4. PRF SELECTION SIMULATOR

a. Purpose

The prf selection simulator (Figure 13) is used for training tracking-station personnel in the selection of prf for best radar performance. For a given altitude, considering the elevation beam pattern and depression angle, there will be an optimum prf setting. For a different altitude, the prf for optimum performance will change. The prf is selected by visual examination of the return followed by a manual adjustment of the prf selection switch. Prior to an actual mission the operators can become familiar with the techniques involved by use of the prf selection simulator.

b. Background Theory

Refer to Figure 14. Assume that the radar is at point S transmitting a beam toward the ground. A pulse leaves the radar and arrives at point S_1 at range R_1. This point will be somewhat down on the beam pattern and the radar return for an average target will be of amplitude E_1. For point S_2 the return amplitude will be maximum since the target is at the center or maximum power point of the antenna beam. For point S_3 the return will again be down. The resultant return for a uniform target distribution will be peaked as shown in curve 1. The peaking effect will be compensated for by the sensitivity time control (stc), curve 2, provided the prf is properly selected to center the radar return about the mid-point of the stc curve.

In Volume I, Figure 16, the stc wave form was shown to occur at a fixed time following the transmitted r-f pulse. The prf is adjustable from 8215 (step 15) to 8735 (step 0) pulses per second in 16 steps. This represents a change of 114.5 to 121.7 microseconds or about 1/2 microsecond per step. Since about 16 prf pulses are sent out before the first pulse is returned from the ground, this results in the stc being delayed or advanced approximately eight microseconds per prf step relative to the radar return.

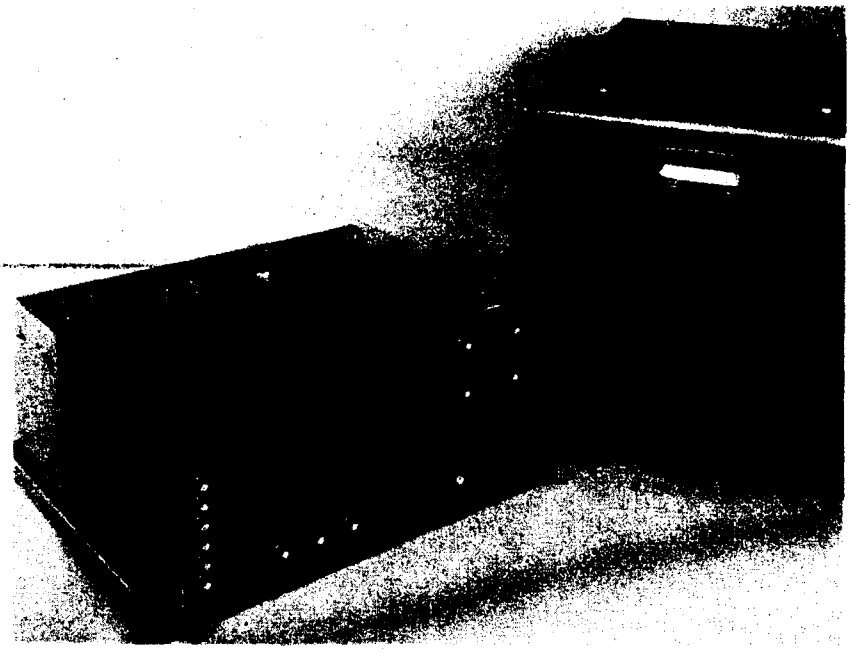

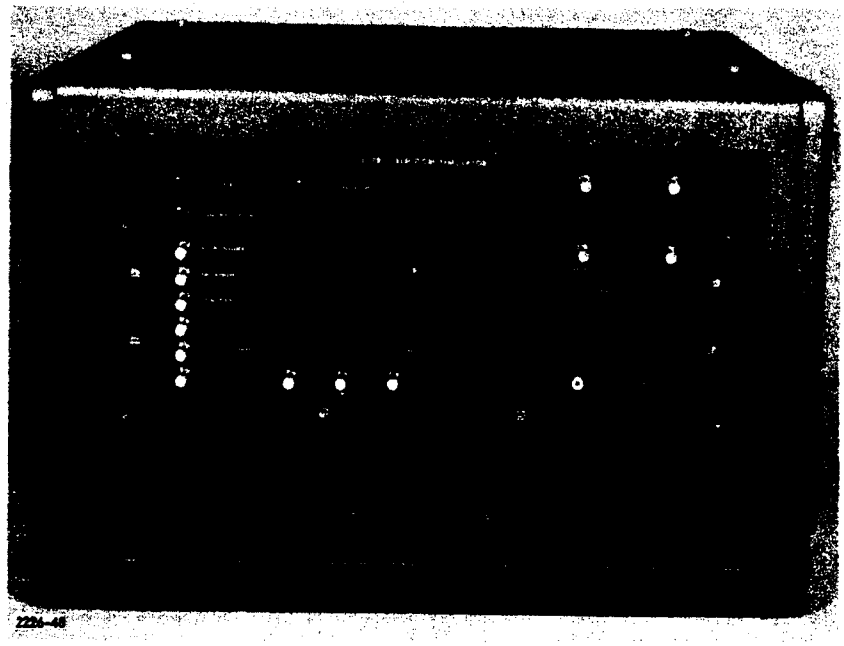

Figure 13 - Prf Selection Simulator

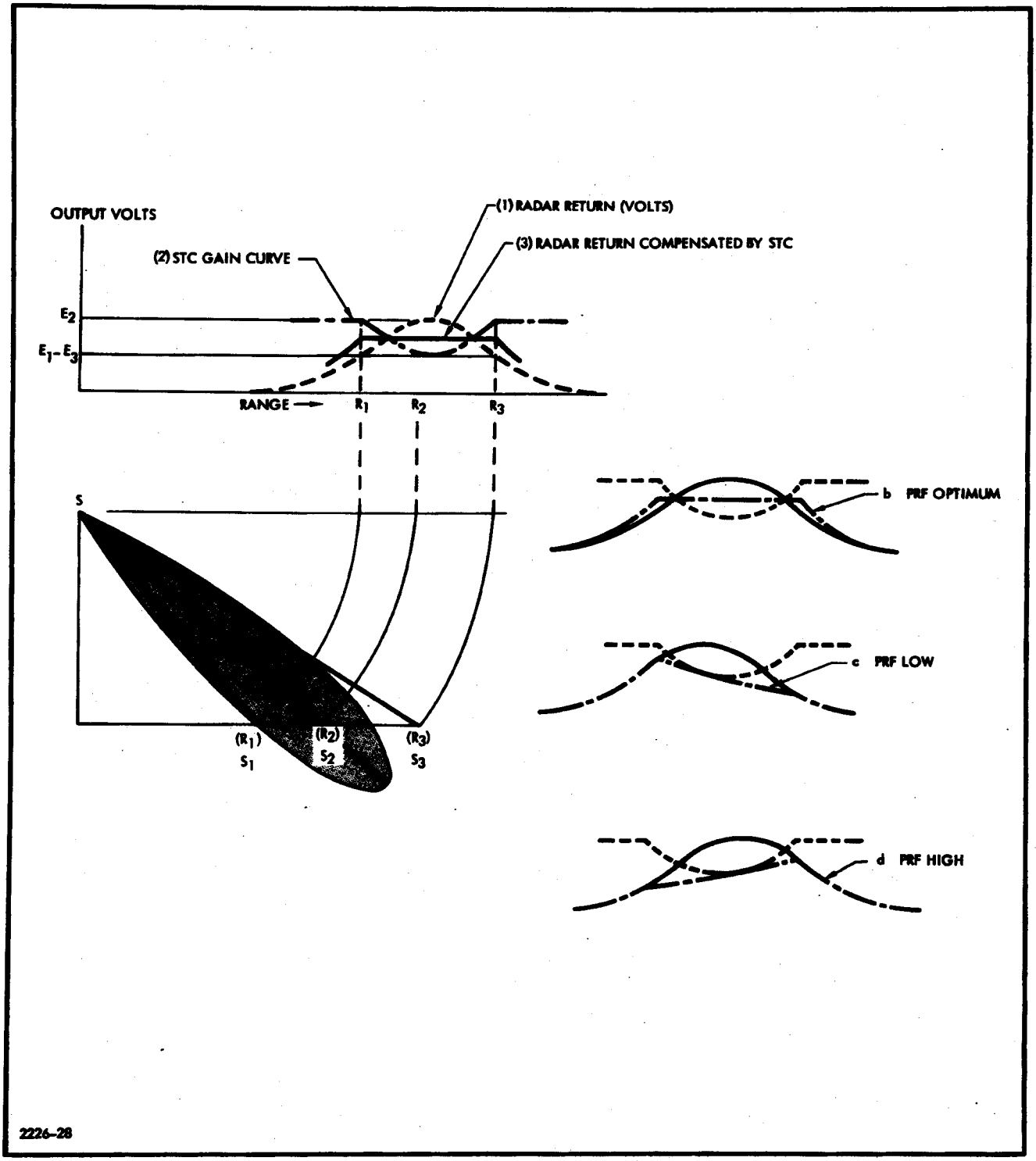

Figure 14 - Sensitivity Time Control

Figures 14(b), (c), and (d) show the radar return (upper envelope only) at a constant altitude (based on an assumed uniform target distribution) for low, high and optimum prf. Prf refers to actual rate of transmission of radar pulses. Similar results are obtained (except for slight changes in the radar return envelope) for other than nominal altitudes as the prf is stepped to either side of the optimum value. Figure 15 shows the prf selection simulator in block diagram form and the envelope of the output wave form of the simulator.

The noise generator G-1 (Figure 15(a)) generates a random noise voltage which simulates the target return. The frequency range of the noise is approximately 250 kc to 10 mc. The noise voltage is fed to two modulators M_1 and M_2. The first modulator modifies the noise voltage with the stc wave form. The output of the first modulator serves as an input to the second modulator. The modulating signal for the second modulator is the resultant of an addition of a sine wave and a low-variable-frequency wave form. The sine wave provides the simulated antenna beam envelope, and the low frequency, a variable "terrain" input.

The output of the second modulator is amplified in a four-stage amplifier A-1 to obtain the desired signal level. The amplified modulator output is inhibited for five microseconds every 114 to 121 microseconds. This is accomplished by clamping to a d-c level the output of one of the amplifiers with the On-Gate generator G-2. The amplified output of the modulator is fed to summer S-2 where it is added to the sync pulse.

The combined signal (modulated noise and sync pulse) is then passed through a limiter L-1. The output of the limiter is adjustable from the front panel of the noise generator. The output of the limiter is Output 1. Output 2 on the front panel is the output of the limiter after it has passed through an additional stage of amplification (see Figure 15(b)).

A noise adjustment located on the front panel provides a means of combining the output of the second modulator with additional noise.

The prf selection switch located on the front panel is a ten-deck switch. The "A" deck is used to supply one of 16 d-c levels to a vco. The oscillator

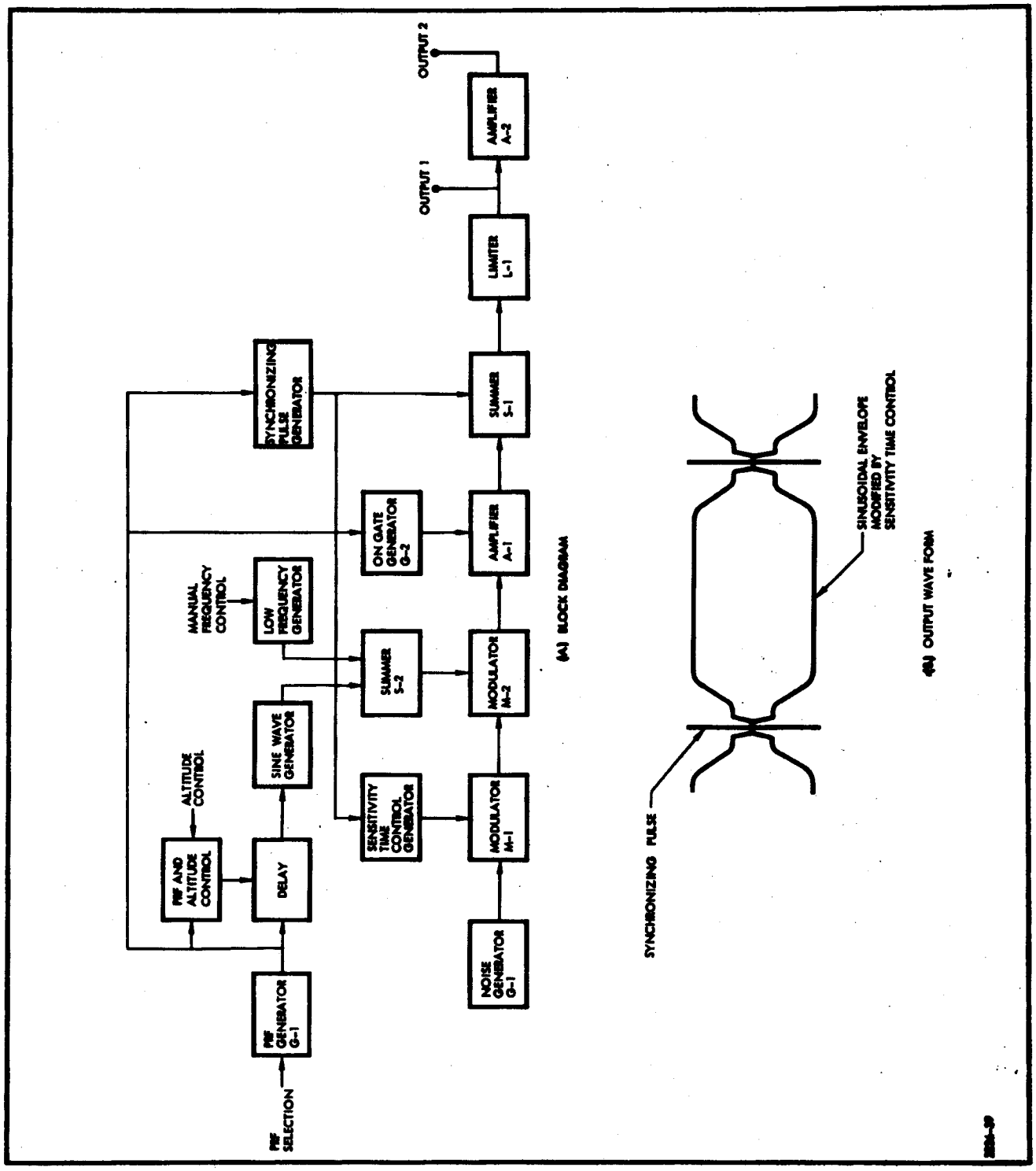

Figure 15 - Block Diagram of Prf Selection Simulator

output is used to generate the prf trigger at any one of 16 selected rates. The prf trigger is the basic trigger and all other signals are generated with respect to this trigger. The ALTITUDE switch selects one of eight voltages for routing to the delay generator. Thus the d-c level selected as an input to the delay generator is determined by the setting of altitude and prf. The output of the delay generator provides a trigger which in turn generates a square wave. The square wave generates the sine wave mentioned above.

The negative-going edge of the sync pulse is delayed 10 microseconds from the prf trigger. The start of the stc wave form is delayed approximately 20 microseconds from the negative-going edge of the sync pulse. The negative-going edge of the sync pulse is differentiated and is called "scope sync".

c. Video Simulator

The video simulator was an airborne version of the prf selection simulator. The video simulator provided an output wave form representative of only the correct prf setting at nominal vehicle altitude. The video simulator was used as a signal source to provide modulation of a Lockheed Type VIII transmitter. Both the simulator and the transmitter were placed on board a jet aircraft which was used to simulate the video link output of the orbital vehicle during collimation of the 60-foot receiving antenna at the tracking stations. While collimation checks were being conducted, the tracking station personnel became familiar with the signal and the tuning techniques that were required during orbital operations.

SECTION IV - GROUND TEST PROGRAM

1. GENERAL

This section covers the tests which were performed for both qualification and acceptance of the radar equipment. Each test is briefly described with particular emphases placed on the problems encountered. The material in this section provides a background for the more detailed discussion in Section V of problems and corrective actions.

2. QUALIFICATION TEST PROGRAM

The qualification tests were begun at Goodyear Aerospace and completed at LMSC. The tests were performed on a radar system (Serial No. 1) which was set aside for this purpose. The tests were performed at both unit and system levels. The qualification test program will be discussed with the aid of the flow chart in Figure 16.

a. Unit Design Approval Tests

Following fabrication, each unit was subjected to an Adjustment and Calibration Procedure (ACP) as a preliminary to the Design Approval Test Procedure (DATP). The DATP consisted of a low level vibration test and a thorough functional test. The units came through these tests with very few problems. The individual unit maintenance testers (refer to Section II: Ground Support Equipment) were used to perform the tests.

b. System Design Approval Tests

Following the unit DATP's, the units were tied together in a system configuration with the system tester (refer to Section II) and subjected to the system ACP and then the system DATP.

The system design approval tests were selected to verify that the system was operating as designed and that it would deliver the required radar data with sufficient quality to meet the design goals. The results of system design approval testing illuminated some incompatibilities between the

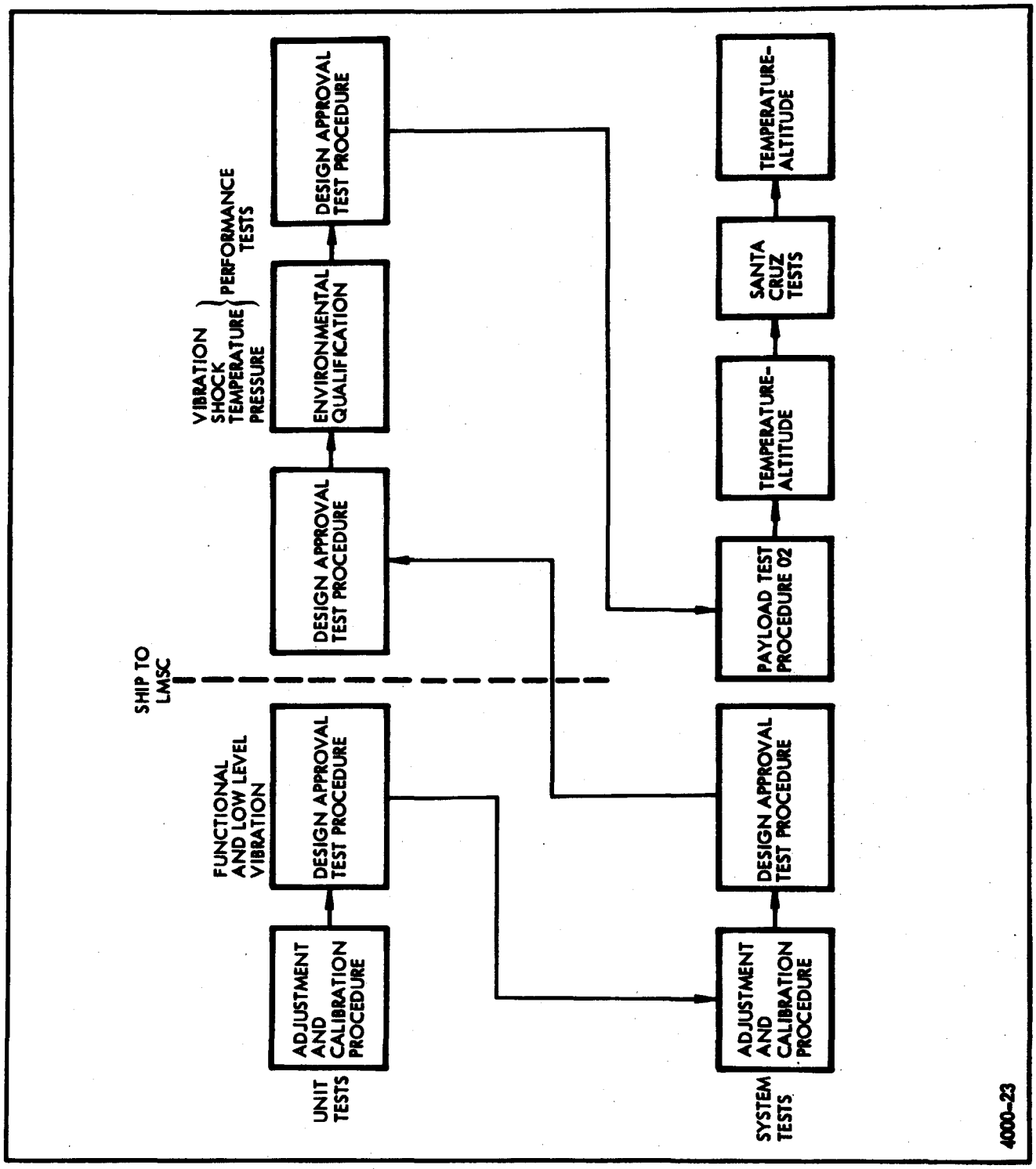

Figure 16 - Qualification Test Program

radar system and tester. Additionally indicated were other problems relating to system timing, conditioned signal outputs, recorder crt bias, and repeatability of film exposure and development.

All of these problems were corrected during the testing phase. In one area, the original design approval tests failed to uncover a serious system problem. This problem, in connection with the clutterlock operation, is discussed in detail in Section V, paragraph 7.c.

c. Unit Environmental Tests

At the conclusion of the design approval tests, the Serial No. 1 radar system was shipped to LMSC for environmental qualification testing. There, the electrical portion of each unit design approval test was repeated to ensure proper unit operation after shipping. The individual units were then subjected to vibration, shock, and temperature-altitude environmental tests in accordance with the specification requirements. The problems which appeared during environmental testing are included in the discussion of problems and corrective actions in Section V following.

(1) Vibration

The units experienced few serious problems in the vibration tests but a number of attaching hardware problems appeared. A switch came loose on the Transmitter-Modulator. Two loose choke coils, a loosened connector, and a broken wire on a printed circuit board were found in the testing of the R-F/I-F unit. In the Recorder a choke coil vibrated loose. The Reference Computer and Control unit suffered no damage. The most serious problem occurred in the Recorder when the crt changed brightness. This necessitated a later redesign of the gun structure.

(2) Shock

The problems encountered during shock testing were not serious and were easily corrected. The Transmitter and Control unit had no

failures. In the R-F/I-F unit a cold solder joint was found after testing. The Reference Computer developed a short circuit in a coaxial insert, with an additional short circuit caused by human error during testing. The power supply studs came loose in the Recorder and the inserts pulled out of some lead weights on one of the isolation roller assemblies.

(3) Temperature-Altitude

Many problems which were encountered later in temperature-altitude testing at system level in the temperature-altitude-simulation (TAS) chamber did not show up in the TAS unit testing phase. A single high-voltage problem appeared in the Transmitter when arcing in the plotted connector of the pulse transformer caused erratic operation. In the R-F/I-F unit the pre-amplifier displayed symptoms of temperature instability. An instability of r-f power output, possibly caused by a loose connection, disappeared when the pre-amplifier was replaced.

The Reference Computer and Recorder underwent the tests without difficulty. In the Control unit a power supply overload recovery problem appeared which was traced to a diode which did not meet all the design requirements as a function of input voltage and load conditions. The problem was corrected by selecting an improved component.

At the conclusion of the unit environmental tests, each unit was re-tested to the unit DATP and the results compared with the results of the same procedure run prior to environmental testing.

d. System Temperature-Altitude Test

The units were subsequently assembled in the vehicle nose section and checked to Payload Test Procedure PLTP02. The complete nose was then placed in the TAS chamber for environmental qualification at the system level. Several difficulties were experienced with the Transmitter-Modulator during the temperature-altitude tests. The thyratron triggering circuit was shown to be voltage sensitive and design changes were made.

A klystron and inverse diode were inadvertantly destroyed because of a test error and a pulse-forming network failed. After these malfunctions were corrected, twelve simulated orbits were completed without a failure and the system was sent to a test range for field tests with the antenna.

e. Santa Cruz Tests

The field series of tests was conducted at an LMSC antenna test range in the coastal mountains near Santa Cruz, California. The radar and antenna were mounted on a tower on one peak and a pair of corner reflectors placed on an adjacent peak. The tests, in addition to showing the resolution to be within specifications, provided a valuable check on round trip gains and losses through the radar system and antenna. The only malfunction was a t-r tube which failed during the tests and had to be replaced.

f. Repeat of System Temperature-Altitude Tests

Following the Santa Cruz tests the temperature-altitude tests were repeated in the TAS chamber. Momentary interruption of the high-voltage power supply was experienced during several operate cycles. The difficulty was traced to a faulty inverse current overload relay in the Transmitter-Modulator.

3. FLIGHT EQUIPMENT TEST PROGRAM

a. General

The flight radar system was tested as shown in the flow chart of Figure 17. The test program included both unit and system tests.

b. Unit Acceptance Tests

The formal acceptance tests were started at Goodyear Aerospace Corporation. Each unit upon completion was coupled to its particular unit maintenance tester and subjected to a component Adjustment and Calibration

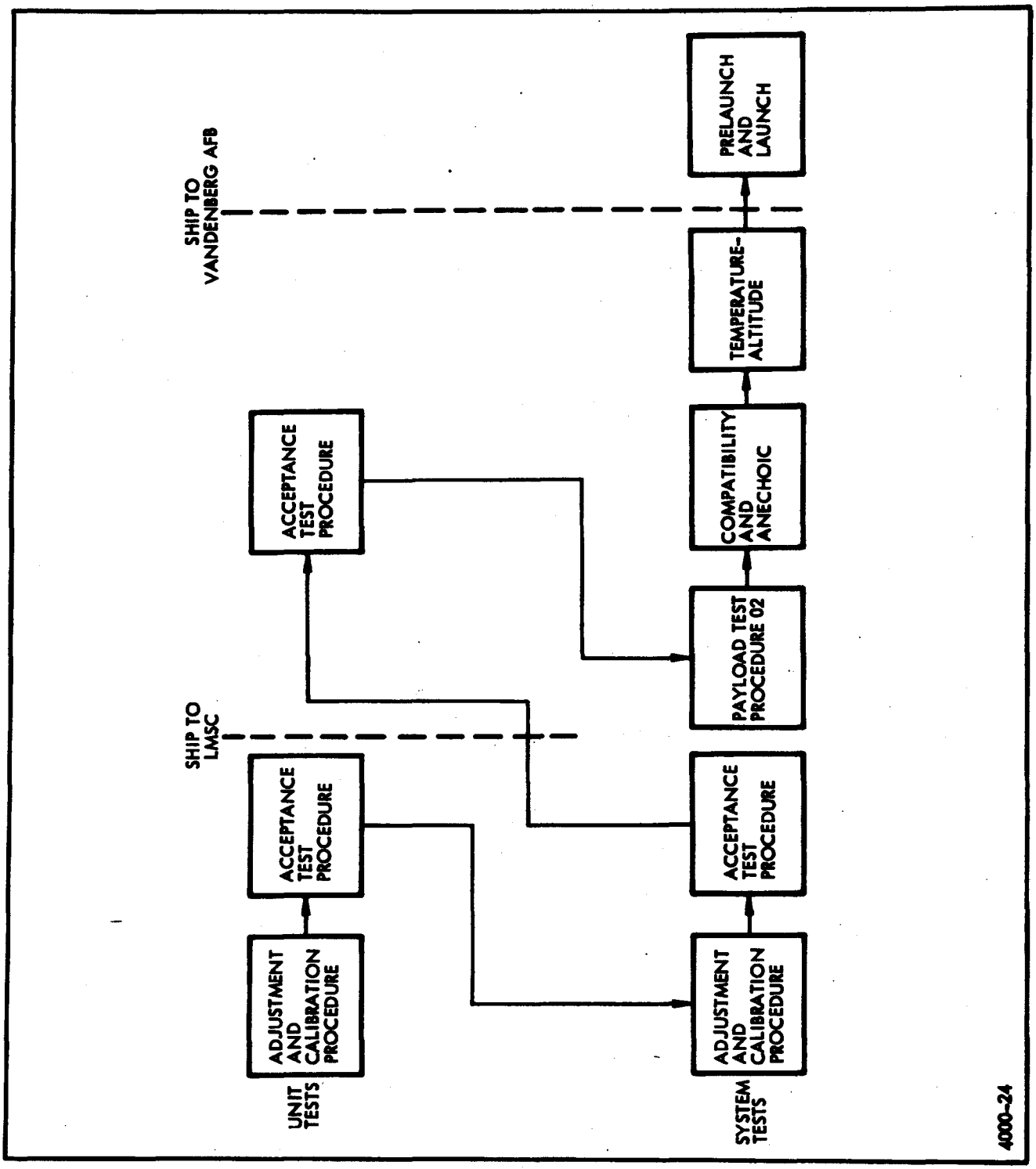

Figure 17 - Flight Test Program

Procedure (ACP) and then to an Acceptance Test Procedure (ATP) designed to prove that the unit was functioning correctly.

c. System Acceptance Tests

Upon completion of the unit acceptance tests, the units were cabled together with the system tester and subjected to the system ACP and then to the system ATP. Upon completion of the system ATP, the units comprising the system were shipped to LMSC.

d. Payload Tests

(1) Agena Nose Section Tests

After arrival at LMSC, each unit was retested to the unit ATP to ensure operation after shipping. The units were then installed in the Agena nose section and tested to the first of the payload test procedures (PLTP02). This procedure, which was similar in content to the system ATP, was designed to show proper operation of the radar set with the associated equipment in the barrel. A battery simulator was used as the primary power source.

(2) Agena Compatibility Tests and Anechoic Chamber Tests

The nose section was next moved to the Agena assembly area for preliminary compatibility tests, anechoic chamber tests, and final compatibility tests. The anechoic chamber tests were conducted with the entire Agena assembled in the anechoic chamber and tested as an entity, self-powered by batteries and remotely controlled. No troubles were encountered with the payload and the tests were completed in June, 1964.

(3) System Temperature-Altitude Tests

In this test, the nose was installed in the TAS chamber and a series of tests run which were designed to simulate actual orbit times,

temperatures, and pressures. The problems which occurred during this test included one voltage breakdown each in the klystron, inverse and charging diodes, and pulse transformer. Also included were capacitance changes in some of the radio frequency interference filters and a short circuit in one radio frequency interference filter. These problems, which occurred from September through November, 1964, are discussed in detail in Section V. At the time of completion of the test on 1 December 1964, a total of 152 hours had been spent at simulated altitude in the TAS chamber.

(4) Prelaunch Tests

Following the TAS chamber tests, the radar system was shipped to Vandenberg Air Force Base, California, for final tests prior to launch. A bearing failure in the data film supply cassette resulted from a human error. This malfunction was corrected and the satellite was launched on December 21, 1964.

SECTION V - PROBLEMS AND CORRECTIVE ACTIONS

1. GENERAL

The problems which appeared during the ground testing of the radar set mostly originated as a direct result of the high-altitude environment and, to a lesser extent, to the high vibration levels. This section discusses the unit and system failures and problems which appeared during testing, together with the corrective actions which were taken to prevent recurrence.

2. TRANSMITTER-MODULATOR

Failures of this unit usually resulted either from vibration or from the combination of high-voltage and high altitude environment.

a. Vibration Problems

Early in the program it was decided that all of the units would be hard mounted to the vehicle structure. It soon became apparent that this approach was not adequate for the Transmitter-Modulator. Vibration amplifications up to 50 times at various frequencies between 100 and 1000 cps were experienced. Accordingly, a center-of-gravity mounting using stiff vibration isolators was designed. This type of mounting minimized the vibration problem. Table VI lists the various problems encountered in the Transmitter-Modulator. Of these problems, items 1, 2, and 3 can be classified as resulting from vibration.

b. Pressure Altitude Problems

Those problems which can be classed as voltage breakdown resulting from the high altitude environment include items 4 through 12 of Table VI. These failures were invariably initiated during exposure to reduced pressure and resulted from various causes such as improper bonding of potting materials at high-voltage points, voids in potting, air bubbles or reduced pressure in oil filled units, and contamination of potting. They were corrected by

extensive testing in altitude chambers, thorough failure analysis programs, and close process control.

c. Other Causes

Items 13 through 16 were miscellaneous problems. Items 12 and 13 were design deficiencies requiring design changes. Items 14, 15 and 16 required no corrective action other than parts replacement since they were either secondary failures or resulted from use of substandard parts.

3. RF-IF

The majority of the problems in this unit, as in the Transmitter-Modulator, were the result of the high voltage in combination with the high altitude environment. In Table VII, items 1, 2, and 3 are vibration problems and items 5, 6, 7, 8 and 9 are high voltage/high altitude problems. Items 10 and 11 are failures involving only replacement of parts in test and monitor circuits. Items 12, 13 and 14 were design deficiencies requiring circuit redesign.

4. REFERENCE COMPUTER

This unit was very reliable throughout the program. Item 1, Table VIII, was a design deficiency associated with the clutterlock and built-in-test (BIT) circuitry and was corrected by circuit modifications and adjustments. (This problem is discussed in paragraph 7.c.) Item 2 was a workmanship problem.

5. CONTROL UNIT

This unit was very reliable and had only two problems (refer to Table VIII). The first was an end seal problem in the rfi filters which was solved by elimination of the filters from the circuit. These particular filters were found to be unnecessary. The second problem, failure of the +300 vdc supply to recover following a short circuit overload, occurred only for low input voltages or low temperatures and was corrected by a component type change.

TABLE VI - TRANSMITTER-MODULATOR PROBLEMS

Item	Number of failures	Problem description	Corrective action
1	1	Overload switch vibrated loose	Redesign switch mounting
2	2	Klystron filament shorted	Reduce heater feed-through diameter to provide better support
3	2	Charging choke open, broken wire	Change to stranded wire, fill with epoxy sand
4	1	High-voltage breakdown, potted area around pulse transformer bushing	Change potting procedure
5	2	Klystron breakdown, potted area around cathode	Eliminate vendor use of silicon grease prior to potting. Contamination problem
6	4	Pulse-forming network, shorted capacitors	Redesign case to maintain oil pressure at high altitudes. Use bellows, epoxy sand, stiffer case
7	3	Pulse transformer, internal breakdown, shaping coil to ground	Redesign shaping coil mounting. Use fiberglass insulation, change tuning slug
8	5	Thyratron high-voltage breakdown	Modify metal container, change potting procedure and material
9	2	Cracked klystron window	None. Test error, wave guide pressure
10	4	Inverse diode, high-voltage breakdown	Change to epoxy potting. Change case. X-ray diodes
11	2	Charging diode, high-voltage breakdown	Change to epoxy potting. Change case. X-ray diodes

TABLE VI - TRANSMITTER-MODULATOR PROBLEMS (Continued)

Item	Number of failures	Problem description	Corrective action
12	1	Breakdown of high-voltage interconnecting leads	Change method of shield braid termination
13	1	Thyratron multiple triggering	Redesign triggering circuit
14	1	Apparent inverse overload and thermal switch operation	Replace bad relay. By-pass inverse and thermal overload circuits for flight
15	1	Delay timer inoperative	Replace timer. By-pass delay timer for flight
16	2	Inverse resistors, high-voltage breakdown	None. Secondary failures

TABLE VII - R-F/I-F PROBLEMS

Item	Number of failures	Problem description	Corrective action
1	1	Varactor frequency multiplier detuning as a result of vibration	Bonding of coil turns to coil form. Bonding of capacitors. Use of foam potting
2	2	R-f choke coils broken loose in i-f switch because of vibration	Design change, better fastening
3	1	Broken wire on printed circuit board because of vibration	Design change, board attachment
4	1	Cold solder joint to relay. Discovered in vibration testing	Resolder
5	1	2-kv (twt) supply voltage breakdown	Use of potting
6	1	Varactor frequency multiplier voltage breakdown	Use of foam potting
7	1	TWT high voltage breakdown	Vacuum potting of high voltage leads
8	3	Voltage divider high voltage breakdown	Redesign for better spacing. Change to epoxy potting material
9	1	Spiking indicated on 2-kv supply monitor	Design change
10	1	Defective coaxial test connector	Replace
11	1	Defective temperature monitor	Replace
12	1	Defective twt output monitor circuit	Design change
13	1	Defective r-f power monitor	Design change
14	-	Poor wave form, r-f to transmitter monitor	Redesign signal conditioner circuit

TABLE VIII - REFERENCE COMPUTER AND CONTROL UNIT PROBLEMS

Item	Number of failures	Problem description	Corrective action
		Reference Computer	
1	-	Clutterlock circuit not operating properly and BIT loop gain incorrect. Design deficiency	1. Filter addition, On-Gate line 2. Addition of ground plates and straps on coaxial connectors 3. Circuit changes 4. Change BIT loop gain
2	-	Short in coaxial connector	Repair. (Workmanship problem)
		Control Unit	
1	2	Rfi filters, oil leaks	Elimination of filters from circuit
2	-	±23 vdc supply failure to recover from short circuit overload. Design deficiency	Circuit design change (component change)

6. RECORDER

The Recorder unit had very few problems (refer to Table IX). Item 1 was a light level shift in the crt induced by vibration or shock. This problem was corrected by a vendor redesign of the crt gun structure. Items 2 and 3 were also vibration problems. Items 4 and 5 were intermittent and shorted capacitors in the rfi filters. One filter type was eliminated from the circuit and the other was simply replaced. Item 6 was an open magnetic brake coil. Item 7 was a temperature sensitive light monitor circuit which was redesigned. Item 8 was not a failure since the drive speed was well within specifications. The meter drum drive was changed to further minimize short term film speed variations.

7. SYSTEM PROBLEMS

During the system design approval and acceptance tests at Goodyear Aerospace and during the following tests at LMSC, certain system problems arose which required system modifications.

a. Timing

During the design approval tests the chirped pulse (see Volume I, Figure 17) could not be made to fall within the klystron high-voltage pulse. The source of error was traced to a 0.25-microsecond delay occurring in a pulse transformer in the transmitter. The transformer was replaced with an avalanche pulse circuit which eliminated most of the delay. A 0.1-microsecond delay line was later added in the transmitter trigger line to further improve the timing between the chirped and klystron pulses.

b. Line Filter

When the radar system was assembled with the 400-cps inverter power source in the Agena, the filters contributed substantially to a poor power factor which in turn created a severe distortion of the input wave shape to the Recorder as a function of load changes. The distortion was particularly objectionable as the crt regulated high-voltage supply output and therefore the sweep amplitude is affected by distortion. The sweep amplitude tended

TABLE IX - RECORDER UNIT PROBLEMS

Unit	Number of failures	Problem description	Corrective action
1	1	Light level change in crt because of vibration	Redesign of crt gun by vendor
2	1	Inserts in lead weights on twiddle roller assembly pulled out during vibration	Material change, lead to stainless steel
3	1	Choke on printed circuit board damaged during vibration	Component bonded to board
4	1	Rfi filter oil leakage problem	Eliminate filters from circuit
5	1	Rfi filter shorted	Replace filter
6	1	Magnetic brake, open coil	Replace coil
7	1	Photocell in crt light monitor temperature sensitive	Change photocell type, change circuit
8	0	Variations of film drive speed	Change meter drum drive to minimize variations

to change as the drive motor, which also uses 115 vac, 400 cps, was turned on and off. The rfi filters were replaced with insulated feed throughs and the power factor correction capacitor values were changed for the drive-on condition. A near-unity power factor was finally obtained which greatly reduced the wave shape distortion.

c. Clutterlock

The original system tests failed to point out a problem involving excessive error in the clutterlock loop. The problem was finally brought into focus late in the system test program at LMSC. Test work at Goodyear Aerospace pinpointed the principle source of error as leakage of 70-mc signals (both c-w and prf/4 phase stepped) between the Reference Computer and the RF-IF. These leakage signals were entering the RF-IF on the On-Gate line and on the other interconnecting cables. The shields of these cables were "hot" because of inadequate grounding in the Reference Computer.

The corrective action consisted of the addition of braided ground straps and grounding plates on each printed circuit board connector containing shielded coaxial pin connectors. In addition, a small potted r-f rejection filter was installed in the On-Gate line just prior to its output to the R-F/I-F unit. These changes proved adequate to give the clutterlock loop of flight system No. 1 an operational capability at least 10 db better than that required.

d. Crt Bias Setting and Video Gain

As the optimum brightness setting of the crt could not be verified by a series of flight tests as in a piloted aircraft radar, a great deal of study and ground experimentation was required in advance of the Agena launch.

The crt bias level and video gain settings are major factors in obtaining high over-all system performance. In the KP-II system three recorders, one airborne and two ground based, were used, each requiring proper setting prior to flight.

NRO APPROVED FOR RELEASE
DECLASSIFIED BY: CHART
DECLASSIFIED ON: 9 JULY 2012

To establish the crt bias point, it was first necessary to measure the crt transfer function of bias volts versus light output. A microphotometer was used to make films having incremental steps of light output for film developing tests. Various developer types and processing times were evaluated to provide the desired range of film densities (or square root of film transmissivities, $\sqrt{T}$). The values of $\sqrt{T}$ were then plotted as a function of crt bias to produce an S-shaped curve. The high transmissivity end of the curve is determined primarily by the cut-off characteristics of the crt and the low transmissivity end by the maximum density of the film.

From the theoretical standpoint of linear recording, the bias point should coincide with the $\sqrt{T}$ being equal to 50 percent. However, measurement of the relative amount of film noise as a function of $\sqrt{T}$ showed that film noise could be reduced by choosing the bias point slightly lower than the 50 percent value.

The video gain was then selected to linearly record small signals and to allow large signals to be limited by the crt-film characteristics. This choice was made to ensure adequate ground painting.

To resolve these problem areas, close coordination was required between Goodyear Aerospace, [redacted], LMSC, and, especially, the Air Force Satellite Photographic Processing Laboratory (SPPL).

8. PROBLEM STATUS AT LAUNCH

a. General

There were four radar problems remaining just prior to launch. These were evaluated and judged to be not serious and are discussed here for completeness.

b. Transmitter Power Output

The transmitter power was 0.5 db below the minimum specified in the test specification (specification value was 74.7 dbm; actual was 74.2 dbm). This could have been corrected by a re-adjustment to increase the drive

power from the twt, but the problem did not warrant removal of the R-F/I-F unit to make last minute adjustments.

c. Sensitivity Time Control Wave Form

The sensitivity time control wave form was outside of the specification limits in two respects: the ratio of maximum to minimum amplitude should have been 2.0 ±0.1 but was actually 2.2; and the delay of the sensitivity time control start should have been 31 microseconds maximum but actually measured 35 microseconds. It was decided that this condition would not degrade the final maps.

d. TWT Output Interruptions

The TAS chamber tests exhibited a number of momentary spikes on the -2 kv monitor F11, and the r-f power to transmitter monitor F-72 during high altitude operation. Extensive retests of the R-F/I-F unit in an altitude chamber at Goodyear Aerospace indicated the problem to be non-destructive in nature.

e. Accelerometer

Tests showed the accelerometer in the Transmitter-Modulator unit to be inoperative. As this accelerometer was used only for flight test instrumentation, no corrective action was taken.

This page intentionally left blank.

NRO APPROVED FOR RELEASE
DECLASSIFIED BY: CHART
DECLASSIFIED ON: 9 JULY 2012

SECTION VI - ORBITAL OPERATIONS

1. MAPPED AREAS

The areas mapped during the flight test are shown in Figure 18. Each trace on the map represents a mapped interval which is approximately 10 nautical miles wide (5.95 nautical miles in slant range) and several hundred miles long. Table X gives the approximate latitude and longitude (determined by examination of the map film in all but one pass) of the start and finish of each pass.

2. PRE-RECOVERY OPERATING MODES

For the first seven payload operate periods (passes 8, 9, 14, 16, 24, 25, and 30), no attempts were made to determine the radar system limits, as the primary purpose of the mission was to demonstrate the feasibility of operating a satellite-borne radar system and early experiments could have placed the primary goal in jeopardy. Immediately after pass 8 the data obtained from the wide band telemetr link were sent by courier to be processed and correlated at the [redacted] This step was taken to verify that the radar was operating properly. During these first seven active passes only OPERATE, PRF and OFF commands were sent to the radar system. The necessary prf commands were determined from the A-scope presentation in the screen room at the tracking stations.

3. POST-RECOVERY OPERATING MODES

On pass 33 the data film from the satellite was recovered. On the next active pass (40), the automatic gain control (agc) circuitry in the radar was commanded off and fixed amounts of receiver (r-f/i-f) attenuation (step 2 and step 3) were selected.

Again, on pass 41, the radar was operated with several steps (0, 3, 4, 5) of fixed attenuation.

No experiments were conducted on pass 46 but on pass 47 the prf was stepped through all of its 16 positions. On pass 56 a command to short the integrator output (clutterlock circuitry) was sent. On pass 57 clutterlock time constant number 2 was selected and on pass 72 additional fixed attenuator settings were

selected. Table XI shows the status of the various radar functions, which were subject to commanding from the tracking stations, during the active orbital life of the vehicle. Table XII is a time analysis of the mission.

TABLE X - ORBITAL PASS COORDINATES

Pass no.	Pass direction	Start		End	
		North latitude	West longitude	North latitude	West longitude
8	S-N	38° 56.0'	86° 58.5'	45° 47.5'	82° 52.5'
9	S-N	32° 28.9'	112° 33.5'	39° 46.5'	109° 06.2'
14	N-S	42° 03.0'	79° 51.0'	34° 46.2'	76° 12.1'
16	N-S	41° 27.5'	124° 48.5'	35° 55.1	121° 49.0'
24	S-N	39° 23.5'	88° 49.0'	46° 51.3'	84° 19.0'
25	S-N	33° 11.5'	114° 22.5'	42° 00.9'	109° 24.6'
30	N-S	47° 23.5'	85° 29.8'	34° 09.0'	78° 01.5'
40	S-N	40° 40.1'	90° 08.0'	46° 54.1'	86° 20.5'
41	S-N	32° 42.2'	116° 46.0'	41° 24.2'	112° 27.0'
46	N-S	45° 37.5'	86° 21.5'	34° 06.5'	80° 10.0'
47	N-S	44° 47.5'	108° 23.1'	33° 57.5'	102° 42.5'
56	S-N	41° 41.8'	91° 37.8'	47° 38.2'	87° 58.0'
57	S-N	32° 51.6'	118° 28.7'	43° 34.2'	113° 22.5'
72	S-N	46° 17.5'	90° 50.0'	51° 01.2'*	87° 15.6'*

*S-Look data

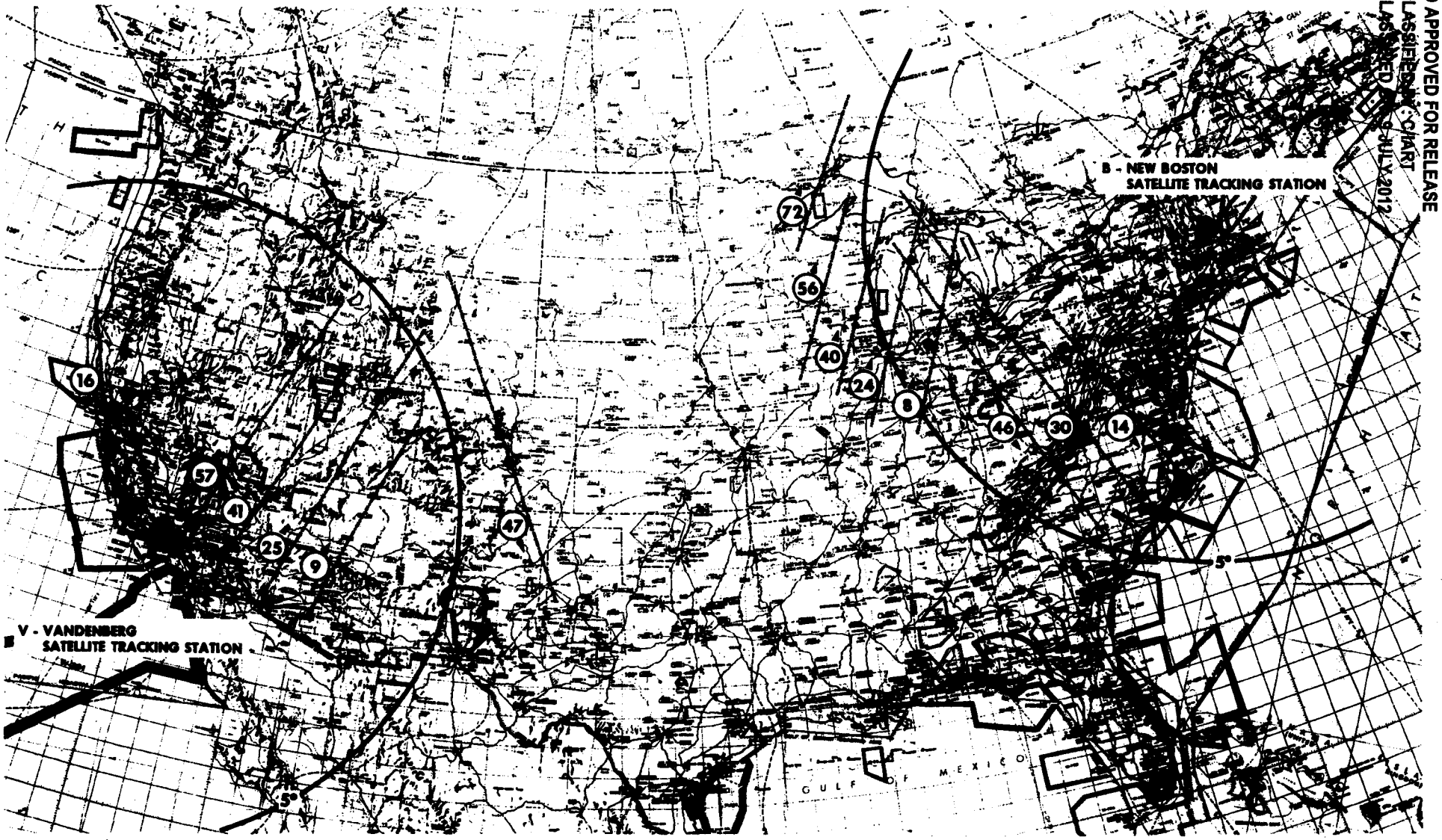

Figure 18 - Traces Depicting Radar Coverage of United States by The KP-II Radar, December 1964

This page intentionally left blank.

TABLE XI - STATUS OF RADAR FUNCTIONS

Pass no.	Automatic gain control	Fixed attenuator steps	Prf initial (at OPERATE on) step	Prf changes step	Clutterlock time constant	Clutterlock integrator output
8	Yes	None	14	13-12-11-10	TC No. 1	Normal
9	Yes	None	10	5-6-7-8-9	TC No. 1	Normal
14	Yes	None	10	9-8	TC No. 1	Normal
16	Yes	None	10	None	TC No. 1	Normal
24	Yes	None	11	10	TC No. 1	Normal
25	Yes	None	11	10-9	TC No. 1	Normal
30	Yes	None	8	9-8	TC No. 1	Normal
33	Recovery of Data Film					
40	App. 5 sec	2, 3	8	None	TC No. 1	Normal
41	No	4, 5, 4, 3, 0	9	None	TC No. 1	Normal
46	Yes	None	8	7-6	TC No. 1	Normal
47	Yes	None	6	All 7-15, 0-6	TC No. 1	Normal
56	Yes	None	6	7-8	TC No. 1 (approx 7 sec)	Shorted
57	Yes	None	9	8	TC No. 2	Normal
72	App. 36 sec	0, 7	8	7-6	TC No. 2	Normal

TABLE XII - MISSION TIME ANALYSIS

Active pass no.	Payload warm-up time (T_w) (min)	Payload pre-operate time (T_p) (min)	Operate (time (T_p) (min)	Total payload ($T_w + T_p + T_o$) cycle (min)	Time to next active pass (hr)
8	5.5	2.5	2.0	10.0	1.3
9	4.5	3.8	2.1	10.4	7.7
14	4.5	3.6	2.1	10.2	2.8
16	4.5	2.4	1.6	8.5	11.4
24	4.5	1.4	2.2	8.1	1.3
25	4.5	3.4	2.8	10.7	7.7
30	4.5	2.2	3.7	10.4	14.4
40	4.5	2.4	1.8	8.7	1.3
41	4.5	4.0	2.4	10.9	7.7
46	4.5	2.7	3.2	10.4	1.3
47	5.1	0.2	3.0	8.3	12.9
56	4.5	2.3	1.7	8.5	1.3
57	4.5	4.1	2.9	11.5	22.4
72	4.5	3.3	1.4	9.2	
Totals	64.6	38.3	32.9	135.8	93.5

Total payload cycle time ($T_w + T_p + T_o$) = 2.3 hr
Time from launch to pass 8 = 11.4 hr
Pass time = 93.5 hr

Total orbit time = 107.2 hr
(from launch to end of pass 72)

SECTION VII - ENVIRONMENTAL FLIGHT DATA

1. GENERAL

The various units of the KP-II radar system were instrumented so that component and unit characteristics could be monitored under the thermal and dynamic environments encountered during ascent and orbital conditions. Sensors were installed to measure unit and component temperature, vibration, shock, and pressure responses under the flight conditions.

Thermistors (Fenwal 918, 919, and General Electric DO 53) were used as the temperature sensors in the equipment. These resistive elements are used in circuits energized by the vehicle's 28.3-volt regulated power supply. Resistance of these thermistors is inversely proportional to the component temperature. The conditioned signal of the monitor circuit thus decreases as the body temperature increases, and vice versa. These sensors were mounted on particularly high heat dissipating or temperature sensitive components as well as on unit cases. Skin temperatures of the conical support and the cylindrical vehicle section were monitored. Temperatures on the cylindrical section were measured in the area of the Transmitter-Modulator and the Control unit.

Piezoelectric accelerometers were used to measure equipment dynamic response. These devices were used in conjunction with amplifiers for supplying conditioned signals to the telemetry subcarrier oscillators. The monitor system has a frequency response from 0 to 2000 cps and is capable of measuring acceleration levels up to 15 g (zero to peak). Accelerometers were mounted on the primary structure of the Transmitter-Modulator, R-F/I-F, and the Recorder units. These sensors were oriented in the vehicle longitudinal (X-X) direction.

Pressure sensors were installed in the vehicle payload compartment and in the equipment to measure in-flight pressures. Five Pirani gages were used, two sensors were placed in the vehicle payload compartment, and one sensor each in the Transmitter-Modulator, Recorder, and in the interconnecting wave guide between the Transmitter-Modulator and RF-IF. A complete list of the various

monitor sensors used to determine equipment environmental characteristics are given in Tables XIII, XIV, and XV.

Flight temperature, vibration, and pressure information was relayed to ground tracking stations by narrow band telemetry. Flight results and analyses of these results are presented in the following paragraphs.

2. FLIGHT TEMPERATURE DATA

a. General

Equipment temperatures were monitored during vehicle ascent and during each active (equipment operating) orbit. Temperature measurements were made primarily during the equipment OPERATE-ON mode although temperature data were also obtained before and after the active phase of several orbits. Temperature data taken before the OPERATE-ON mode included data from the payload WARM UP and PRE-OPERATE modes. Most components contained within the various units, with the exception of the Transmitter-Modulator, utilized full power during both the PRE-OPERATE and OPERATE-ON modes.

b. Ascent Heating

Aerodynamic heating occurring during ascent resulted in slight heating of the radar equipment. From an initial temperature of 55-60 degrees F (precooled on launch pad) the unit temperatures specified in Table XVI were experienced.

The Recorder unit located in the vehicle conical section (estimated maximum average skin temperature - 460 degrees F) reached the highest temperature. This maximum temperature occurred approximately 2800 seconds after lift-off. The Transmitter-Modulator and the R-F/I-F units located in the vehicle cylindrical section reached their maximum temperatures approximately 4000 seconds after lift-off. The maximum recorded ascent temperature of the Reference Computer and Control units occurred at 5400 seconds after lift-off and was probably still increasing

TABLE XIII - FLIGHT INSTRUMENTATION: TEMPERATURE MONITORS

Unit	Telemetry number	Locations
Control	F20	Power supply
	F21	Unit case
Reference Computer	F22	Video amplifier
	F23	Gate sequencer
	F24	Sine x/x pulser
	F25	Timer A
	F26	Audio synchronizer demodulator
	F27	Unit case
Recorder	F28	Deflection amplifier
	F29	High-voltage power supply
	F30	Unit case
RF-IF	F31	Traveling wave tube (twt)
	F32	Frequency multiplier
	F33	Transmit-receive tube (t-r tube)
Transmitter-Modulator	F34	Klystron collector
	F35	Klystron body
	F36	Unit case
	F37	Pulse transformer

TABLE XIV - FLIGHT INSTRUMENTATION: VIBRATION MONITOR

Unit	Telemetry number	Locations
Recorder	F83	Primary structure - Longitudinal axis
RF-IF	F84	Primary structure - Longitudinal axis
Transmitter-Modulator	F86	Primary structure - Longitudinal axis

TABLE XV - FLIGHT INSTRUMENTATION: PRESSURE MONITOR

Telemetry number	Pressure monitored
F100	Vehicle payload compartment
F101	Vehicle payload compartment
F102	Recorder unit - Internal
F103	Transmitter-Modulator unit - Internal
F104	Wave guide between the Transmitter-Modulator and the R-F/I-F units

TABLE XVI - UNIT TEMPERATURES DURING ASCENT

Unit	Temperature 5400 seconds after lift-off (F)	Maximum ascent temperature (F)
Transmitter-Modulator	80	86
RF-IF	85	93
Reference Computer	75	75
Control	80	80
Recorder	92	98

slightly. This condition occurs because of the unit geometry and location and local vehicle skin condition.

c. Orbital Temperature Data

A summary of unit and component orbital temperature data is presented in Figures 19 through 24. Figure 19 shows typical temperature cycles of two components. One component is energized during both the PRE-OPERATE and the OPERATE-ON modes, and the other component dissipates power primarily during the OPERATE-ON mode. Component cooling is shown for 1260 seconds after the operate-off command.

The orbital heating characteristics for the Transmitter-Modulator, R-F/I-F, Reference Computer, Control, and Recorder units are given in Figures 20 through 24. These plots show the component temperature rise during the OPERATE-ON mode for each active orbit. It is noted that three temperature monitors – F24, F25, F26 – are not plotted. These thermistors, located within the Reference Computer unit, indicated a maximum orbital temperature of 91 degrees F with cyclic variations similar to other monitors within the Reference Computer unit (F22 and F23).

No temperature response curve is presented for the klystron collector (Transmitter-Modulator, F34). The temperature sensor for this component was calibrated over the temperature range 350-575 degrees F. Conditioned signal data indicated that the klystron collector temperature was below the 350 degree F calibration minimum during all operating phases. No information on temperature variation with time was obtained.

In analyzing temperature data, a slight temperature drop was found to occur when the equipment was energized. This abnormal temperature variation is believed to be caused by a decrease in voltage output of the regulated 28.3-vdc power supply during the equipment operating modes. This is the voltage source for the temperature monitoring circuits and thus temperature compensation was required. Temperature data were normalized accordingly.

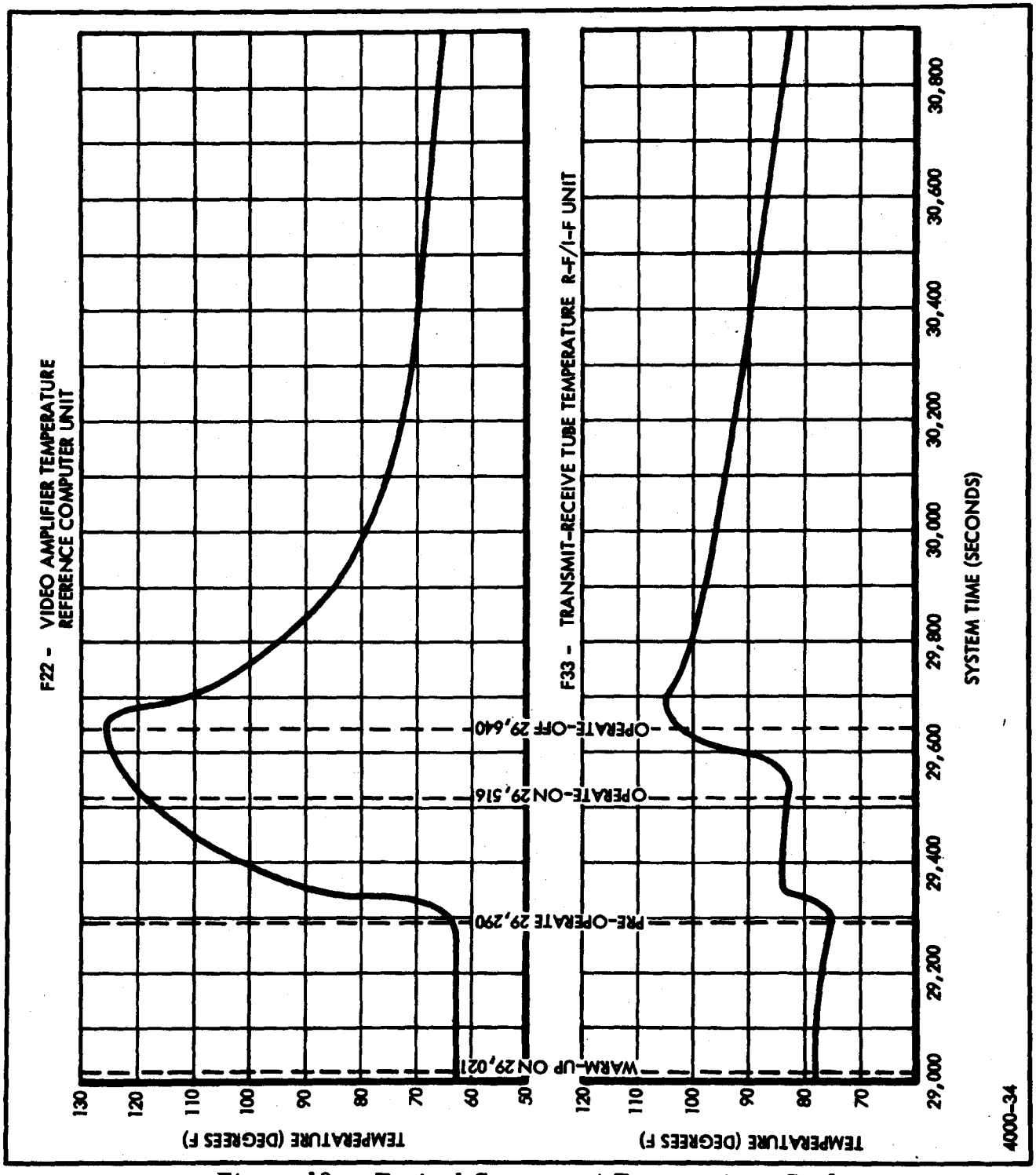

Figure 19 - Typical Component Temperature Cycle

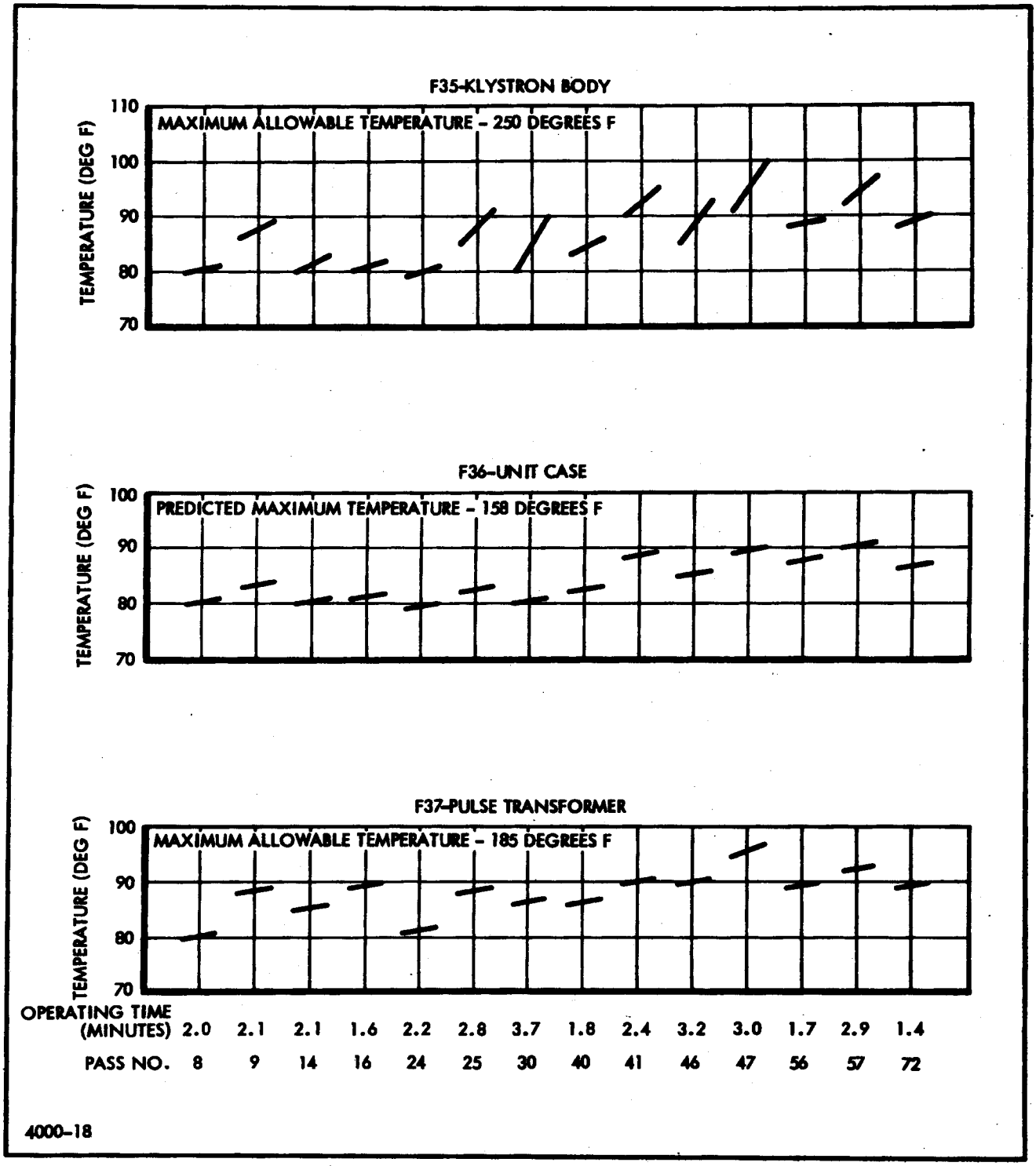

Figure 20 - Orbital Temperature History - Transmitter-Modulator Unit

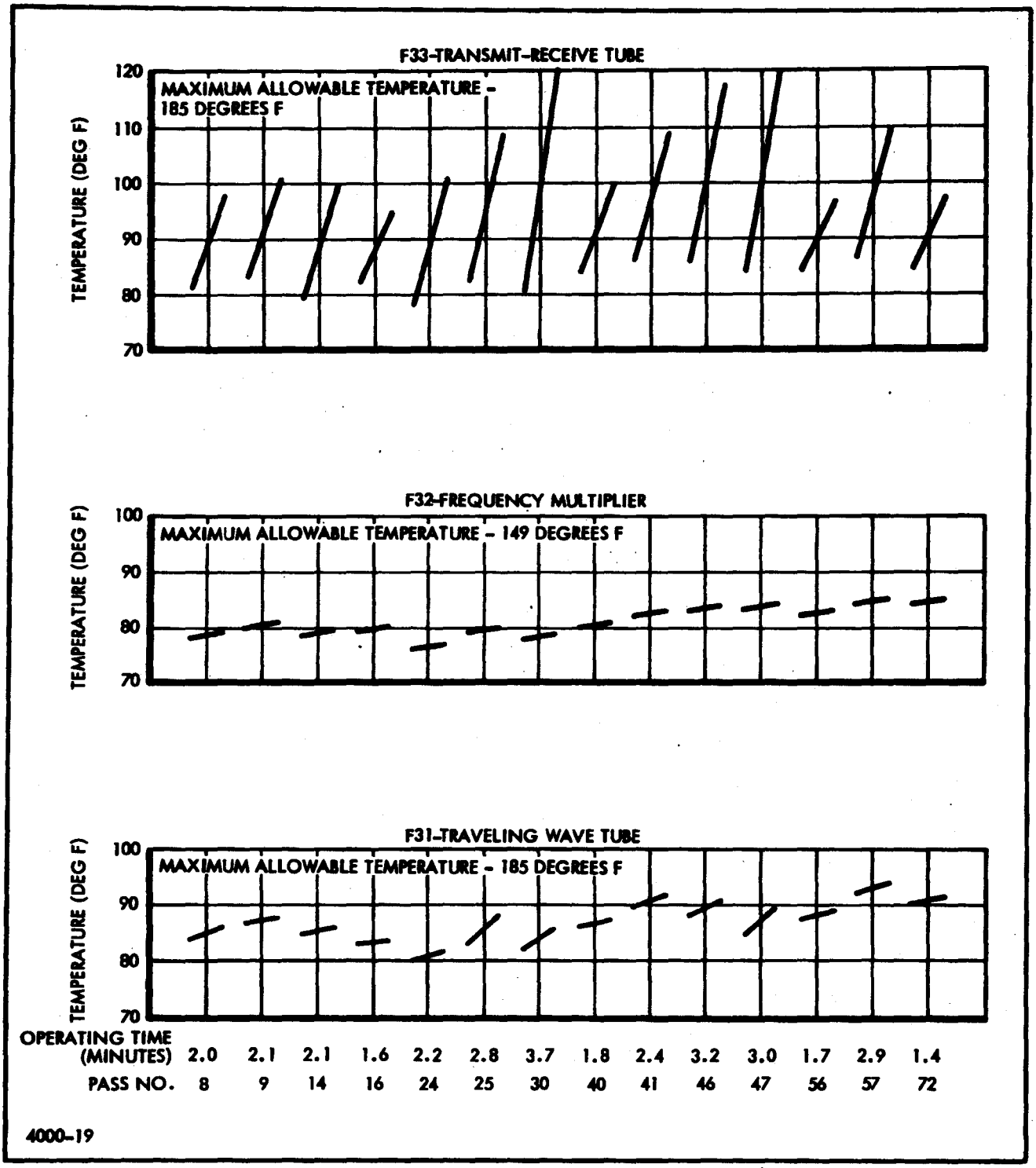

Figure 21 - Orbital Temperature History - R-F/I-F Unit

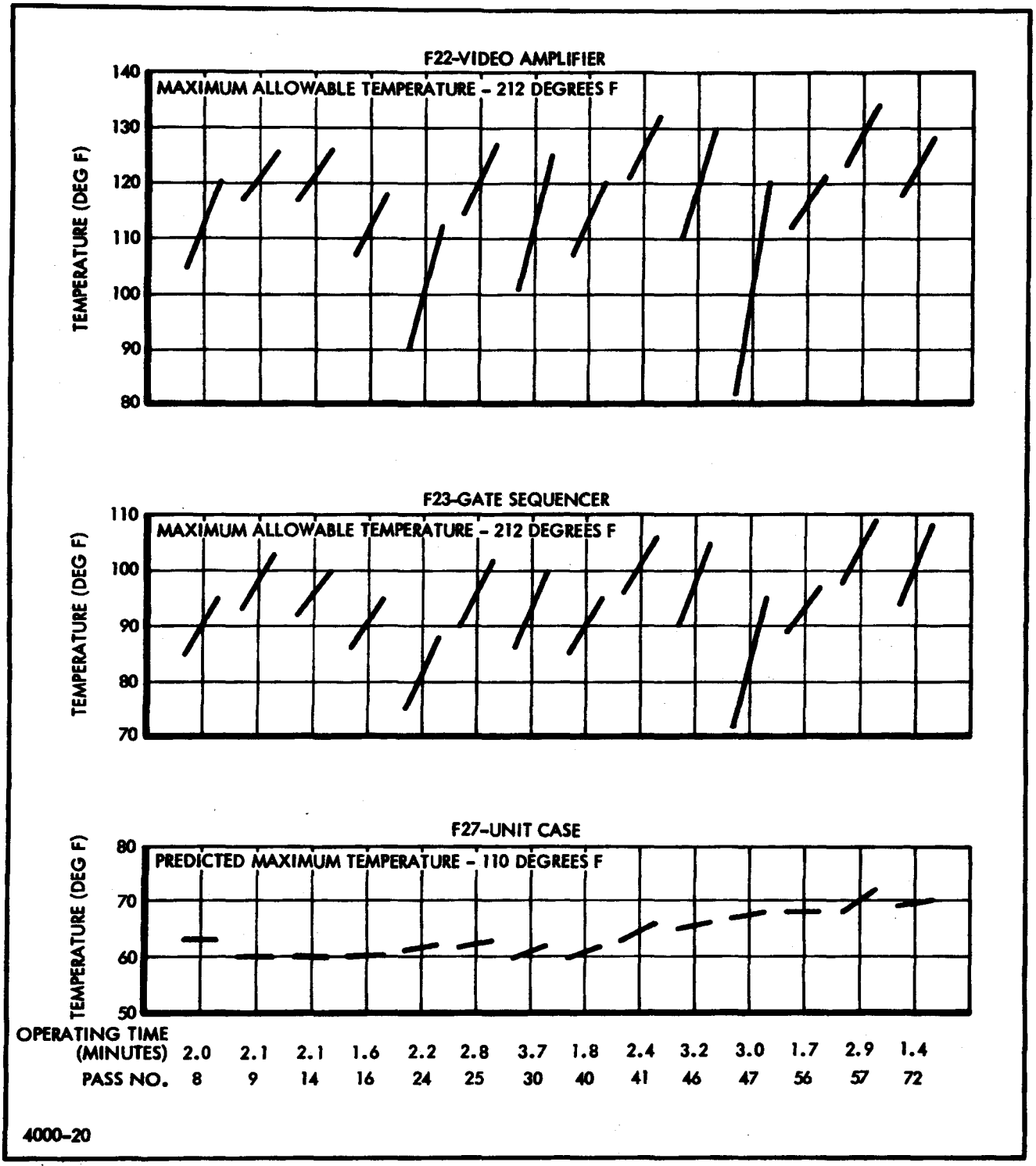

Figure 22 - Orbital Temperature History - Reference Computer Unit

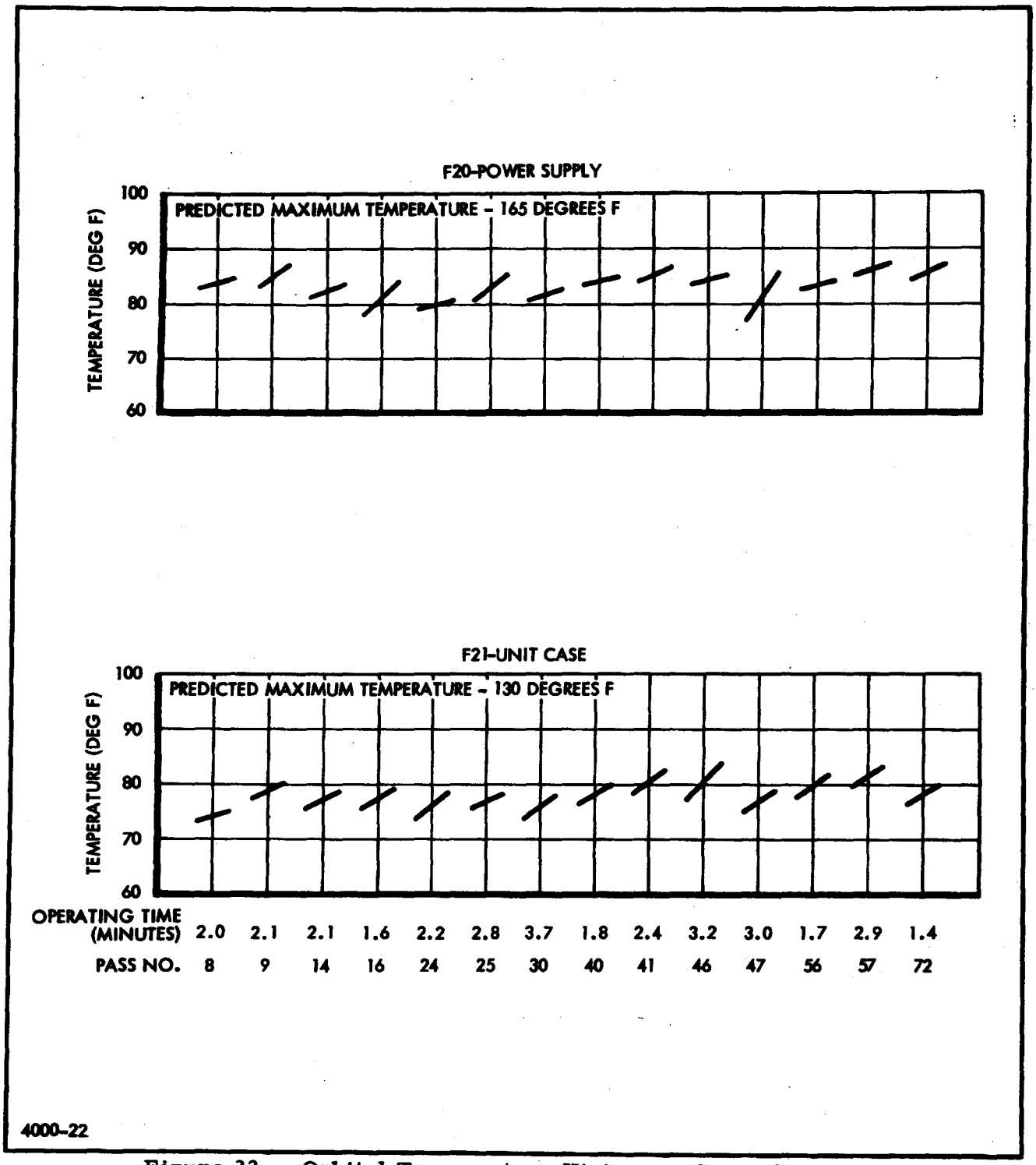

Figure 23 - Orbital Temperature History - Control Unit

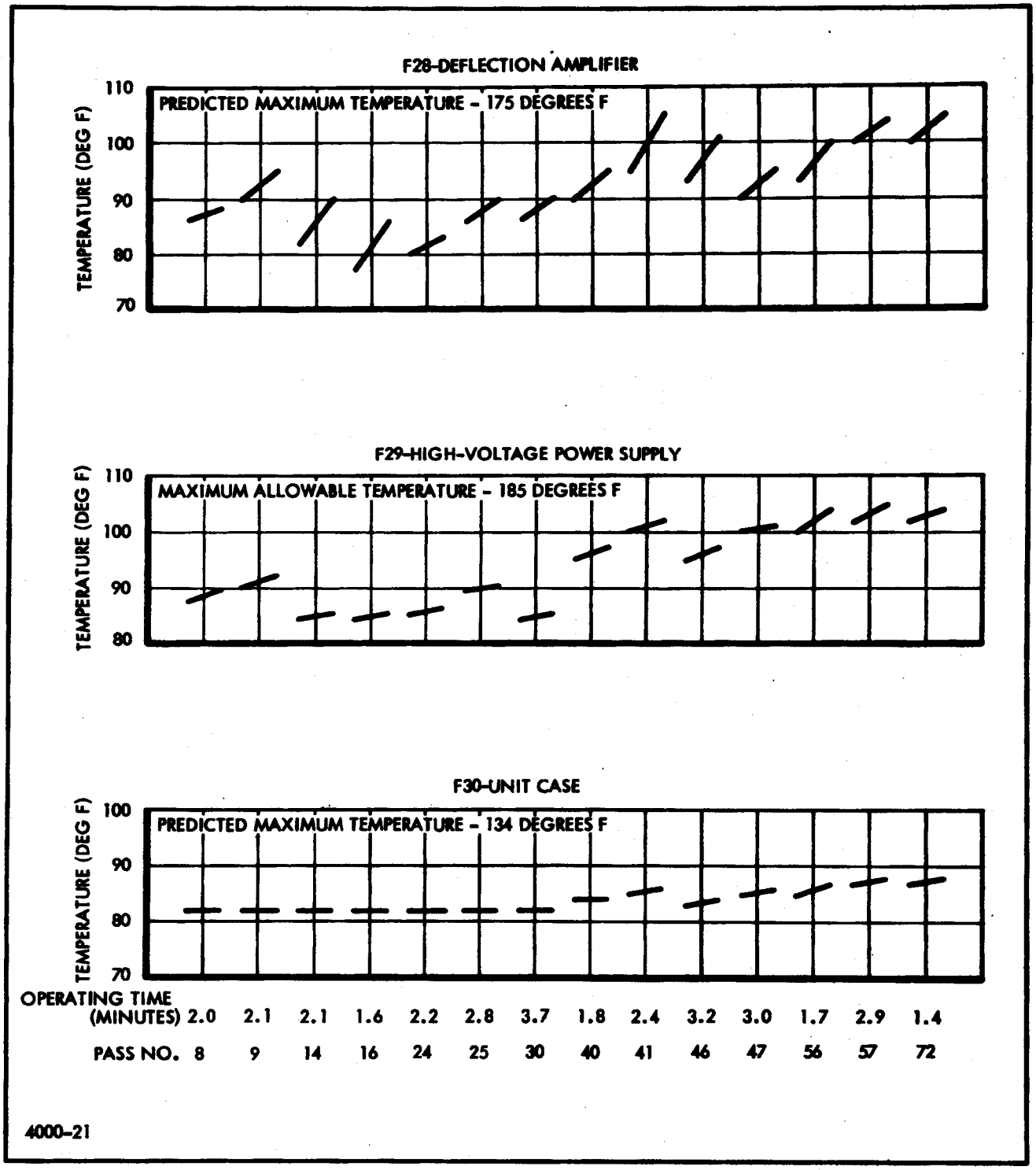

Figure 24 - Orbital Temperature History - Recorder Unit

Examination of flight temperature data indicates that the equipment remained well within predicted and allowable maximum temperature limits. Temperature history data show normal accumulation of heat and a gradual heating trend.

Variations in the orbital operating temperature data and apparent inconsistencies in the temperatures experienced at the start of the various cycles are explained somewhat by considering the effect of the pre-operate mode on the equipment thermal response. Figure 19 showed that components experience the greatest rate of heating shortly after being energized. Furthermore, components in Figures 21 through 24, with the exception of the t-r tube, are fully energized during the pre-operate mode. Therefore, the temperature at the start of a particular orbital operating cycle (operate-on mode) and the rate of heating (temperature slope) is directly dependent upon the length of the pre-operate condition. A comparatively short pre-operate period results in a lower initial temperature as well as a steeper temperature slope.

3. FLIGHT VIBRATION AND SHOCK DATA

Vibration and shock response of the equipment was monitored during vehicle launch and ascent for approximately 330 seconds. Satisfactory data were received via the telemetry link from sensors in the R-F/I-F and Recorder units. No meaningful data were obtained from the monitor in the Transmitter-Modulator. It was determined that this accelerometer was not functioning properly during prelaunch checkout. No repair or replacement was effected.

A summary of the vibration and shock data for the R-F/I-F and Recorder units is presented in Table XVII. Vibration or shock levels, duration and frequency characteristics, where applicable, are given for various stages of vehicle ascent.

Both shock and vibration responses were measured during ascent. The vibration spectrum encountered was, in general, complex. It was not possible to determine the frequency components of a particular response spectrum in most

TABLE XVII - FLIGHT VIBRATION AND SHOCK DATA

System time	Function	Recorder Response			R-F/I-F Unit Response		
		Level (g's)*	Duration (sec)	Remarks	Level (g's)*	Duration (sec)	Remarks
68935.62	Lift-off	6	3.5	±3 g, 15 cps sine with high frequency vibration, ±3 g superimposed	2	3.5	±2 g, 15 cps sine with high frequency vibration, ±1.5 g superimposed
68951.22	0.54 Mach number	7 (max)	6	High frequency vibration. Random amplitude	2(max)	6	High frequency vibration
68959 to 68963.3		2.5 (max)	–	High frequency vibration. Random amplitude	0.5 to 0.75	–	High frequency vibration
68963.3 to 69001.1		1	–	High frequency vibration. Random amplitude	Negligible response		
69001.1	Booster separation	Negligible response			Negligible response		
69072 to 69086.5		2	–	20 cps, sine	2	–	20 cps, sine
69086.5	Main engine cut-off	6	0.2	Shock pulse, triangular	6	0.2	Shock pulse, triangular
69095.4	Vernier engine cut-off	4	0.1	Decaying vibratory burst. Decay time: 0.1 sec	1	0.1	Decaying vibratory burst. Decay time: 0.1 sec

* Zero-to-peak acceleration

TABLE XVII - FLIGHT VIBRATION AND SHOCK DATA (Continued)

System time	Function	Recorder Response			R-F/I-F Unit Response		
		Level (g's)*	Duration (sec)	Remarks	Level (g's)*	Duration (sec)	Remarks
69101.1	Agena separation	6	0.1	Decaying vibratory burst. Decay time: 0.1 sec	3	0.1	Decaying vibratory burst. Decay time: 0.1 sec
69105.3	Fairing separation	6	0.08	Decaying vibratory burst	1.5	0.08	Decaying vibratory burst
69115.3	Ulage rocket firing	0.5	0.5	Vibration: 60 cps	0.5	0.5	Vibration: 60 cps
69128.5	Agena burn	2	0.5	Decaying shock	1.5	0.5	Decaying shock
69368.7	Agena engine cut-off	9	–	Decaying shock. First pulse duration approx 0.016 sec Decay time: 0.15 sec	7	–	Decaying shock. First pulse duration approx 0.014 sec Decay time: 0.15 sec

* Zero-to-peak acceleration

cases. Vibration amplitude (acceleration level) also varied considerably (random amplitude) for a particular response. Values given in the summary are the maximum values that occurred. Vibration response between the listed times was small and of little consequence. Most equipment vibration occurred within 60 seconds of lift-off. Maximum vibratory acceleration levels were reached at lift-off and during the transonic range of vehicle ascent. Several shock pulses and short bursts of decaying (highly damped) vibration (probably shock induced) were encountered at various other stages of vehicle ascent.

Comparison of vibration levels encountered in the Recorder and R-F/I-F units (assuming comparable vehicle input to the two units) shows the effectiveness of the isolation system used on the R-F/I-F unit. As a result of this system, the high frequency vibration response of the R-F/I-F unit was 50 to 80 percent less than the acceleration levels encountered in the hard-mounted Recorder unit.

The equipment was designed and qualified to more stringent environmental requirements than those encountered during vehicle ascent. The ascent vibration levels, although somewhat comparable to design requirements, were of such short duration that the occurrence of equipment damage is extremely unlikely. Relatively high vibratory acceleration levels occur for only 4 to 6 seconds during ascent as compared to the qualification test duration of 3 minutes per vibration frequency octave. Shock levels were also well below design criteria.

4. FLIGHT PRESSURE DATA

Pressure information obtained under flight conditions was extremely limited. No meaningful orbital pressure data were obtained. The Pirani vacuum gages used to monitor pressure have an operating range from 2 to 100 microns. These gages proved to be inadequate for this application. Conditioned signals from all sensors indicated that the pressure went below the calibrated range. Off-scale readings occurred at the times listed in Table XVIII.

TABLE XVIII - FLIGHT PRESSURE DATA

Telemetry number	Time of off-scale reading
F100	300 seconds after lift-off
F101	300 seconds after lift-off
F102	Between pass no. 2 and pass no. 8
F103	300 seconds after lift-off
F104	3600 seconds after lift-off

SECTION VIII - UNIT FLIGHT TEST ANALYSIS

1. GENERAL

This section analyzes the flight performance of each of the five units of the radar set. The analyses were performed by studying the telemetered signals. Each of the telemetered signals from the radar was examined and the signals which were most indicative of the status of the units are discussed in detail in the subsequent paragraphs.

2. TRANSMITTER-MODULATOR

a. General

The conditioned signals furnished for telemetering by the Transmitter-Modulator unit are listed in Table XIX.

TABLE XIX - TRANSMITTER-MODULATOR CONDITIONED SIGNALS

F-number	Signal
F13	Klystron filament voltage
F14	High-voltage supply
F16	Inverse current
F17	Klystron wave form
F56	Operate Transmitter-Modulator

Two other signals, the F72 input to the Transmitter-Modulator and the F73 output from the Transmitter-Modulator, indicate the input and output power levels and are furnished by the R-F/I-F unit.

From these signals, the klystron filament voltage, high-voltage supply, input to Transmitter-Modulator, and output from Transmitter-Modulator, have been chosen for discussion and are plotted in Figure 25. The klystron

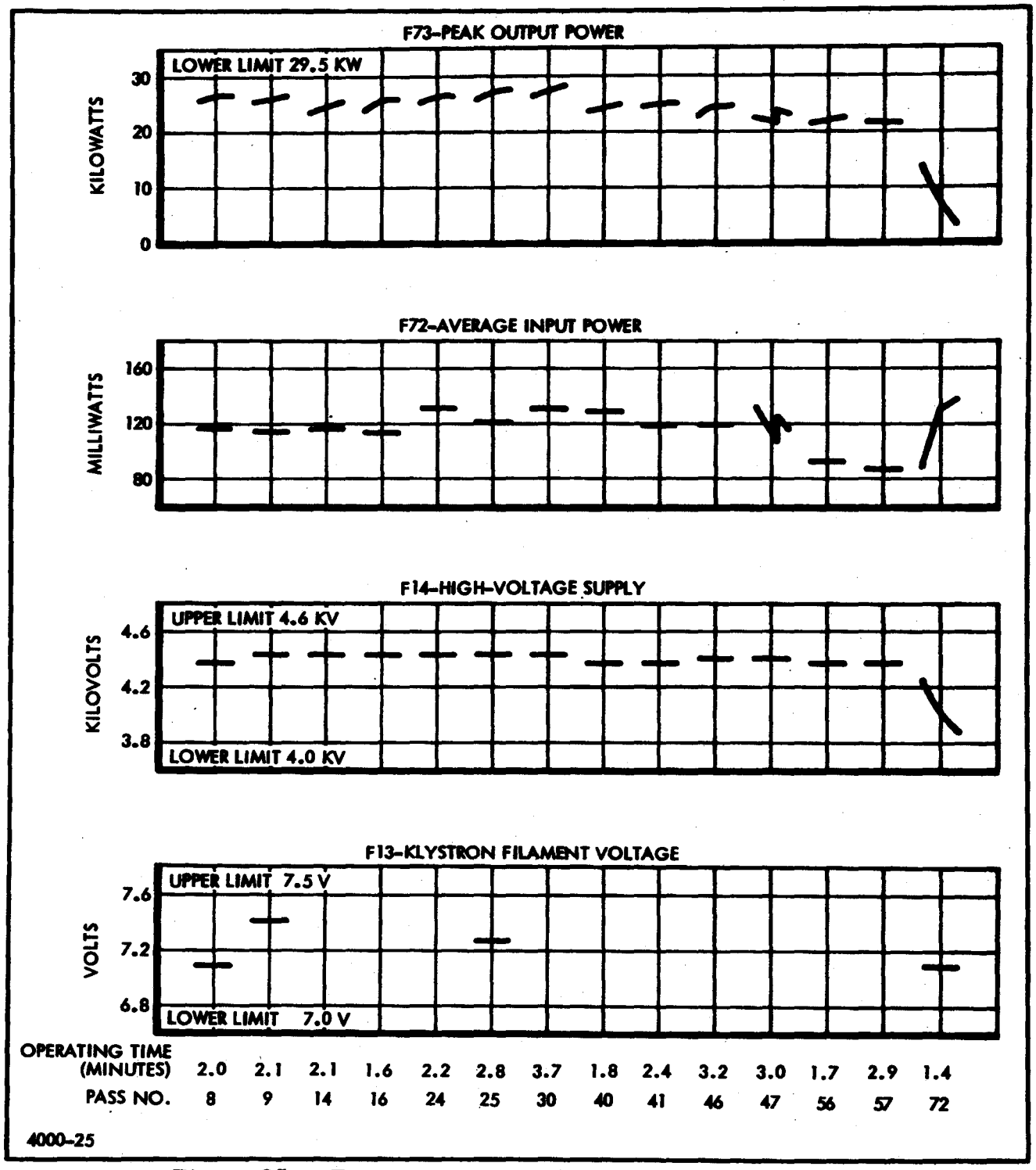

Figure 25 - Transmitter-Modulator Unit Monitor Signals

wave form and inverse current signals, although useful for trouble shooting, are not discussed as the unit behaved normally. The operate Transmitter-Modulator signal indicates the status of certain control signals in the unit.

b. F13 - Klystron Filament Voltage

The klystron filament voltage data were furnished for only four passes. The plot shows that the klystron filament voltage was within the prescribed limits of 7 to 7.5 volts.

c. F14 - Transmitter-Modulator High-Voltage Supply

The Transmitter-Modulator high-voltage supply plot shows that the supply voltage was well within the limits of 4 to 4.6 kv except for the last pass. The supply voltage decreased rapidly on the last pass because of the battery voltage falling below the regulating range of the high-voltage power supply.

The Transmitter-Modulator high-voltage supply reached the operating level approximately ten seconds after the operate command was given.

d. Transmitter-Modulator Average Input Power

The r-f drive power furnished to the Transmitter-Modulator unit by the R-F/I-F unit is adjustable at the R-F/I-F unit. The r-f drive power is normally set to a value just below saturation for each klystron. The value of the r-f drive power required by the klystron varies with each individual tube. As delineated in Section V, paragraph 8.b., and in paragraph e. following, the klystron drive power was set slightly below the level required for the particular klystron used in the flight Transmitter-Modulator.

On pass 47 the average input power decreased linearly, then rose abruptly and decreased again. This behavior was caused by the changes in prf during the pass, as average power varies directly with prf. The pass started with prf step 6 (8519 cps) and was decreased in consecutive steps to prf step 15 (8215 cps), which accounts for the linear decrease in average

power. The prf was then changed from step 15 to step 0 (8215 to 8735 cps), which accounts for the sudden increase in average power. The prf was again decreased in consecutive steps to step 6, which accounts for the decrease in average power after the jump. Changes in average power on other passes where the prf was varied were not as readily discernible as on pass 47 where the prf was varied through the entire range.

On pass 72 there was an apparent increase in the average input power to the klystron; however, since the vehicle batteries were low and the telemetry link was not functioning properly, this is believed to be an incorrect indication.

e. F73 - Transmitter-Modulator Peak Output Power

The Transmitter-Modulator peak output power data were corrected to incorporate the final test measurement before launch. The final test measurement was 74.2 dbm which corresponded to a conditioned signal of 1.32 volts hardline and 1.29 volts telemetering. This measurement was taken as a calibration point, and the received data were corrected by adding 0.3 db. The calibration point represents a peak power of 26.5 kilowatts. This is below the system specification minimum value of 29.5 kilowatts because of insufficient drive power (refer to preceding paragraph d.). The data plotted also take into account the r-f pulse width and the prf. The pulse width measured at the 70 percent point was 0.9 microsecond and was assumed constant. The prf for the plotted power points was taken from the operating log.

The telemetered power data are basically in terms of average power. The average power reading automatically reflects any changes occurring in klystron beam voltage (amplitude and pulse width), filament voltage, r-f drive, and prf. The peak output power would be expected to remain constant provided that the klystron beam voltage, filament voltage, and r-f drive remained constant. As can be seen from the data plotted in Figure 25 the klystron filament voltage, r-f drive power, and high-voltage

supply were not the same for each pass. Consequently, some variation in peak power is expected from pass to pass. It could be assumed that if the factors mentioned above were constant during the pass that the peak power should remain constant. However, the received data showed a slight tendency for the power to increase from the beginning to the end of the pass because of a slight tendency towards an increase in power as the klystron warms up to operating temperature.

It was considered desirable to present the output power data in terms of peak power. This was obtained from the relation,

$$P_p = \frac{P_{av}}{PW \times PRF} \tag{13}$$

where

P_p = Peak output power

P_{av} = Average output power

PW = R-f pulse width at 70 percent amplitude

PRF = Pulse repetition frequency.

The high-voltage supply reached the normal operating level approximately 10 seconds after the operate command was given. In the data plot, the first point for each pass was taken at approximately 20 seconds after the operate command was given.

The plot shows that the peak power decreased from pass 40 to pass 72. The decrease corresponds somewhat with the lower high-voltage supply for these passes. In passes 56 and 57 the input power was slightly below average. Pass 47 shows the effect of the prf change discussed in paragraph c.

On pass 72 the output power started low and dropped off rapidly during the pass. This corresponds quite well with the drop off in high-voltage supply during the pass.

3. RF-IF

a. General

The conditioned signals which are monitored in the R-F/I-F unit are listed in Table XX.

TABLE XX - R-F/I-F CONDITIONED SIGNALS

F-number	Signal
F11	High-voltage supply monitor
F53	Gain control monitor
F72	R-f power to Transmitter
F73	R-f power from Transmitter
F74	Twt pulse monitor
F75	100-Mc output power monitor.

Of the above signals, F11 high-voltage supply, F72 r-f power to Transmitter, F74 twt pulse, and F75 100-mc output power are discussed in detail in the following paragraphs and plotted in Figure 26. F53, gain control, is discussed in Section IX: System Flight Test Analysis. F73 was fully discussed under the Transmitter-Modulator, paragraph 2. e.

b. F11 - R-F/I-F High-Voltage Supply Monitor

The 2000-vdc R-F/I-F high-voltage telemetered plot shows that the high voltage was very near the required twt cathode voltage of 1975 vdc during each of the fourteen passes. The voltage remained well within the specified operating limits for stable twt amplification. Telemetered data

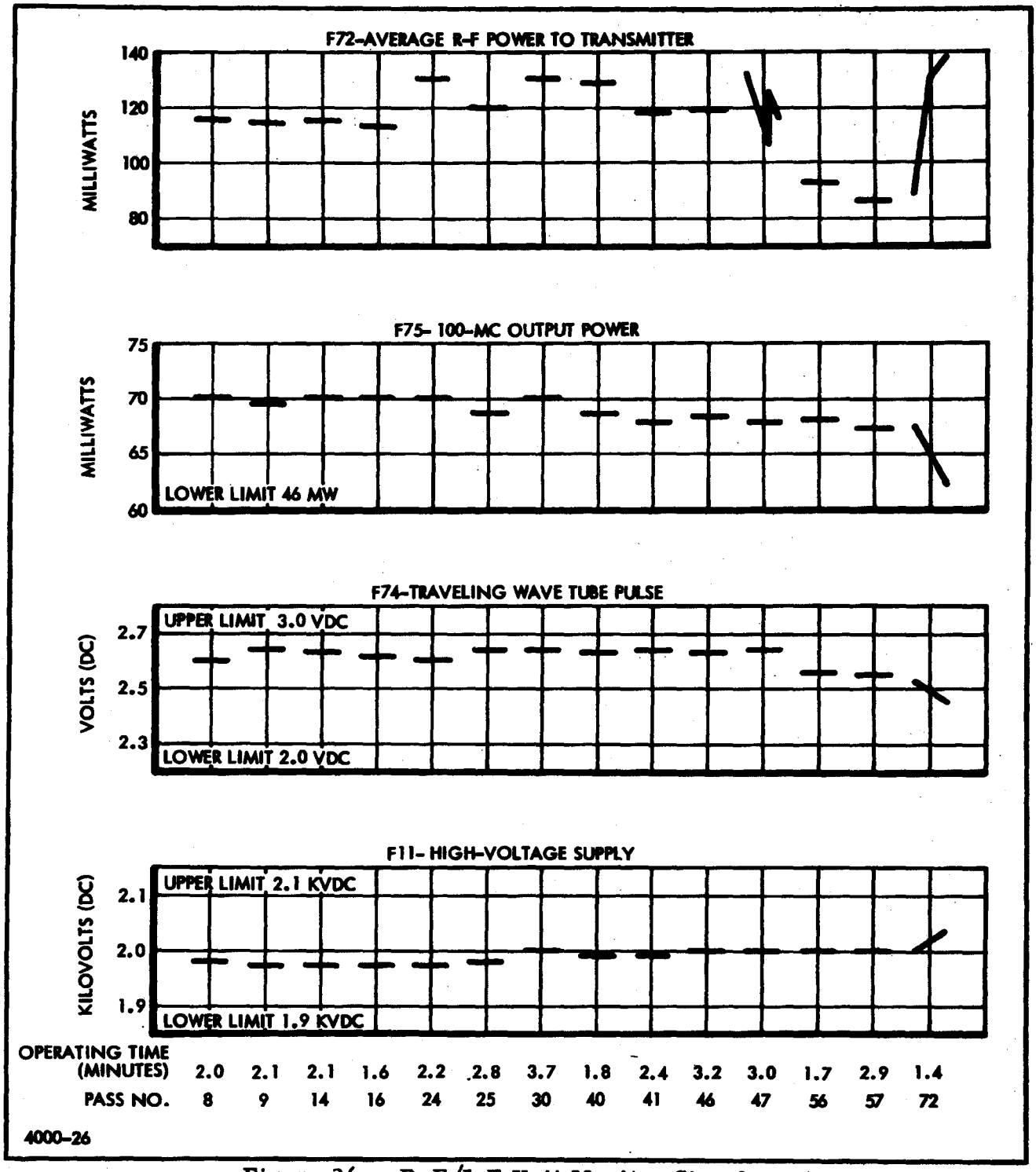

Figure 26 - R-F/I-F Unit Monitor Signals

indicate that the high voltage increased approximately 40 volts during the final operating pass. However, this apparent increase in high voltage was caused by a decrease in the +23.5 vdc connected to the high-voltage monitoring circuit and does not represent a true increase in high voltage. Therefore, as the high-voltage power supply apparently did not drop out of regulation because of the decreased 115 vac, it can be assumed that the output voltage of the high-voltage power supply remained essentially constant throughout the final operating pass.

c. F74 - Twt Pulse Monitor

The telemetered twt pulse data show that the twt pulse remained relatively constant during the entire life of the system and was well within the specified operating limits. The different operating levels are caused by changes in the prf and variations in the telemetering link. The decrease in the operating level during the final pass was caused by a decrease in the +23.5 vdc supply and indicates the general decaying condition of the vehicle batteries.

d. F75 - 100-Mc Oscillator Output Power Monitor

The curve for the average output power of the 100-mc oscillator (see Figure 26) demonstrates that the 100-mc output level remained well above the 46-mw input power level required for satisfactory frequency multiplier operation. The decrease in 100-mc output power during the final pass was caused by low 23.5-vdc inverter supply output voltages and again indicates the low charge level of the vehicle batteries.

e. F72 - R-f Power to Transmitter Monitor

The average output power of the R-F/I-F unit (Transmitter-Modulator input power) was slightly below the calculated system specification value. As previously delineated in paragraph 2: Transmitter-Modulator, the klystron input drive level is adjusted by a variable attenuator in the R-F/I-F unit. This adjustment is made at the system level and varies

for each individual klystron. Although the R-F/I-F unit has a much greater capability, the output power of the flight unit was set slightly below the required drive level of the klystron (see Figures 25 and 26). This condition was known prior to lift-off and resulted from the decision not to remove the R-F/I-F unit covers and re-adjust the klystron input drive power when a new Transmitter-Modulator unit was installed in the flight vehicle.

4. REFERENCE COMPUTER

The conditioned signals monitored in the Reference Computer are listed in Table XXI.

TABLE XXI - REFERENCE COMPUTER CONDITIONED SIGNALS

F-number	Signal
F46	Clutterlock relay
F47	BIT relay
F48	Clutterlock time constant no. 1
F60	Integrator output
F61	Agc
F62	70-mc reference
F63	70-mc offset reference
F64	70-mc single side band
F65	Sweep trigger
F66	0.06-microsecond 70-mc pulse
F67	140-mc pulse
F68	On-Gate

Of the above signals, three have been selected as being indicative of the status of the unit: F62 70-mc reference, F64 70-mc single side band, and F66 0.06-microsecond 70-mc pulse. These signals are plotted in Figure 27. Each signal remained essentially constant throughout the flight. On pass 72, slight variations occurred because of changes in the +23.5 vdc reference and the variations in the telemetry signals. The outputs, however, are still within the established limits of operation.

The remaining signals were analyzed but are not plotted. The first three – F46, F47 and F48 – are relay position monitors. The relays behaved normally during the flight. The next two signals, F60 and F61, are discussed in detail in Section IX. The remaining signals, F63, F65, F67, and F68, held constant within their prescribed limits.

5. CONTROL UNIT

a. General

The signals available for analysis from the control unit are listed in Table XXII.

TABLE XXII - CONTROL UNIT CONDITIONED SIGNALS

F-number	Signal
F1	+23.5 vdc
F3	-23.5 vdc
F4	+300 vdc
F5	+28.3 vdc
F7	115 v 400 cps Phase AB
F8	115 v 400 cps Phase CB
F9	115 v 2 kc
F11	Pre-operate monitor
F12	Transmitter-Modulator timer override monitor

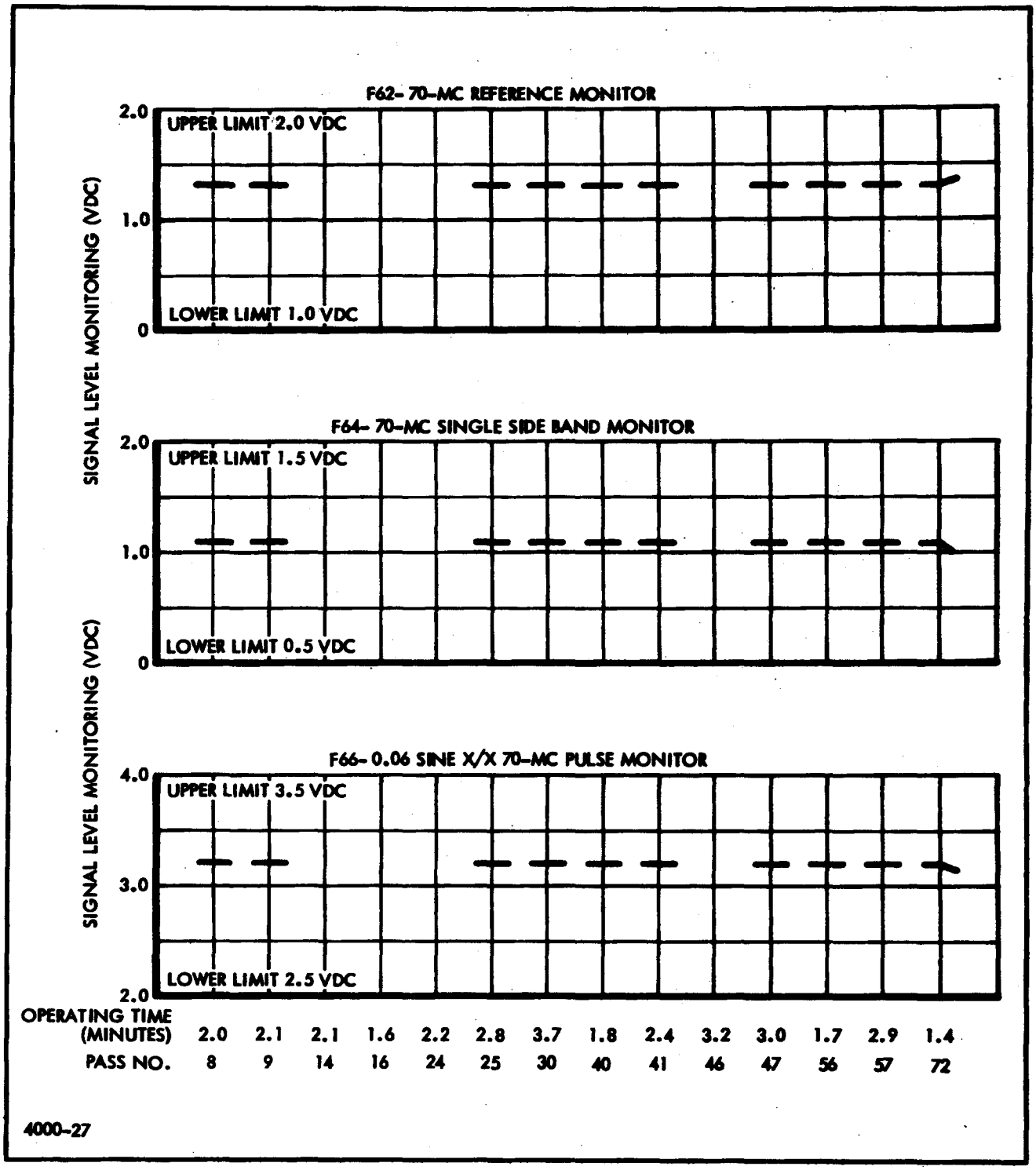

Figure 27 - Reference Computer Unit Monitor Signals

From these signals, F1 +23.5 vdc, F3 -23.5 vdc, and F4 +300 vdc, have been chosen as output signals which show the status of the unit. In addition, F5 +28.3 vdc, F7 115 v 400 cps Phase AB, and F8 115 v 400 cps Phase CB, are included in the analysis since they show the condition of the primary power input.

b. Power Supply Output Voltages F1, F3, and F4

A study of the variations in the telemetered outputs from the Control unit regulated power supplies reveals that each voltage output (+23.5 vdc, -23.5 vdc, and +300 vdc) turned on for each orbit at pre-operate within the ±1 percent regulation specified (see Figure 28). When the radar was switched into operate, however, a jump in each of these voltages was indicated and for some orbits the indicated values were outside of the ±1 percent regulation limits. Since the normal performance of these supplies within their regulating range is well within the specification, and since the load presented to these supplies does not change appreciably when switched to operate, these variations are believed to be caused by variations in the telemetry link.

c. Primary Voltage Inputs F5, F7, and F8

One exception to the above analysis occurred during pass 72. Figure 29 shows the variation of the input voltages. During pass 72 each of the input voltages fell off sharply indicating the end of battery life. During this pass the primary voltages, and also the Control unit power supplies, went out of regulation as the battery voltage went down.

The conclusion reached from the indicated telemetry data during the pre-operate mode, and from the quality of the data during each operating mode, is that the Control unit operated within specifications for all orbits.

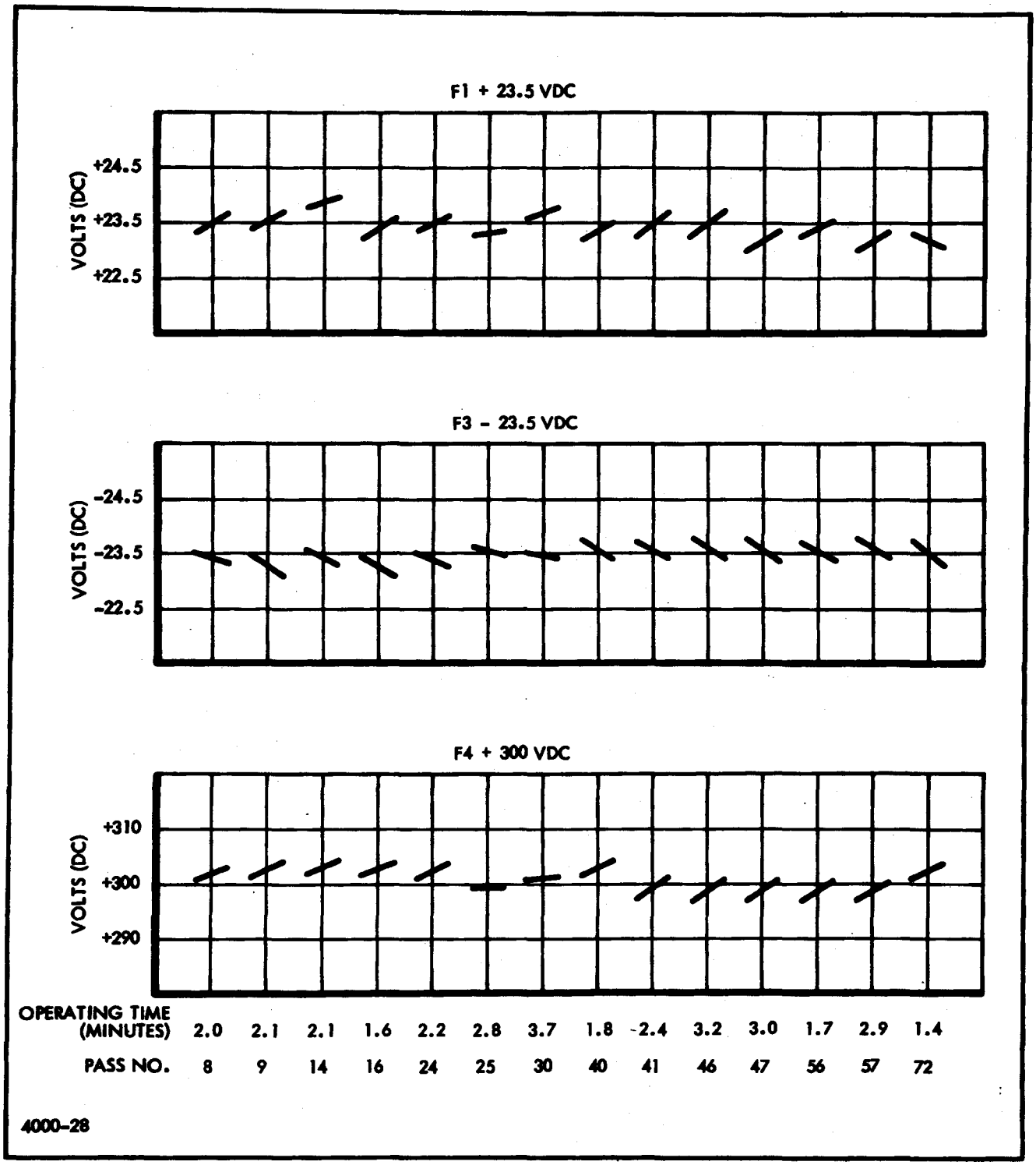

Figure 28 - Control Unit Regulated Voltages Monitor Signals

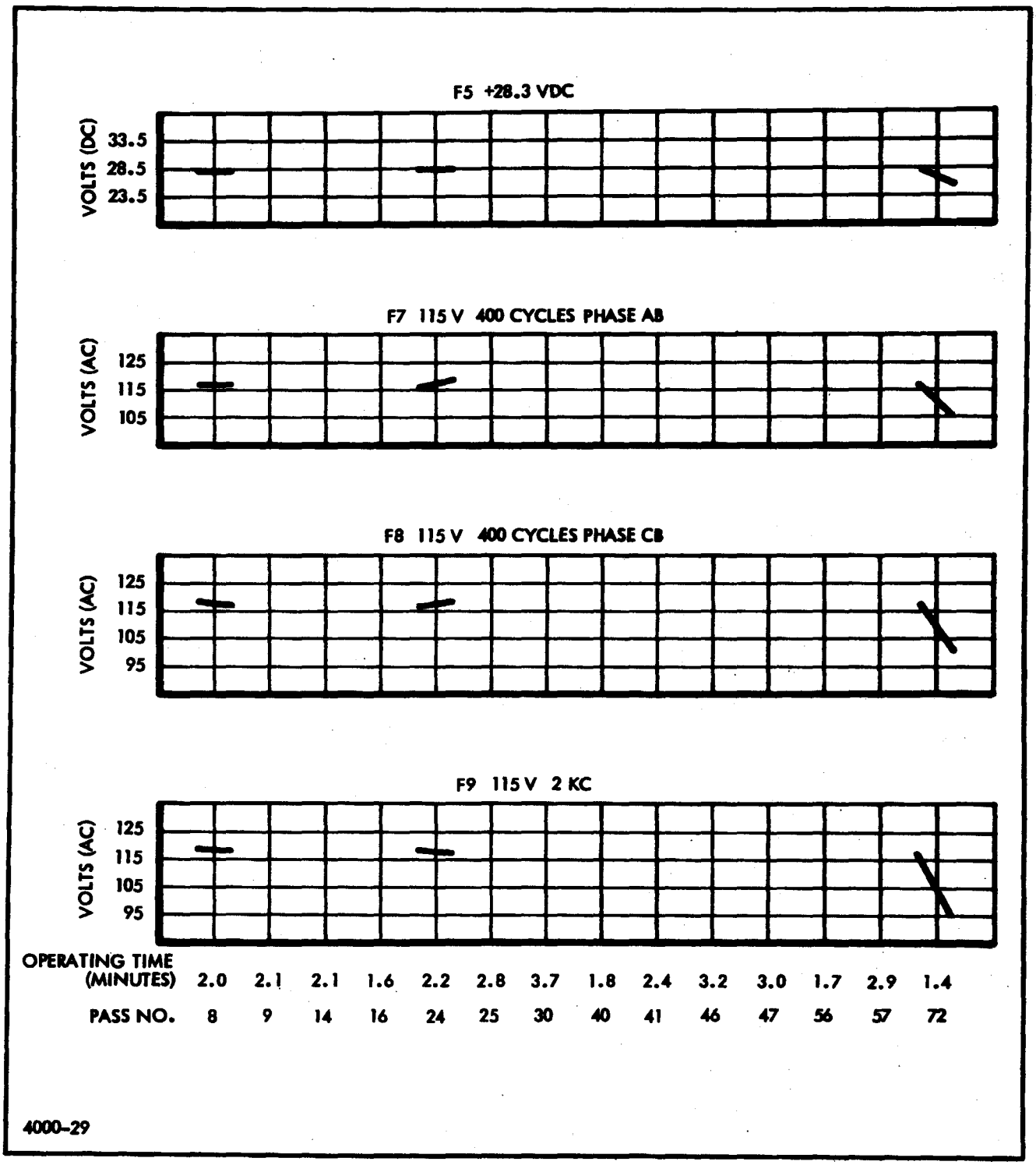

Figure 29 - Control Unit Primary Power Monitor Signals

6. RECORDER

a. General

The Recorder unit furnished the conditioned signals listed in Table XXIII for telemetering.

TABLE XXIII - RECORDER CONDITIONED SIGNALS

F-number	Signal
F10	10-kv supply
F18	Deflection current
F49	Film motion
F51	Operate Recorder
F52	Isolation roller position
F55	Ramp output
F70	Video output
F71	Crt light output

From these signals five were selected for detailed discussion. These are F10 10-kv supply, F55 ramp output, F71 crt light output, F49 film motion, and F52 isolation roller position. The first three signals show the condition of the sweep circuits and crt. The last two signals show the condition of the film drive system.

Of the remaining signals, the deflection current monitor samples the positive-going portion of the deflection current wave form. The output was correct during the test. The operate recorder signal indicates the position of the film drive relay. The video output signal will be discussed in Section IX.

b. F10 - 10-Kv Power Supply

This monitor circuit is a resistor divider network across the 10-kv power supply. As shown in Figure 30, the power supply output voltage remained constant during the active passes, thus indicating proper operation. The function is plotted only through pass 30. The film was recovered on pass 33.

c. F55 - Ramp Output

The ramp generator produces a linear voltage ramp which is proportional to the slant range to the target. The ramp monitor signal was well within the limits which were set up prior to the flight test (0.9 to 1.3 vdc).

d. F71 - Crt Light Output

The crt light monitor uses a photosensitive resistor in a voltage divider network. The output, which varies with light level on the face of the crt, is fed to an emitter follower. This level was set prior to launch with no video present at a relative brightness level of 64 percent as measured on a microphotometer. The crt brightness varies with the amount of video present which is also a function of the terrain and of the i-f gain (attenuator step setting). For the pre-recovery passes shown in Figure 30, the radar set was in the agc mode (passes 8 through 30 inclusive).

e. F49 - Film Motion

The film motion monitor indicates the position of the cam-operated switch on the output isolation roller assembly. (Refer to Volume I for a detailed description of the function of the switch in controlling film speed.) The microswitch opens and closes as the cam cycles either side of center position producing a 0.375 percent change in film speed. Figure 31 shows the cycling of the switch. Fast speed is indicated on the graph by the higher voltage (4.3 vdc). Film speed control was normal throughout the mission.

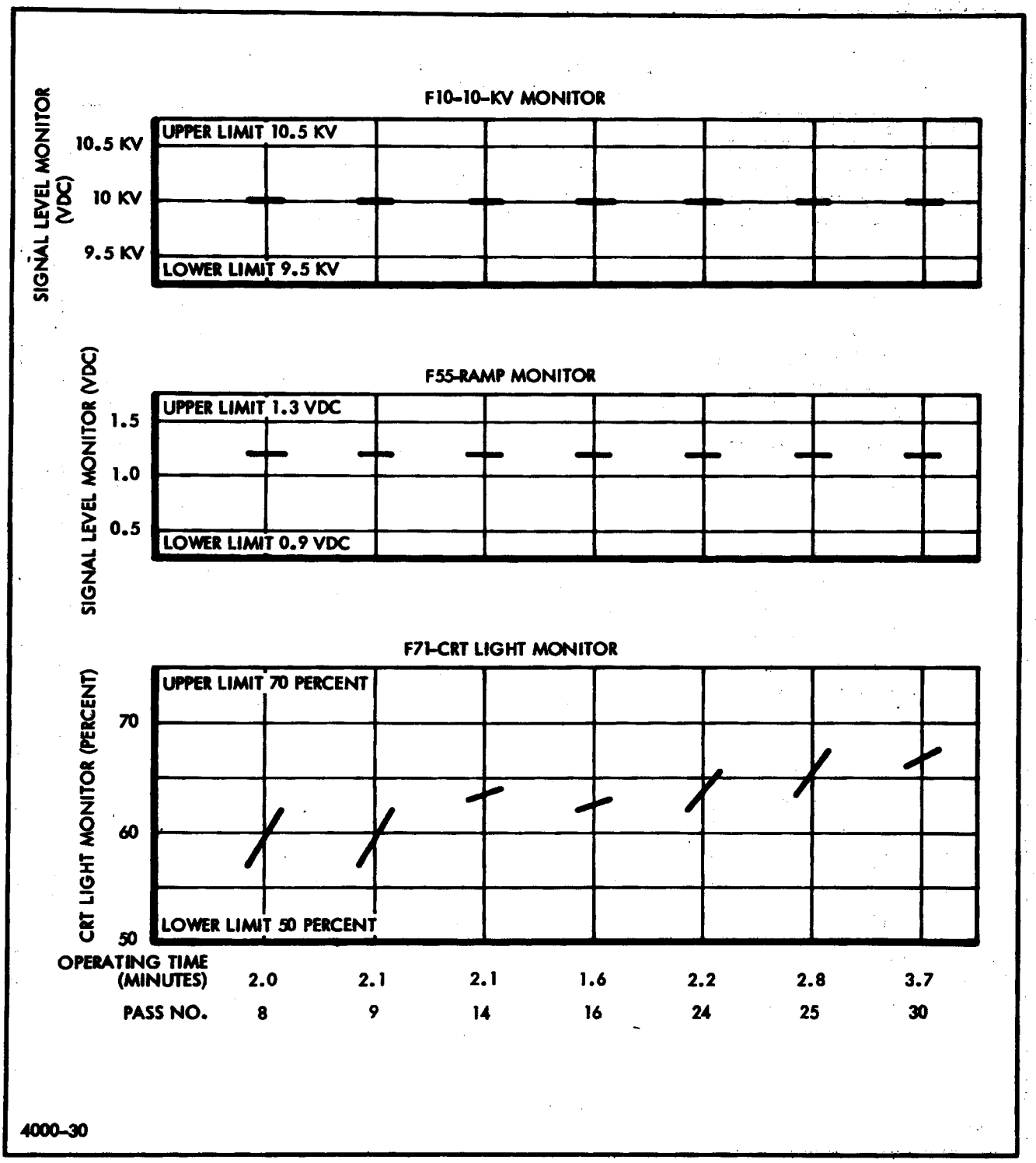

Figure 30 - Recorder Monitor Signals

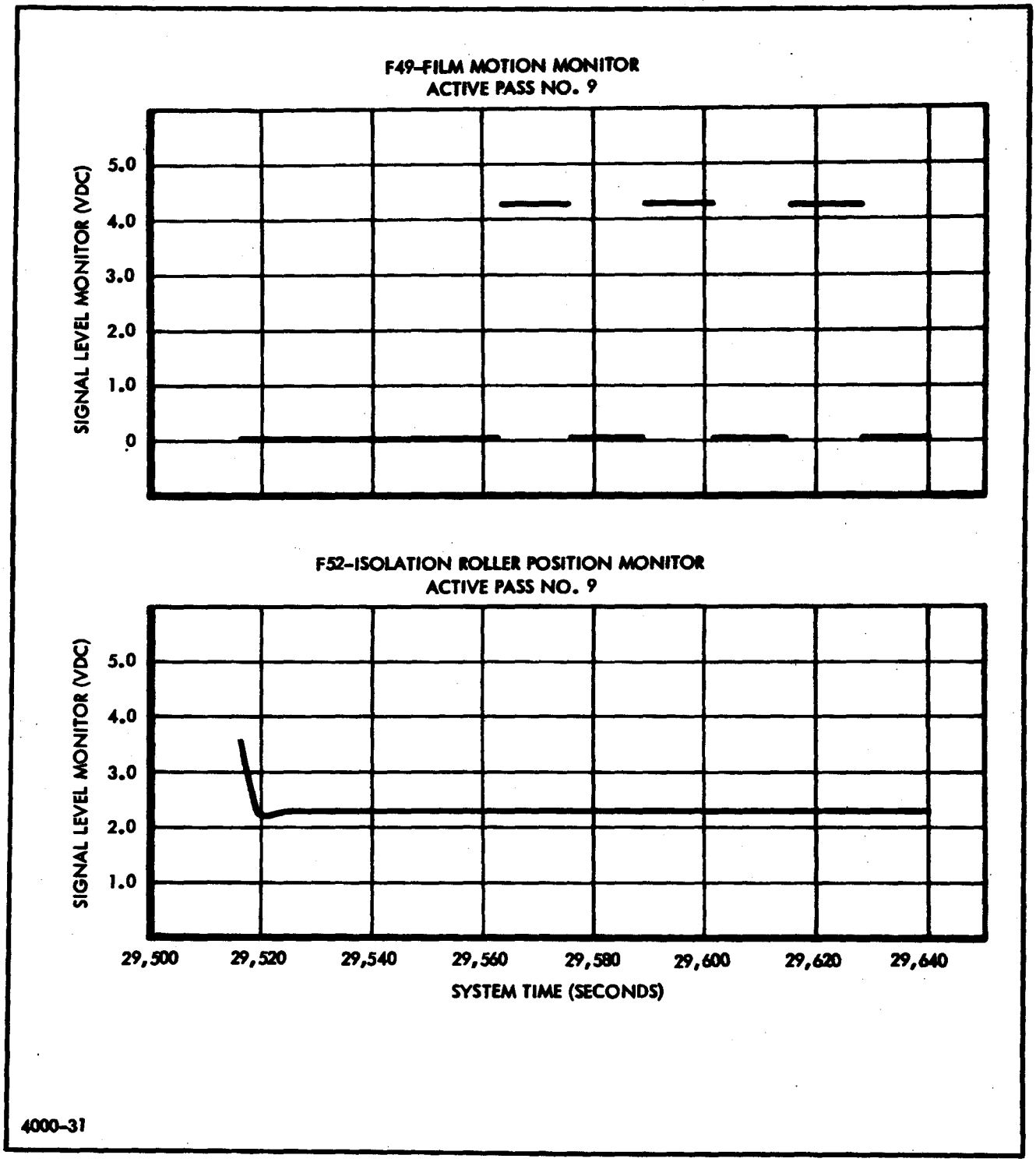

Figure 31 - Recorder Film Motion Monitor Signals

f. F52 - Isolation Roller Position

The isolation roller monitor indicates the position of a potentiometer driven by the input isolation roller assembly (refer to Volume I, pages 139-140, for detailed description of operation). Figure 31 shows that the potentiometer moved immediately after initiation of film drive to stabilize the film tension at 2.5 pounds. Film tension control was normal throughout the mission.

This page intentionally left blank.

NRO APPROVED FOR RELEASE
DECLASSIFIED BY: C/HART
DECLASSIFIED ON: 9 JULY 2012

SECTION IX - SYSTEM FLIGHT TEST ANALYSIS

1. GENERAL

This section presents an analysis of the radar system operation during the orbital flight test. The purpose of this analysis is to establish that the radar functioned properly throughout the test. No attempt is made to analyze the radar performance in terms of resolution or to discuss over-all picture quality. These results are presented in a separate report by [redacted]

In the following pages, a short subsection is presented showing some typical radar mapping results of the flight. Following this, various functions which are important from an over-all system standpoint are discussed by reference to the telemetry and radar map data. The radar pictures, unless otherwise noted, are enlarged 2.6 to 1 from the original data film size. The map scale is 3.6 miles per inch in range and 2.2 miles per inch in azimuth.

2. TYPICAL RADAR PICTURES

Figure 32 shows a section of a 1953 topographic map of East Chicago, Illinois. Figure 33 is a picture of the same area made with the KP-II satellite-borne radar enlarged 4.8 to 1 from the data film size. Several landmarks are identified by numbers on the topographic map and by corresponding numbers on the overlay to the radar map.

Figure 34 shows other radar maps taken with the KP-II radar. Figure 34(a) is the radar return from Richmond, Virginia, and Figure 34(b) the return from Wurtsmith Air Force Base on Saginaw Bay in Michigan.

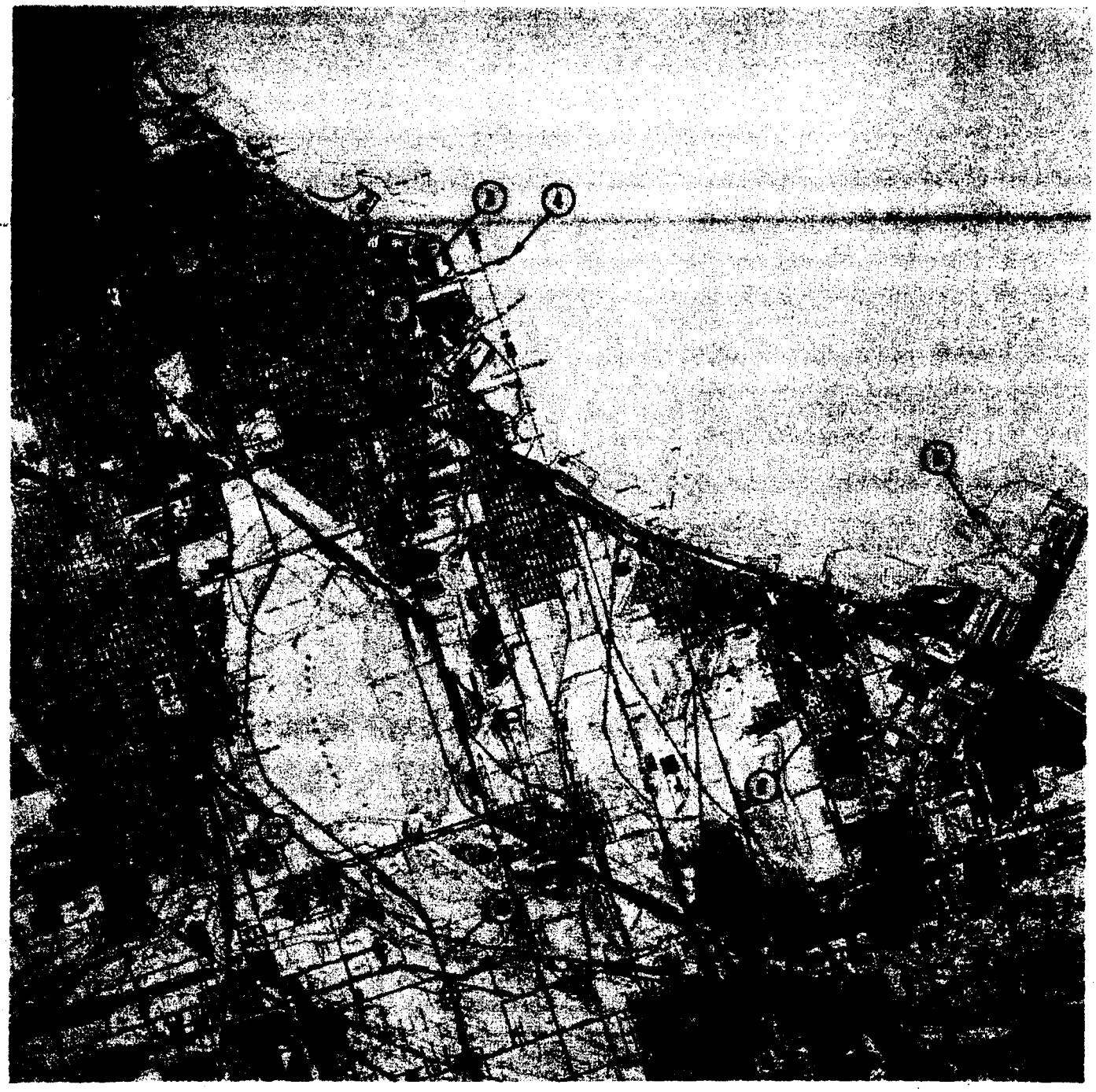

Figure 32 - Topographical Map of East Chicago, Illinois

1. ILLINOIS CENTRAL RAILROAD
2. OAKWOOD CEMETARY
3. HEAVY INDUSTRY
4. BREAKWATER
5. CHICAGO SKYWAY
6. INDIANA HARBOR
7. LAND FILL
8. OIL STORAGE AREA
9. RIVER BARGE
10. CALUMET FREEWAY
11. TRAIN
12. LITTLE CALUMET RIVER

Figure 33 - Radar Return from East Chicago, Illinois

This page intentionally left blank.

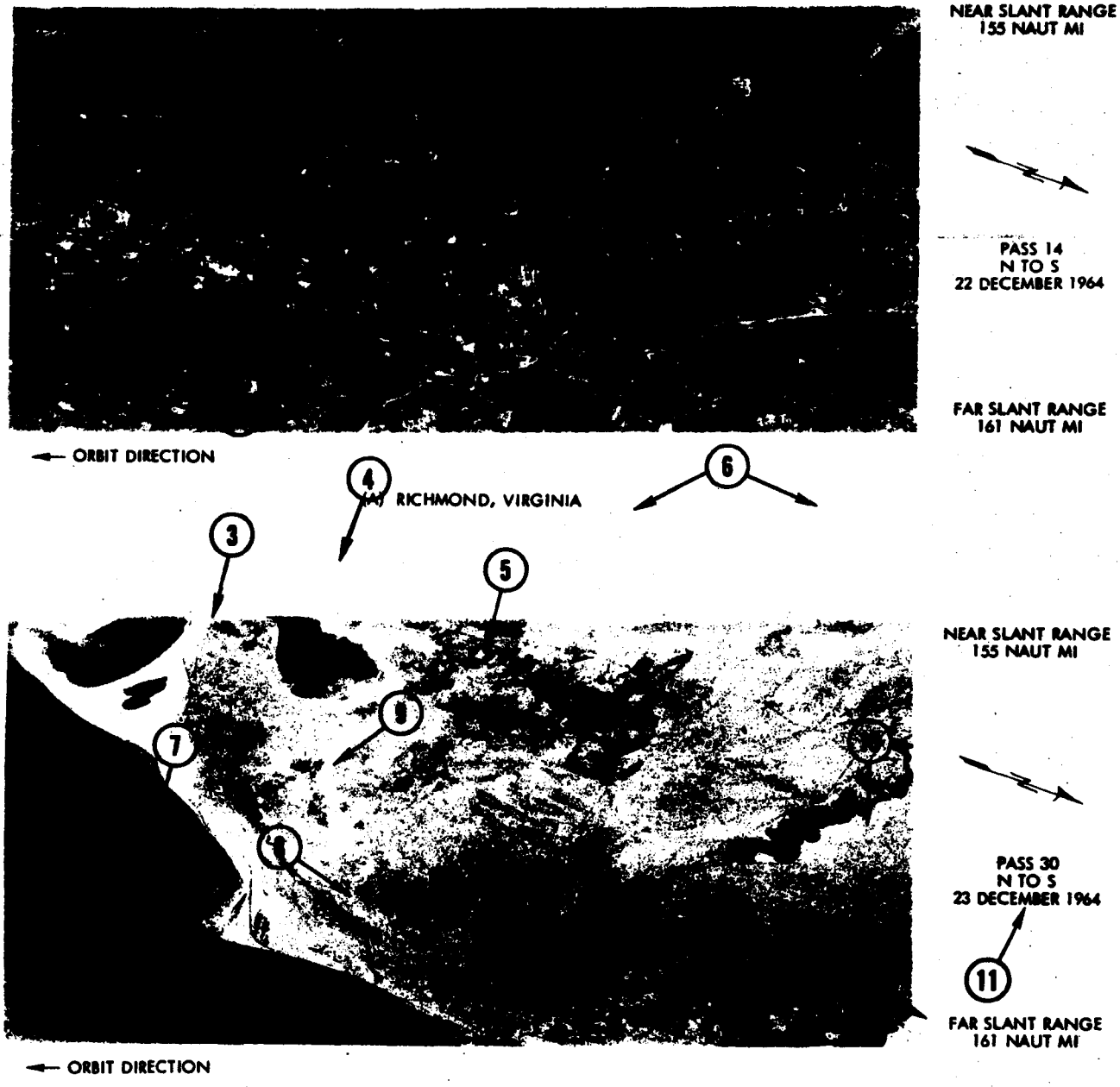

(B) WURTSMITH AFB, MICHIGAN

1. AIRPORT
2. GRAND CANAL
3. SHOPPING CENTER
4. CENTRAL AVENUE
5. STATE FAIRGROUNDS
6. HIGH RISE BUILDINGS
7. BLACK CANYON FREEWAY
8. GRAND AVENUE
9. THOMAS ROAD
10. ALUMINUM PLANT
11. US HIGHWAY 80
12. OIL STORAGE AREA

4000-37

Figure 34 - Typical Radar Maps

This page intentionally left blank.

Figure 35 shows a 1953 topographic map of part of Phoenix, Arizona. (Note: Many changes have occurred in Chicago and Phoenix since the topographic maps were made.) Figure 36 is the radar return from the same area, enlarged 7 to 1 from the data film. The upper part of the radar map is somewhat dark as a result of a one-step misadjustment of the prf. This will be discussed further in paragraph 5 following.

3. AUTOMATIC GAIN CONTROL (AGC)

a. General Operation of Agc

The automatic gain control permitted the receiver gain to vary as a function of the amplitude of the signal returned to the receiver from the terrain being mapped. For large returned signals, such as those from residential or manufacturing areas, the receiver gain was automatically reduced. For low signal returns, such as those from desert or sea areas, the gain of the receiver was increased. The dynamic range of the agc was measured prior to the flight and found to be 35 db.

b. Agc Operation During Pass 34

The effect of the agc action on the map film can be seen in Figure 37(a). The increases of receiver gain over open water areas produce lighter areas on the film. These light areas are seen to correspond to the decreases in agc voltage on the graph, Figure 37(b).

c. Agc Operation During Pass 30

Measurements on a non-flight system showed that the agc time constant was 32 milliseconds for a 10-db step increase in received power and 26 milliseconds for a 10-db step decrease in received power. A land-water boundary occurred at system time 57460

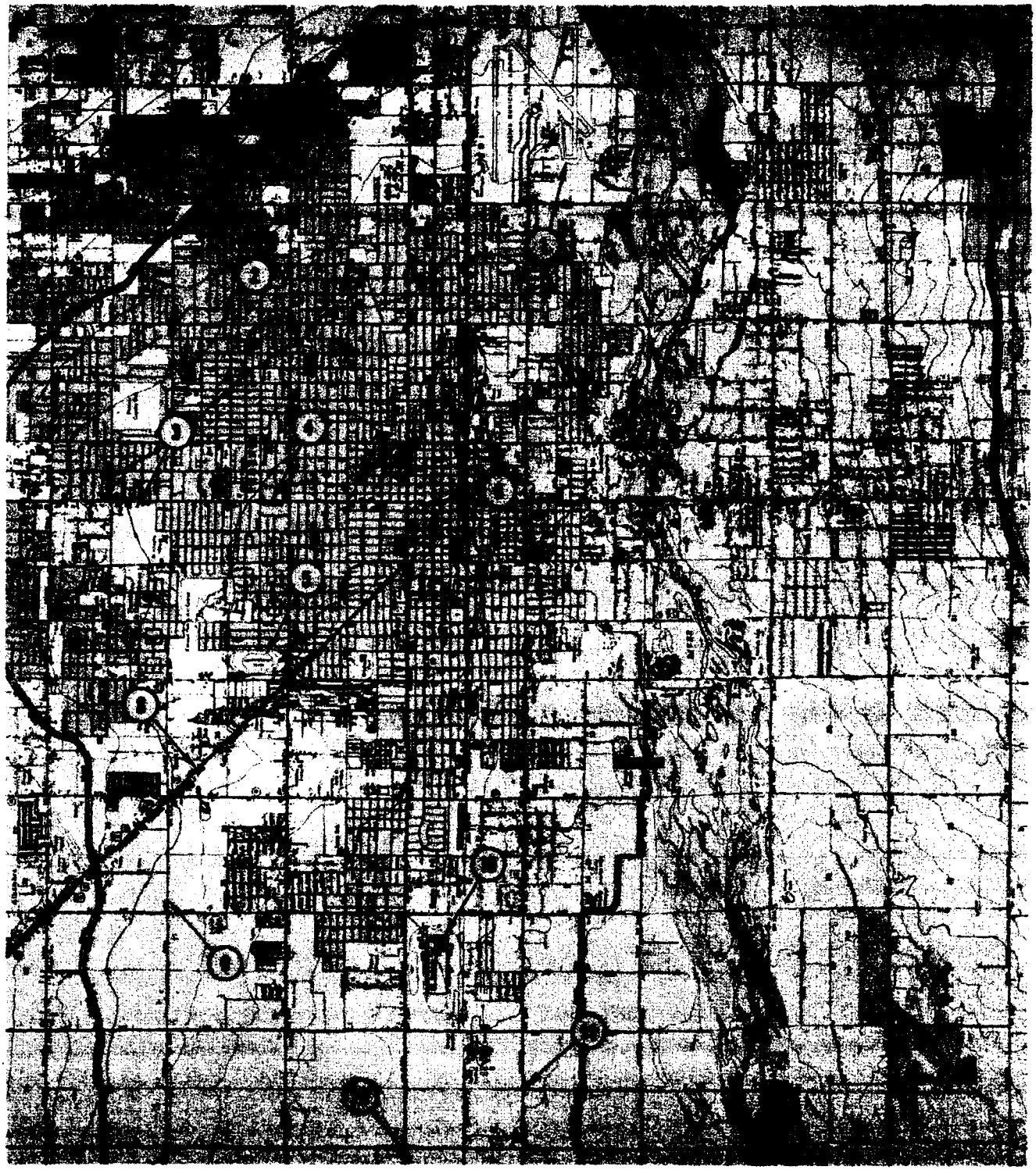

Figure 35 - Topographical Map of Phoenix, Arizona

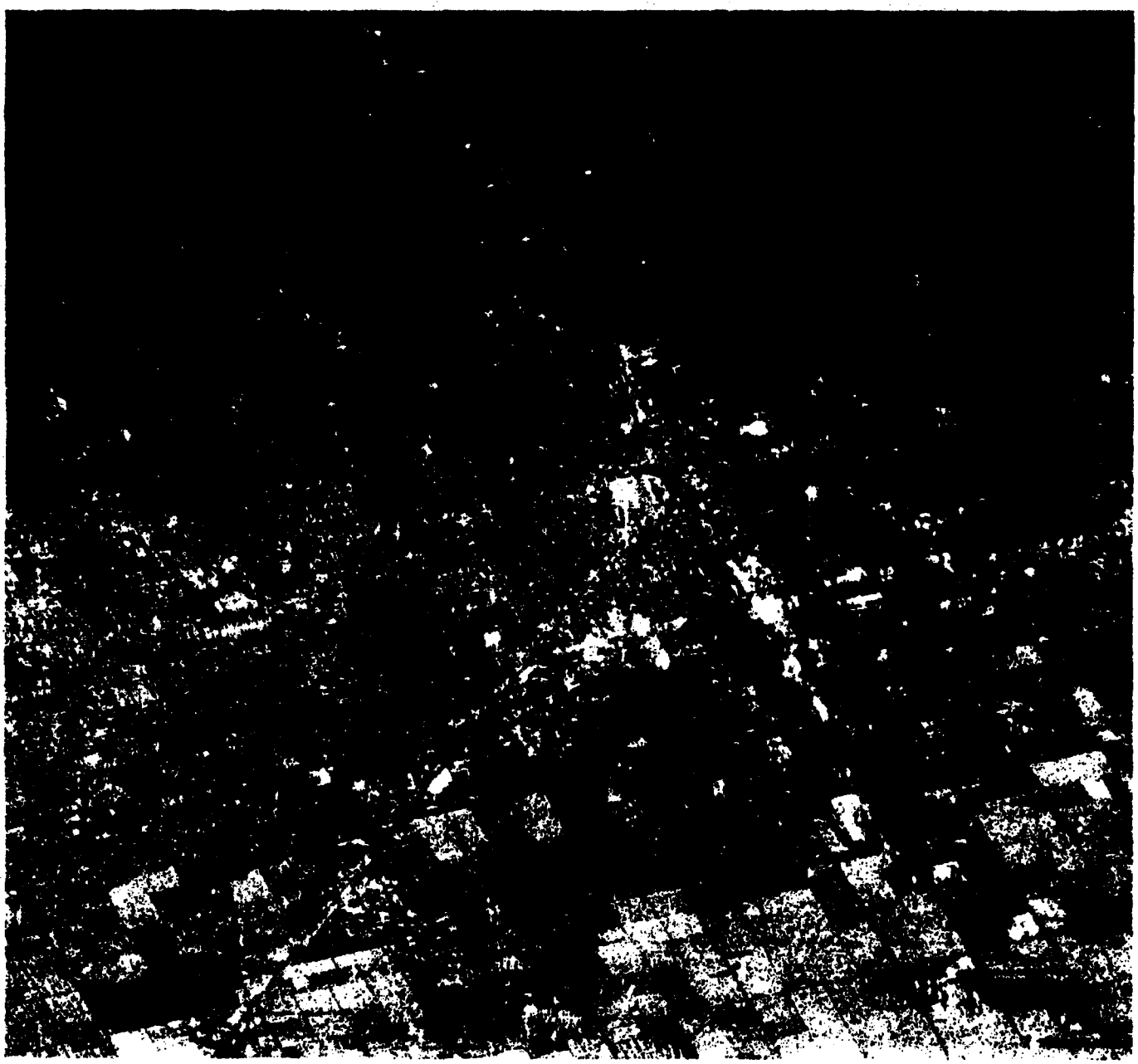

Figure 36 - Radar Return from Phoenix, Arizona

This page intentionally left blank.

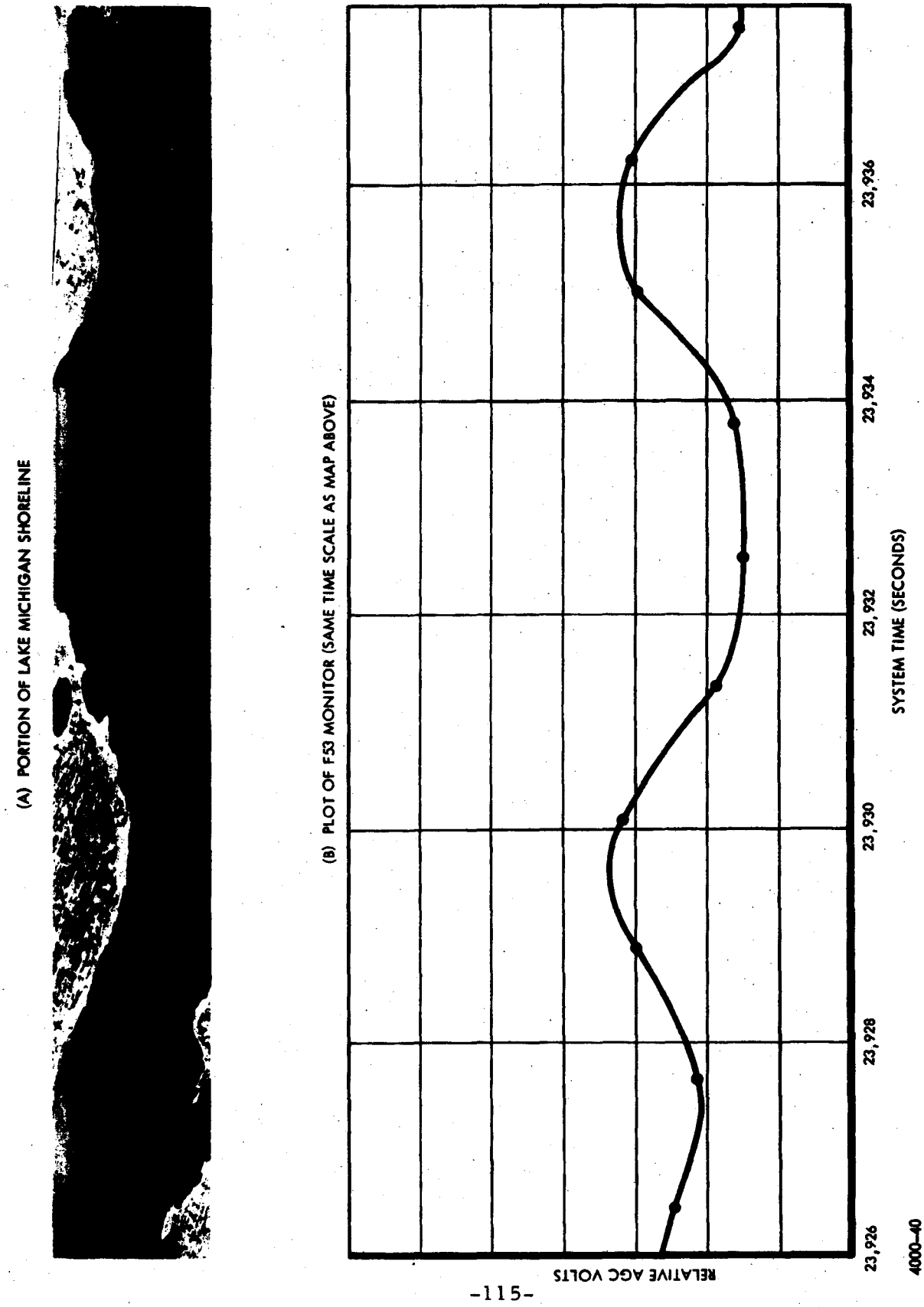

Figure 37 - Automatic Gain Control Operation

This page intentionally left blank.

seconds during pass 30. From Figure 38(a) it is seen that the monitor voltage decreased by 0.78 volts from 2.02 to 1.24 volts, corresponding to a decrease in received power of approximately 10.7 db (see Figure 38(b)). Figure 39(a) is a photograph of the land-water boundary and approximates a step function in terms of power received by the satellite-borne radar system. As the land-water boundary did not represent a perfect step function and as the telemetry samples are too far apart for accurate time measurements, it is not possible to measure the agc time constant with accuracy.

It is interesting to note that the sharp increase and subsequent decrease in receiver gain at system times 57426 and 57431 (see Figure 38(a)) occurred as the vehicle crossed Saginaw Bay in Michigan. The decrease in gain at system time 57471 was caused by the high returns from Cleveland, Ohio. The small decrease at system time 57478 was caused by returns from the city of Akron, Ohio.

4. ATTENUATOR CHANGES

a. Attenuator, General Operation

The seven fixed steps of receiver attenuation covered a range from zero to 33.5 decibels. Provision was made to have these steps available for use in the event that the agc circuitry failed to operate properly. The data film recorded over the wide band data link at the New Boston Tracking Station was processed immediately after pass 8 to check the agc operation and other important system parameters. Analysis of early telemetry data and the map film from pass 8 showed that there was no need to use any of the fixed attenuator settings. However, after recovery of the data film from the satellite on pass 33, it was decided to obtain some data with the attenuator in various settings. Figure 40 shows the amount of fixed receiver attenuation for each of the possible attenuator settings (excluding step 1 which is agc).

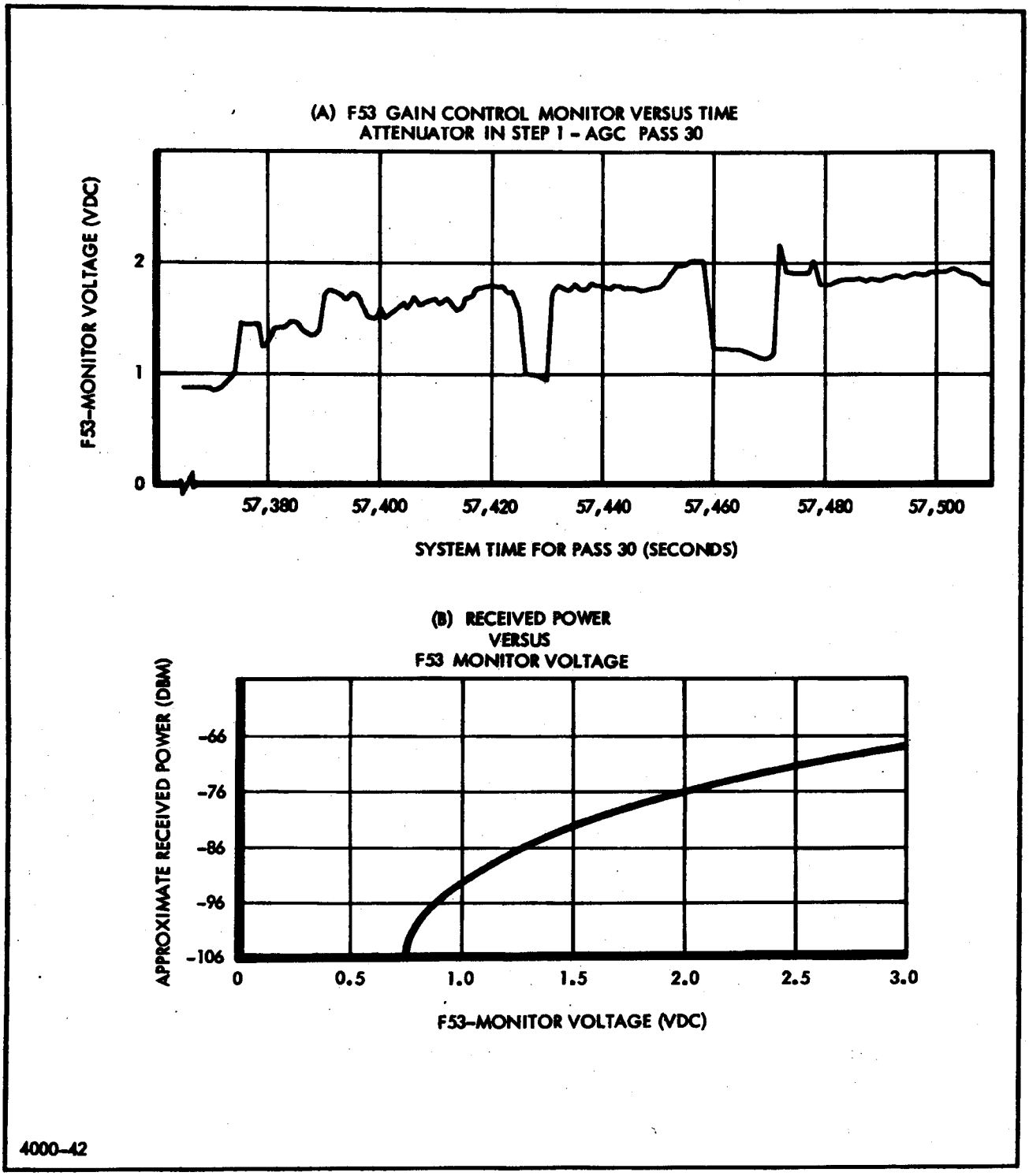

Figure 38 - Gain Control Functions

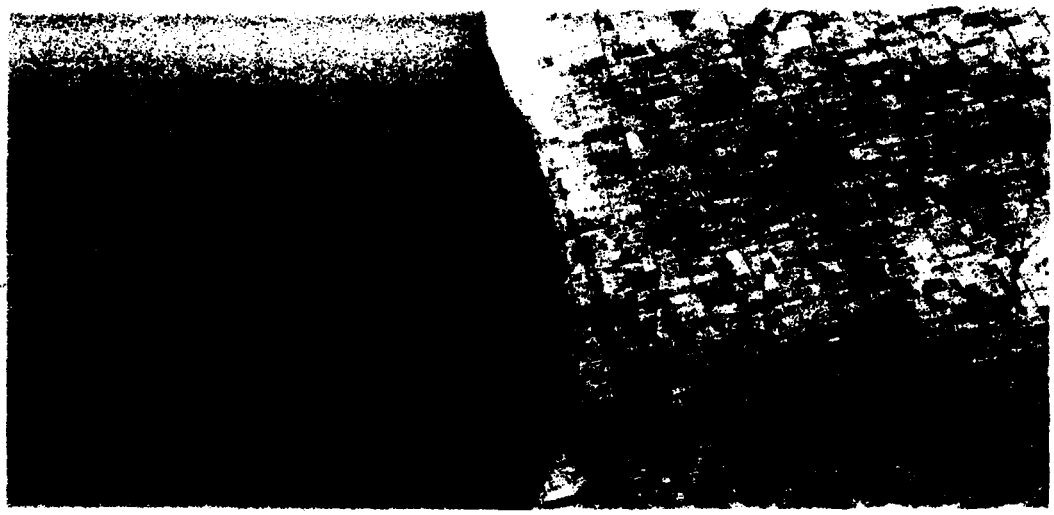

NEAR SLANT RANGE
155 NAUT MI

PASS 30
N TO S
23 DECEMBER 1964

FAR SLANT RANGE
161 NAUT MI

← ORBIT DIRECTION

(A) LAKE ERIE LAND-WATER BOUNDARY
AUTOMATIC GAIN CONTROL

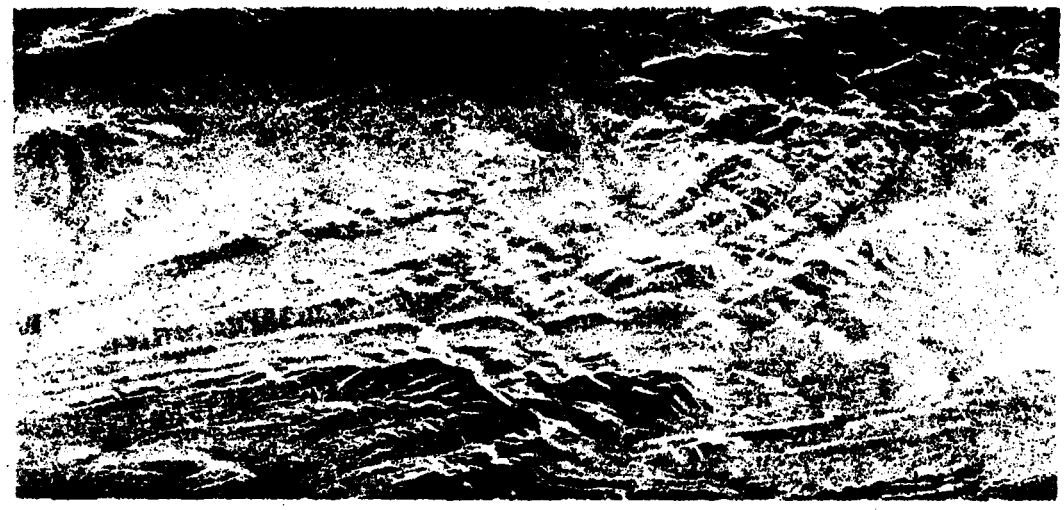

NEAR SLANT RANGE
165 NAUT MI

PASS 41
S TO N
24 DECEMBER 1964

FAR SLANT RANGE
171 NAUT MI

← ORBIT DIRECTION

(B) CONFUSION MOUNTAIN RANGE, UTAH
ATTENUATOR IN STEP 0

4000-41

Figure 39 - Automatic Gain Control and Attenuator Step Zero

This page intentionally left blank.

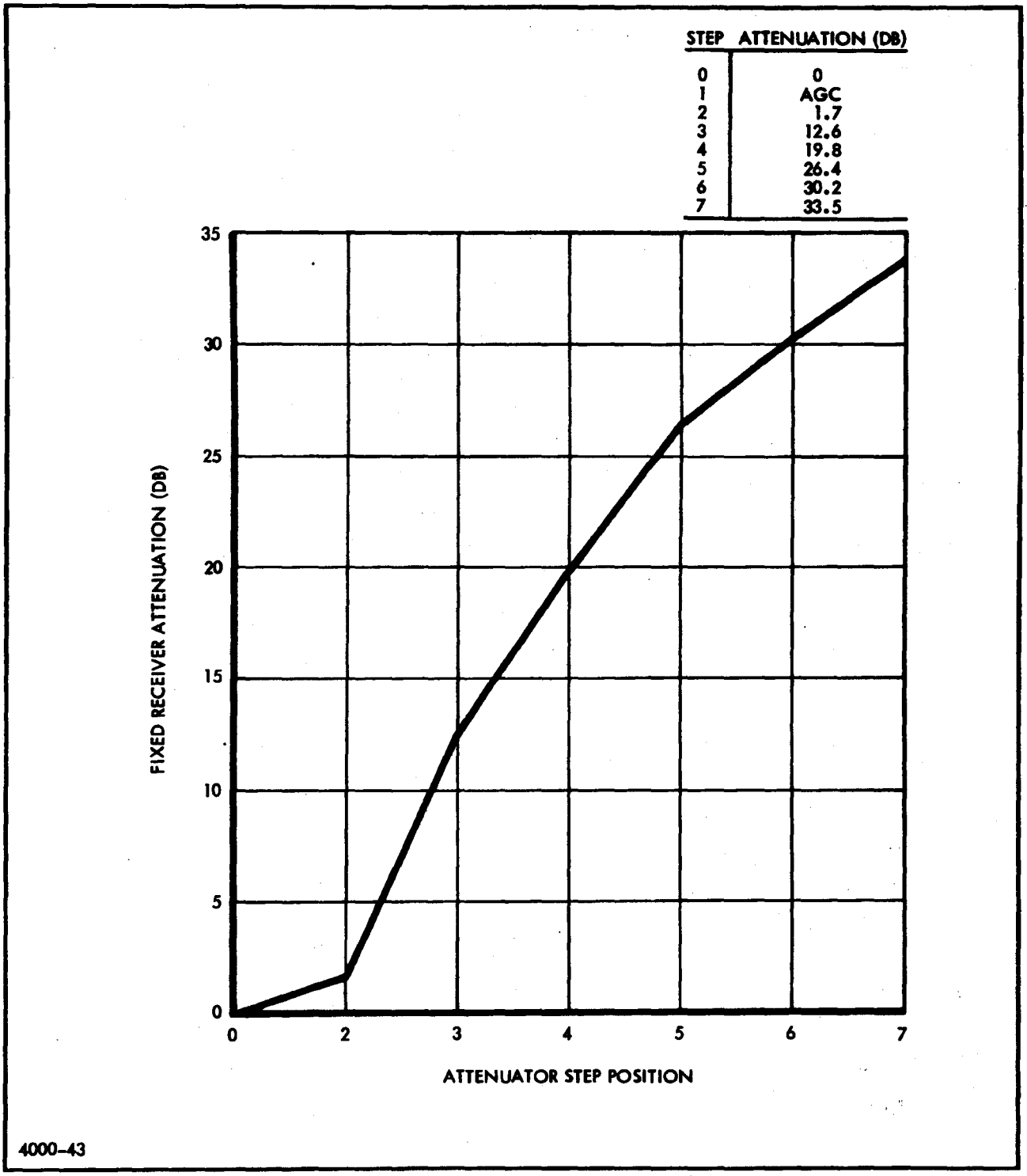

Figure 40 - Receiver Attenuation versus Step Position

Attenuator step 0 allowed the receiver to make use of its full gain. Steps 2 through 7 reduced the receiver gain by fixed amounts.

b. Attenuator Step 0

Figure 39(b) showed a section of the map which resulted after step zero was selected. In step zero, the gain was excessively high. Examination of the results for other attenuator steps shows that the gain for step 3 was near optimum. Based on this selection, the receiver gain in step 0 is approximately 12.6 db above the optimum level. For this map, the correlator was set up to provide the best picture possible for the high-gain conditions. Although some degradation has occurred, the radar map is still useful.

c. Attenuator Steps 2 and 3

Figure 41(a) shows a section of the radar map made over Green Bay, Wisconsin, when step 2 was selected. Some loss of resolution occurred as, based on the above selection of step 3, the gain was approximately 10.5 db too high. Note the ice formations in Green Bay. Figure 41(b) shows Grand Island for attenuator step 3 which is near the optimum gain setting.

d. Attenuator Steps 3 and 4

Figure 42 shows the radar map at the time of switching from step 4 to step 3. Figure 42(a) has been processed to favor step 4 and Figure 42(b) to favor step 3. This comparison demonstrates the versatility of the processor.

e. Attenuator Steps 5, 6, and 7

The map film made with the attenuator in step 5 mainly shows the return from larger targets such as mountains and major cultural areas. Plowed fields and generally level terrain show little return.

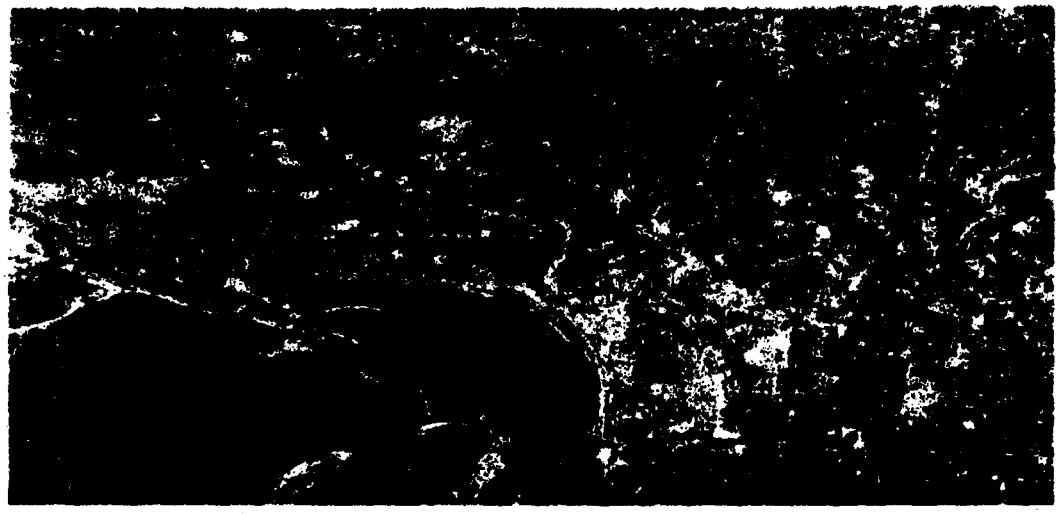

NEAR SLANT RANGE
164 NAUT MI

PASS 40
S TO N
24 DECEMBER 1964

FAR SLANT RANGE
170 NAUT MI

← ORBIT DIRECTION

(A) GREEN BAY, WISCONSIN
ATTENUATOR IN STEP 2

NEAR SLANT RANGE
164 NAUT MI

PASS 40
S TO N
24 DECEMBER 1964

FAR SLANT RANGE
170 NAUT MI

← ORBIT DIRECTION

(B) GRAND ISLAND, LAKE SUPERIOR, MICHIGAN
ATTENUATOR IN STEP 3

4000-44

Figure 41 - Comparison between Attenuator Steps 2 and 3

This page intentionally left blank.

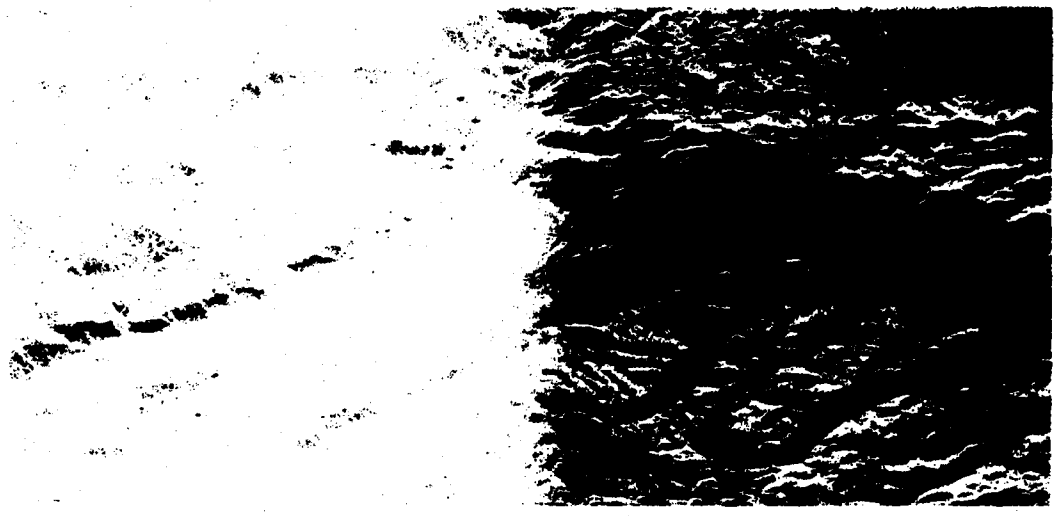

(A) PROCESSED TO FAVOR STEP 4

(B) PROCESSED TO FAVOR STEP 3

4000-45

Figure 42 - Effects of Processing on Radar Imagery

This page intentionally left blank.

No map film was recorded with the attenuator in step 6, but on pass 72, attenuator step 7 was selected. The map film shows no targets at all for step 7.

5. CHANGES OF PULSE REPETITION FREQUENCY

a. Effect on Mapping

(1) General Operation

When the prf setting is correct, a uniformly illuminated map is obtained. Actually, because of the shape of the antenna beam, targets at mid-range are illuminated with more radar energy than targets at near and far ranges, but the radar returns are modified by the sensitivity time control (Volume I, page 32) to attenuate the mid-range returns and produce a uniform map.

By changing the prf, the tracking station operators were able to adjust the time position of the sensitivity time control function for proper compensation. This was usually accomplished within a few seconds after control was turned over to the recorder operators.

During pass 47 the prf was stepped through all 16 of its settings to show the effect of large changes.

(2) Range Shift with Prf Changes

Figure 43(a) shows a portion of the radar map when the prf was set three steps high (left side of picture). After the prf change (step 14 to step 13, right side of picture) the terrain is more nearly uniformly illuminated. It can be seen that even with the prf setting three steps high, the map is still well defined. The primary effect of the prf change on the map film is the range shift, made evident by the discontinuity in the highway (see arrow).

This shift in range is also very pronounced in Figure 43(b), which shows a discontinuity in the Colorado River (see arrow) produced by a prf change from step 8 to 9. In this figure the prf went from two steps low to one step low.

The river is shifted toward the near-range edge of the map after the prf change. The distance between the satellite and the near-range terrain is given by the equation:

$$R_{sn} = \frac{c}{2} \frac{N}{PRF} + K \qquad (14)$$

where

R_{sn} = slant range distance from near-range targets to satellite

c = velocity of light

N = the integer number of interpulse periods between transmission and reception of the radar pulse

PRF = pulse repetition frequency

K = a constant-small compared to $\frac{N}{PRF}$.

A step change from 8 to 9 actually represents a decrease in prf from 8449 to 8415 pps. Hence, R_{sn} is increased by 0.66 nautical mile, assuming a vehicle altitude of approximately 138 nautical miles and a depression angle of 55 degrees (N = 17). That is, the near-range edge of the map is 0.66 nautical mile farther away from the satellite after the prf change. Therefore, the river actually appears closer to the near-range edge of the map film after the prf change.

(3) Effect of Improper Illumination

No photographs showing the prf four steps off optimum are included but in this case the illumination was so low at some ranges that no targets were discernible.

The unequal illumination resulting from a prf five or more steps from optimum produced objectionable results.

(A) LAND MASS NEAR LEBANON, ILLINOIS

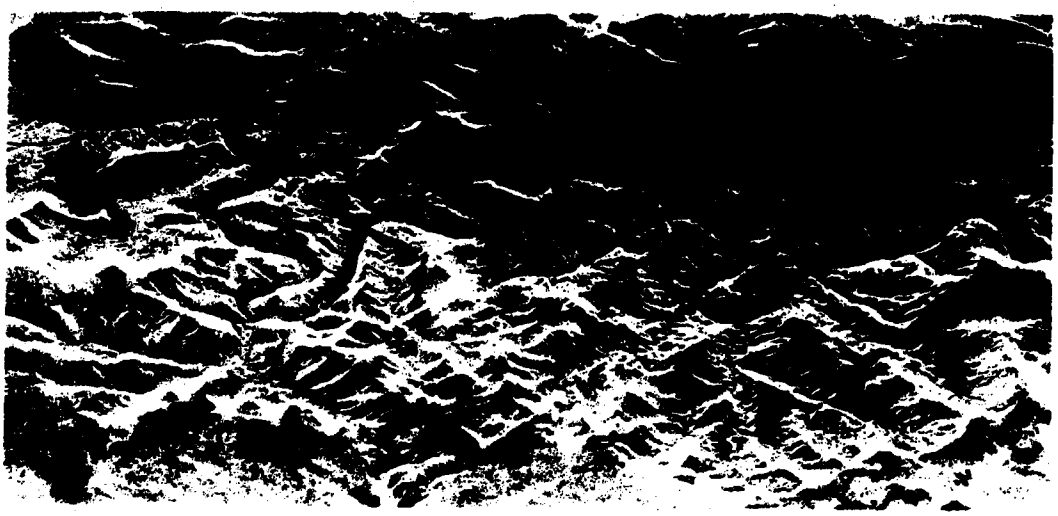

(B) COLORADO RIVER, UTAH

4000-46

Figure 43 - Range Shifts with Prf Changes

This page intentionally left blank.

(4) Range Inversion for Large Prf Errors

For very large prf errors, as were encountered on pass 47 when the prf was intentionally switched throughout its entire range, targets at the near-range edge of the map film are not necessarily the targets that were at the shortest slant range from the vehicle. The prf switching adjusts the time position of the recorder sweep to coincide with the return from a given transmitted pulse. When the prf is set too far off, the trailing edge of one pulse and the leading edge of the next pulse are recorded sequentially, and range inversion is produced.

Figure 44 of Pueblo, Colorado, is an excellent example of this range inversion phenomenon. The center area of the topographic map does not appear; the upper and lower areas defined by the dotted lines are interchanged in the radar display. The railroad tracks (2) are pointed out in both Figures 40(a) and 40(b) to orient the reader. The barely visible crossroads (1) and the curve in the river (3) are to the east of Pueblo in Figure 44(a), and to the west of Pueblo in Figure 44(b).

(5) Transients in Wide-Band Data

The effect of prf change on the data film recorded on the ground usually showed a data loss each time the prf was changed. This data drop-out occurs during the time required for the ground-based recorder crt sweep to lock in with the synchronizing pulse from the vehicle.

b. Operator Recognition Problems

The wave shapes viewed on the "A" scope, located in the screen rooms of the tracking stations, could be easily evaluated by the operator as to the need for prf changes. Errors in setting of the prf could be determined after viewing the "A" scope presentation for only a few seconds. The

integration effects of the human eye play a large part in the recognition of the "A" scope wave shape. If the eye is assumed to have a persistency of only 50 milliseconds, the picture presented to the brain represents an average of the returns from over 400 radar pulses.

Some photographs of the "A" scope presentations are shown in Figure 45. The exposure time on the camera was long enough to simulate the integration effects of the eye. Note that some of the definition of the original "A" scope presentations is lost in the photographs.

Equipment was available at the tracking station for photographing single sweep traces. It was found that these photographs could not be interpreted by the operators, and that they provided no information as to the correct prf as they did not include the effects of integrating a large number of returns.

Sporadically, small groups of targets caused the wave form to have a noticeably higher or lower amplitude than the average signal level. However, these higher or lower points were only a few microseconds in duration and the overall shape of the wave form was clearly defined. Occasionally, lakes or other bodies of water produced "holes" (near zero returns) which lasted for a few seconds and which sometimes moved laterally across the range interval displayed on the oscilloscope. During these occasional short periods, it was not always possible to ascertain whether the prf setting was correct.

c. Evaluation of Prf Selection Simulator

This simulator was used as a training aid in advance of the orbital operation for familiarizing the tracking station operators with the problems which would be encountered later in setting the prf.

As might be expected, there were a few minor differences between the actual wave shape of the returns, as viewed on the "A" scope by an operator, and the wave shapes as generated by the simulator (refer to Section III, paragraph 4). The major difference was that the simulator produced a wave form representative of a uniform terrain. Actually, small groups of targets caused the radar display to have a noticeably higher return during some portions.

FAR SLANT RANGE
152 NAUT MI

PASS 47
N TO S
24 DECEMBER 1964

NEAR SLANT RANGE
155 NAUT MI

ORBIT DIRECTION →

(A) PUEBLO, COLORADO
LARGE PRF ERROR (SIX STEPS OFF)

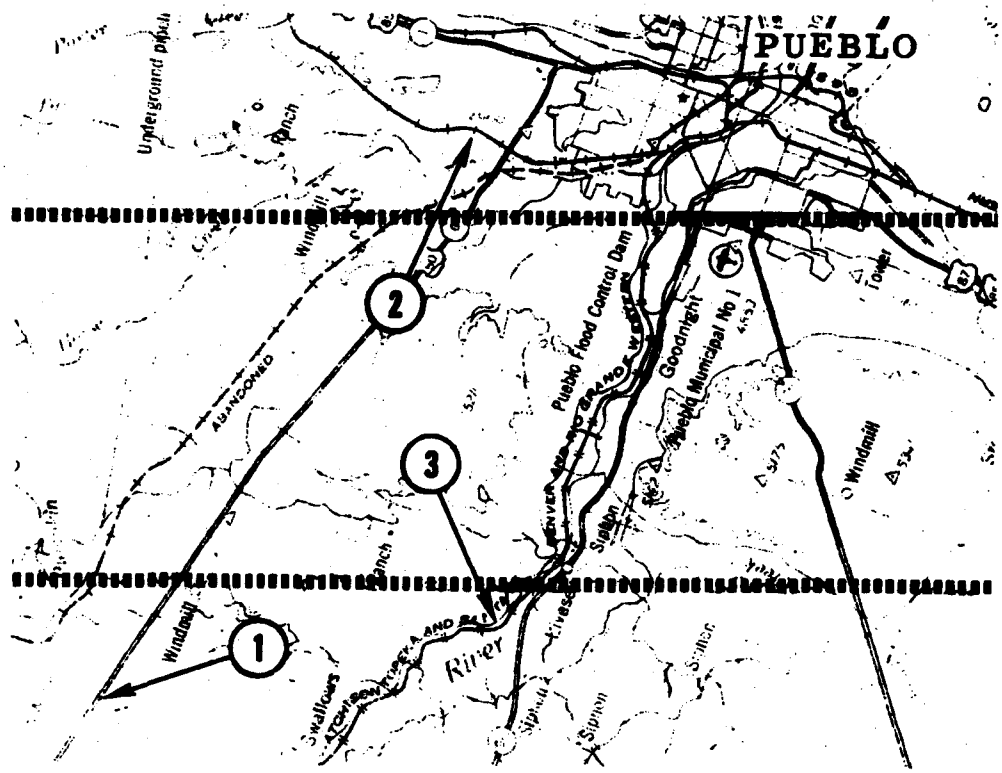

(B) TOPOGRAPHICAL MAP OF PUEBLO, COLORADO

4000-47

Figure 44 - Range Inversion

This page intentionally left blank.

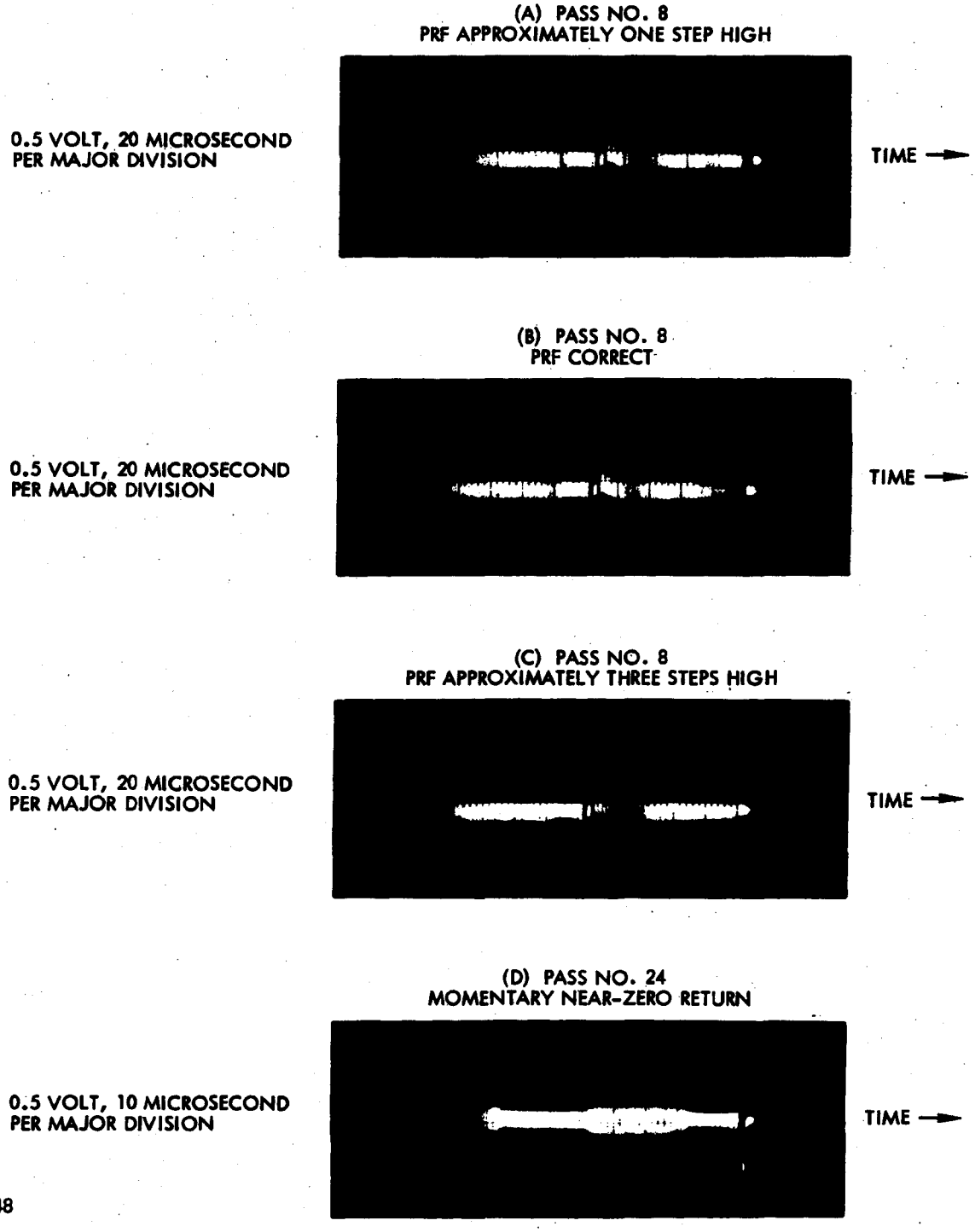

Figure 45 - Oscilloscope Pictures of Tape Playback

This page intentionally left blank.

The simulator wave shape for the condition of the prf being one step off was readily recognized.

It is concluded that the prf selection simulator is a very useful tool for familiarizing tracking station personnel with the wave shapes that are encountered during orbital operations. It is also useful as a signal source during checkout of the wide-band equipment at the tracking stations.

6. CLUTTERLOCK

a. General

The clutterlock loop compensates for angular displacement of the antenna beam with respect to the zero doppler direction. The clutterlock correction signal is telemetered via the F60 integrator monitor. This signal voltage must be converted to an angle in degrees. The angle must then be compared with the error introduced into the antenna beam position by vehicle motion. The vehicle yaw and pitch motions both contribute to clutterlock error. The contribution of roll is minor and will not be considered.

b. Clutterlock Correction Angle

The F60 integrator monitor signal is proportional to the clutterlock offset frequency. The proportionality factor is f (cycles per second) = 1000 × volts dc. The clutterlock angle in degrees is obtained by substituting the offset frequency f_d in the equation:

$$\text{Sin } \phi = \frac{f_d \lambda}{2v} \quad . \tag{15}$$

c. Vehicle Motions

(1) Pitch Reference

The three axes of the vehicle were referred to integrating gyros. The pitch attitude was programmed by an input to the pitch gyro at a fixed rate of four degrees per minute (360 degrees per 90-minute orbit) to

keep the vehicle longitudinal axis generally perpendicular to the local vertical. The pitch attitude was also corrected by sensors which provided a continuous reference to the horizon. At the time of initiation of the operate command, the horizon sensors were switched off and the vehicle was allowed to continue along according to the four-degree-per-minute program.

(2) Yaw Reference

A fixed yaw bias of ±2.44 degrees was provided to align the antenna beam with the relative ground velocity vector. The polarity was switched plus or minus depending on whether the vehicle was in a northbound or southbound pass.

(3) Bias Uncertainty and Deadband

There was a predicted uncertainty of ±0.4 degree for each axis. This bias uncertainty resulted from gyro drift, horizon sensor uncertainty, and other tolerances. A deadband of ±0.18 degree was designed into the attitude correction system. The vehicle tended to hang at one limit of the deadband in pitch, probably as a result of a residual magnetic torque.

(4) Angular Displacement of Antenna

To a close approximation, the resultant angular displacement of the antenna caused by yaw and pitch motions can be shown to be:

$$\theta_a = \frac{R_o}{R_s}\,\theta_y - \frac{h}{R_s}\,\theta_p \qquad (16)$$

where

θ_a = resultant angular displacement of antenna in azimuth direction

θ_y = vehicle yaw angle

θ_p = vehicle pitch angle

R_o = ground range to target

R_s = slant range to target

h = vehicle altitude.

d. Clutterlock Commands

The clutterlock circuitry was designed to close the loop simultaneously with the operate command. However, the circuits were not designed to open the loop with the off command. The opening of the loop after each pass should have been accomplished by sending a clutterlock short command but it was not done. Consequently, the clutterlock loop was open and free to drift during pre-operate for all passes except 8 and 57. No harm was done however, as the integrator does not appreciably drift.

e. Clutterlock Response - Pass 14

For pass 14, the clutterlock loop acted immediately, upon application of transmitter high voltage, to cancel out an error of about 0.37 degree of antenna angular displacement resulting from an error in vehicle attitude. Figure 46(a) shows the section of the radar map and a graph of the corresponding clutterlock correction angle plotted to the same time scale as that of the map. The high voltage was applied at system time 57897 seconds. At this time no targets are visible on the map because of improper sampling of the doppler spectrum. Within a few seconds, the clutterlock loop had compensated for the antenna displacement error and the ground painting was good. A clutterlock time constant of about 2.5 seconds is indicated (see Figure 46(b)) which is in excellent agreement with the design value of 2.5 seconds for the fast time constant which was used for this pass. The radar display is somewhat degraded in this instance because of the reproduction technique employed.

f. Clutterlock Loop Open - Pass 56

During pass 56, the clutterlock loop was opened by means of a shorting relay at the integrator output. The short was applied seven seconds

after the pass began. The short in the loop caused the system to map along the line of zero doppler rather than the line of constant doppler which was centered in the illumination of the physical antenna. Figure 47 is a section of coastline mapped in this condition. The undesirable effects are quite evident. The results obtained are easily explained if it is recalled that the boresight of the antenna and zero doppler line are not usually coincident. When the angular difference is as small as 0.25 degree, the doppler spectrum of the desired targets is not properly illuminated and the level of azimuth ambiguities is greatly increased. The fact that the system mapped properly, just previous to opening the clutterlock loop, verifies that the smeared image is caused by the absence of synthetic beam steering.

g. Clutterlock Operation over Water - Pass 16

The pitch angle, yaw angle, resultant antenna displacement angle (Equation (15)), and clutterlock angle (Equation (14)) are plotted for pass 16 in Figure 48. During this pass the operate command was initiated over water. The clutterlock loop operated immediately, but with a slower response than that over land to correct the vehicle attitude error. Over water, the only signal for clutterlock to operate on is the return from wave patterns. Figure 49 is a radar map of the coastline in the vicinity of the Eel River in Northern California crossed about 12 seconds after the operate command.

h. Clutterlock Performance - Other Passes

Pass 30 is another good example of clutterlock over-water performance. In this case the operate command was initiated over Lake Superior. The pitch angle, yaw angle, resultant antenna displacement angle, and clutterlock angle are plotted in Figure 50 for this pass. At the start of passes 30, 40, and 56 (as in pass 14), the clutterlock had to compensate for

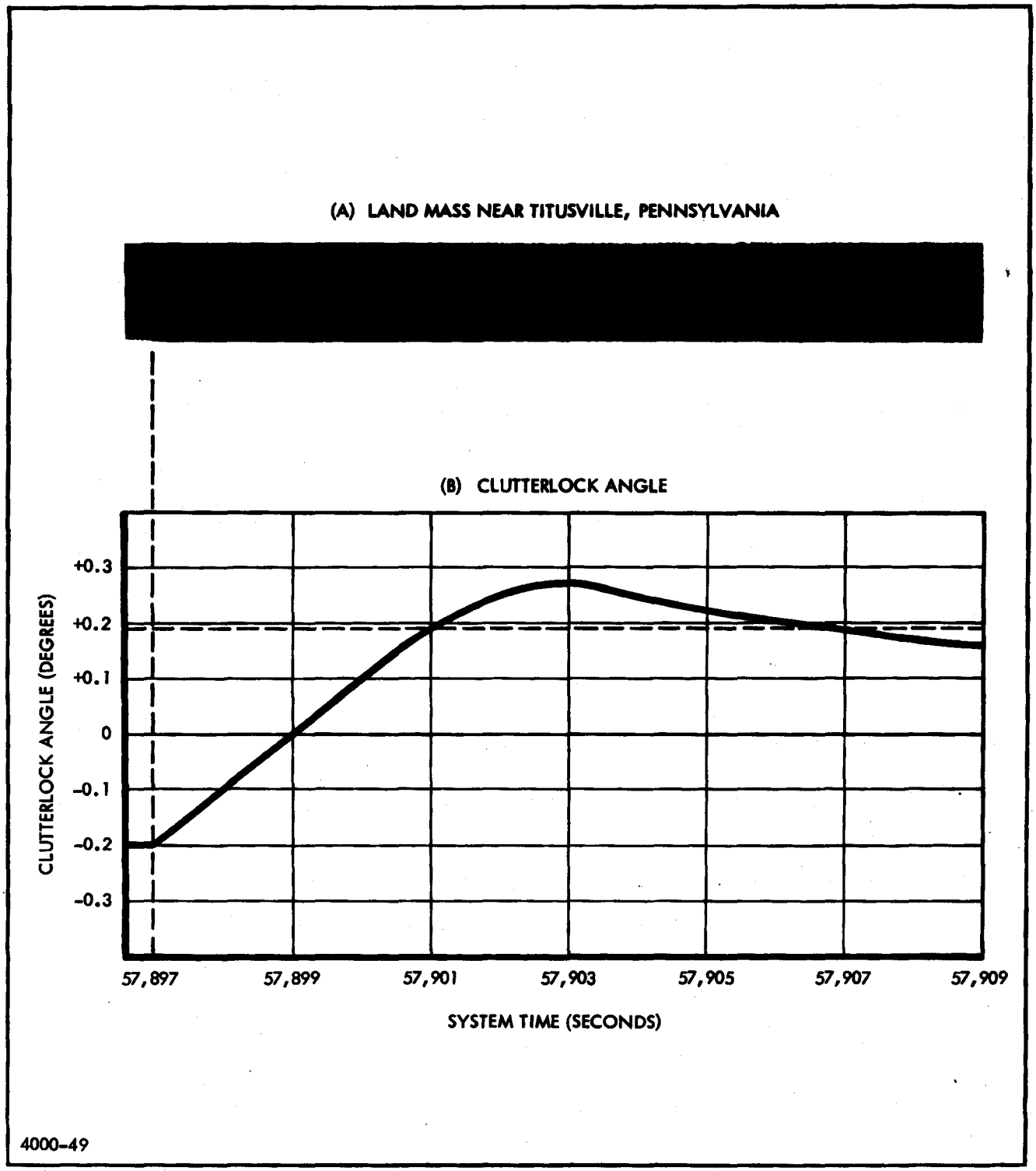

Figure 46 - Clutterlock Response

This page intentionally left blank.

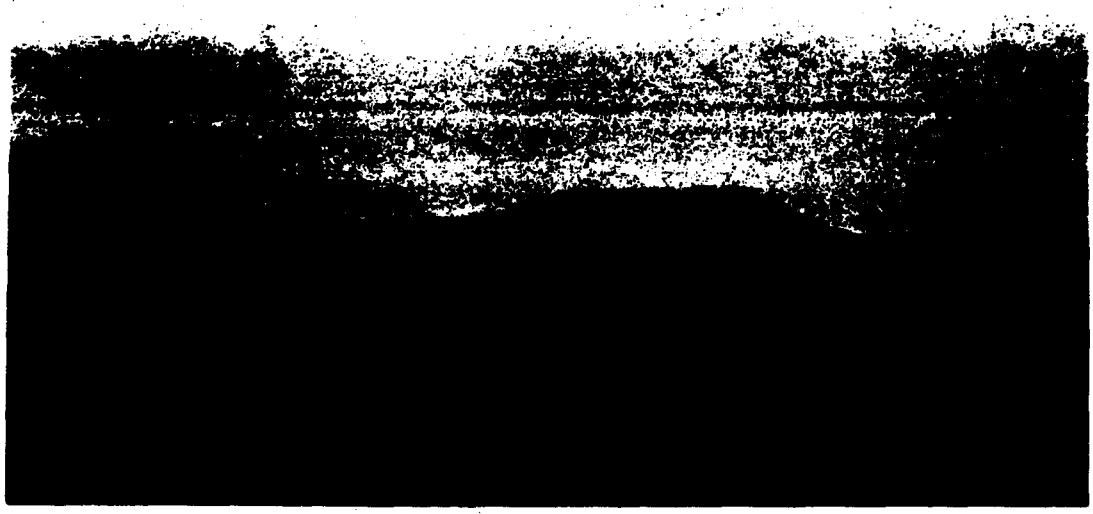

FAR SLANT RANGE
170 NAUT MI

PASS 56
S TO N
24 DECEMBER 1964

NEAR SLANT RANGE
164 NAUT MI

ORBIT DIRECTION →

(A) SHORELINE MAPPED WITH
CLUTTERLOCK CIRCUIT DISABLED

(B) CONFIGURATION OF
ACTUAL SHORELINE

4000-50

Figure 47 - Deterioration of Mapping with Clutterlock Loop Disabled

This page intentionally left blank.

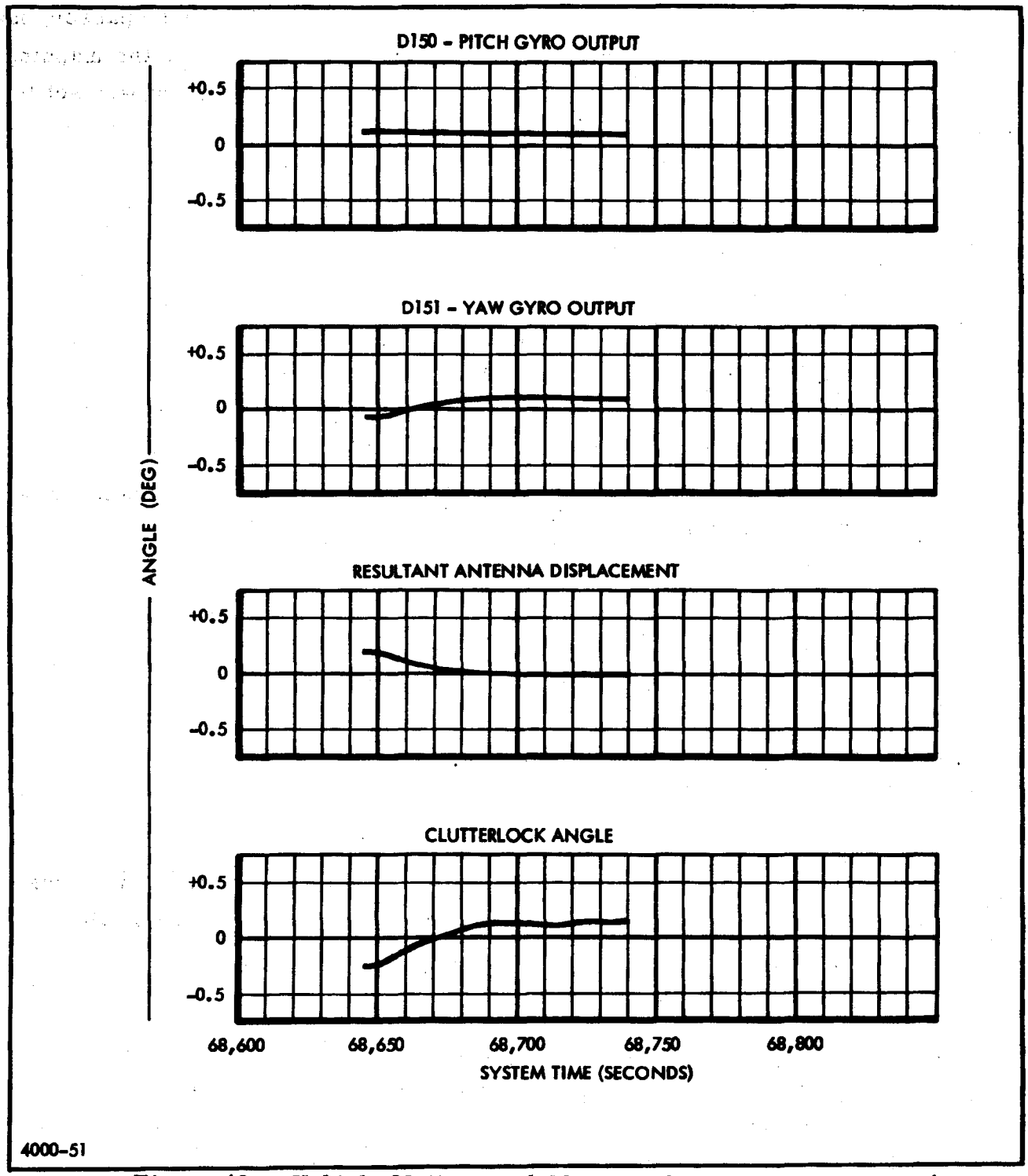

Figure 48 - Vehicle Motions and Clutterlock Response - Pass 16

relatively large errors in vehicle attitude. Initially, for these passes, no targets were present on the map film and after a few seconds the mapping was normal. For all of pass 57, the clutterlock time constant was set to time constant number two (5 seconds). The time constant could not be measured because the vehicle attitude was approximately correct at the start of the pass, but the loop performance appeared to be normal.

7. AZIMUTH AMBIGUITIES

a. General

The angular locations of ambiguities are functions of prf and vehicle velocity (refer to Volume I, Section II, paragraph 3, and Section III, paragraph 4, for a general discussion of azimuth ambiguities).

As was shown in Volume I (page 10), the angle to the first ambiguities is given by the relationship

$$\gamma_1 = \frac{\lambda F}{4V} \tag{16}$$

where

λ = carrier wave length

F = prf

V = vehicle velocity.

These ambiguities are unfocused and do not produce discrete ambiguous images in the final map, but do act to increase the map noise level.

The second ambiguities which appear at $2\gamma_1$ are focused and produce ambiguous images in the final map.

The system was designed to keep the level of azimuth ambiguities below the detectable limit in the final output map. However, under certain circumstances, azimuth ambiguities can become evident. This phenomenon occurred during pass 30 over Cleveland, Ohio.

NEAR SLANT RANGE
156 NAUT MI

PASS 16
N TO S
22 DECEMBER 1964

FAR SLANT RANGE
162 NAUT MI

← ORBIT DIRECTION

(A) EEL RIVER EMPTYING INTO PACIFIC OCEAN
(NORTHERN CALIFORNIA)

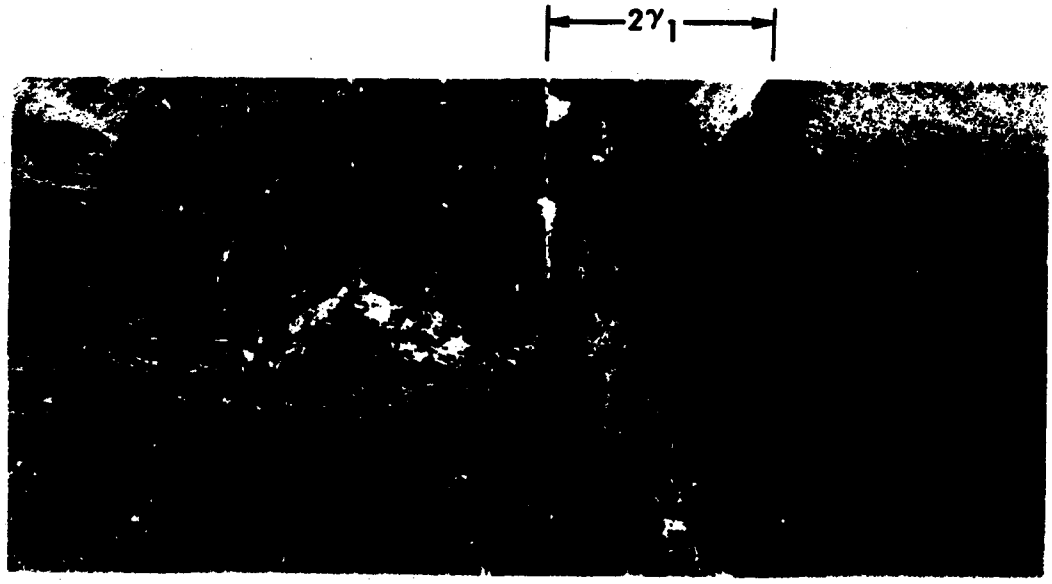

NEAR SLANT RANGE
155 NAUT MI

PASS 30
N TO S
23 DECEMBER 1964

FAR SLANT RANGE
161 NAUT MI

← ORBIT DIRECTION

(B) AZIMUTH AMBIGUITIES WHICH OCCURRED DURING
HIGH GAIN SETTING OVER WATER
(CLEVELAND, OHIO, SHORELINE)

4000-52

Figure 49 - Clutterlock Operation over Water

This page intentionally left blank.

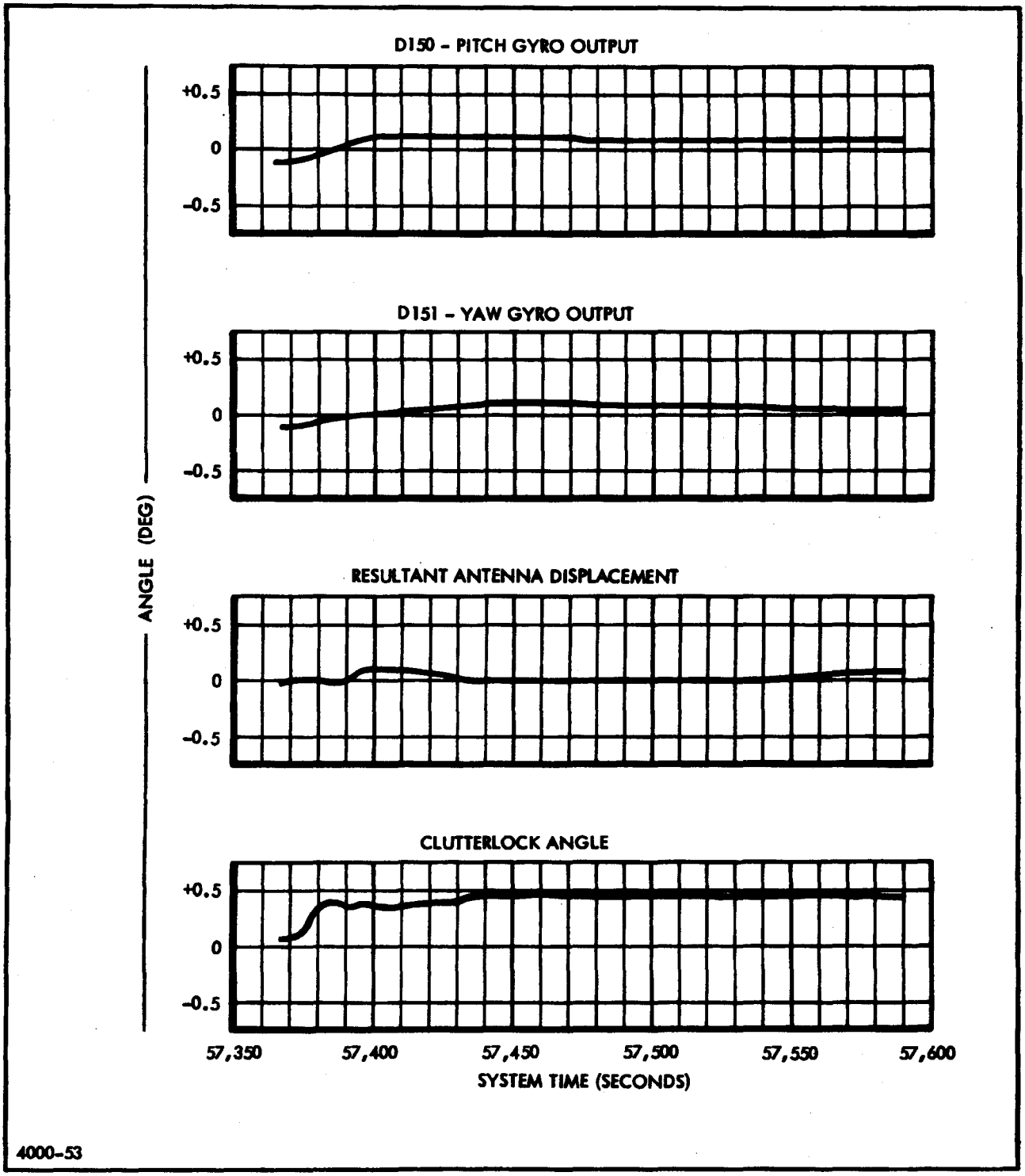

Figure 50 - Vehicle Motions and Clutterlock Response - Pass 30

b. Azimuth Ambiguities in Radar Map

For pass 30, the prf was set at 8415 pps when Cleveland was mapped. At this time some azimuth ambiguities were present (see Figure 49(b)). The relative velocity of the vehicle with respect to stationary targets in the Cleveland area was approximately 25,080 feet per second. These values set the angle to the first focused ambiguity, $2\gamma_1$, to be 0.01712 radian. Relating this to the terrain being mapped, the location of the first focused ambiguity occurs $R_s \times 2\gamma_1$ nautical miles from the actual target, where R_s = slant range to the target. In the case of Cleveland, this distance is 2.7 nautical miles which corresponds to approximately 1.3 inch on the map film shown.

When the satellite approached Cleveland over Lake Erie, the receiver gain was 12 to 15 db higher than when the city of Cleveland was actually mapped (see system time 57471 in Figure 38(a)). This was because the agc action increased gain over areas of low return such as water, and reduced gain over high return areas. The ambiguous targets (one string of which is identified above the radar map) have an angular separation corresponding to $2\gamma_1$.

When the receiver gain is reduced, as is evidenced by lack of return from the water just off shore, no further focused ambiguities can be observed in the water even though strong land targets exist at the proper separation angle. There does not appear to be any evidence of the presence of unfocused ambiguities.

It can be concluded that the criteria chosed for the control of azimuth ambiguities appear to be adequate except for conditions similar to those over the Cleveland land-water area.

8. RANGE AMBIGUITY

a. General

As discussed in Section III of Volume I, it is possible under some conditions for range ambiguous targets to appear on the map film. A likely example of this phenomenon is shown in Figure 51. The mountain along the railroad tracks between Enid and Heaton, Arizona (see arrow on Figure 51) does not appear on the most detailed topographical maps of the region. The return could be that from a low outcropping which does not appear on the map, but it is more likely that it is an ambiguous return from a nearby mountain outside of the mapped area.

b. Ambiguous Interval

At the time the targets in Figure 51 were being mapped, the prf was in error by one step. The prf used was 8381 pps which corresponds to an ambiguous ground range interval of approximately 16 nautical miles. Topographical maps of the area show mountainous terrain located at this distance which could account for the image. The level of range ambiguity suppression in this case was reduced somewhat because of the error in prf setting.

9. OTHER ITEMS OF INTEREST

a. General

Phenomena known as target swallowing and range sticking were detected in some portions of the radar maps. Evidence of film fogging as a result of small light leaks was found. These effects are discussed in the following paragraphs.

b. Target Swallowing

The map of Phoenix (see Figure 36) shows this effect in one area. In the lower right hand corner of the map is a group of large targets from an

oil storage area. The dark area extending to the right of the group is a swallowed area.

Swallowing occurs when a very large target utilizes the entire dynamic range of the system to the exclusion of lesser targets at the same range but slightly different azimuth.

c. Sticking

Side-looking coherent radar systems commonly produce long range streaks when large point targets are encountered. The general effect has been given the name "sticking" as the targets appear as sticks in range instead of points. In the KP-II radar the following malfunctions or misalignments could theoretically cause sticking:

1. Direct leakage through the chirp networks during the recompression (dechirping) process. This could cause a stick on the near range side of the target.
2. Leakage of 70 megacycles through the sine x/x modulator into the i-f channel and thence to the transmitter. This could cause a balanced stick with the target in the center.
3. Demodulator unbalance before or after the sine x/x pulse caused by a base line shift in the sine x/x pulse. This shift can make it impossible to balance the modulator both before and after the pulse. A stick can appear either before or after the target, depending on which balance is chosen.

The map of Phoenix (Figure 36) shows two large targets (6) with long sticks in the far range direction. These are attributed to modulator unbalance caused by base line shift. The sticks appear only on the very largest targets.

Figure 51 - Possible Range Ambiguity

This page intentionally left blank.

d. Film Fogging

A fogging effect was evident approximately 15 inches before the end of each of the recovered map films. Fifteen inches on the map film correspond to approximately 40 inches of data film. This figure places the spot of fogging some 40 inches from the Recorder crt, or somewhere between the Recorder and the take-up spool. Since the film is not running between active passes, any slight light leak in the vehicle could have produced the fogging. The fogging resulted in only an insignificant amount of lost data.

This page intentionally left blank.

SECTION X - CONCLUSIONS

1. GENERAL

This report has documented the KP-II doppler radar program from inception through completion of an orbital test in an Agena satellite. All of the program objectives were realized during the first flight. The success of the mission in large measure resulted from the extensive environmental testing and the associated corrective action program.

2. PROGRAM RESULTS

The results of the KP-II radar program are summarized below:

1. The use of doppler high-resolution radar for mapping of the earth's terrain from an orbital satellite is feasible within the present state-of-the-art.
2. The performance of doppler radar systems at satellite altitudes compares favorably with the performance of lower altitude aircraft-type radar systems. In particular, satellite-borne systems are not subject to the limitation of resolution normally imposed by platform instability in aircraft.
3. Satellite-borne radar systems, as expected, have the ability to map through all weather conditions and either by night or day, thereby overcoming the main limitations of photography.
4. Wide-band video links and ground-based photographic or tape recording provide practical methods of data recovery.
5. The design criteria used for the KP-II radar have provided a firm basis for design of future satellite radar systems.

6. The use of clutterlock for steering the synthetic beam was proved to be highly successful.

7. High altitude radar back-scattering coefficients were shown to be in close agreement with previous low altitude data (refer to Appendix II).

3. RECOMMENDATIONS

A number of improvements could be developed for incorporation in the present equipment or in future systems. A partial list of these is given below:

1. The present radar signal-to-noise ratio could easily be increased by the use of parametric amplifiers. Presently available units could improve the signal-to-noise ratio by 5 to 6 db.

2. The range interval could be extended by three methods:

   a. By eliminating the azimuth image ambiguity. This would extend the range interval by a factor of two. It could be accomplished by arranging the data processing method so as to eliminate the need for an azimuth offset reference.

   b. By the use of a longer antenna. However, the azimuth resolution is theoretically limited to one-half the physical antenna length.

   c. By the use of multiple channels. This can be done by using separate antennas, each operating at different frequencies, and illuminating different range intervals. Alternately, a single transmitter frequency can be used with multiple antenna sections being used for reception.

3. Range resolution could be improved to be more consistent with the present azimuth resolution. This can be readily accomplished by increasing the system band width and increasing the number of resolution elements of the recorder.

4. On-board magnetic or dielectric tape recorders could be used for delayed read out of doppler data.

5. Automatic circuits could be incorporated in the payload for control of prf selection independently of ground commands. The system could then be programmed for operation during any portion of the orbital period.

6. The system could be repackaged for decreased weight and volume. For a system having the KP-II performance a reduction of weight from 340 pounds to 250 pounds is feasible.

7. Real time electronic correlation and display of selected small areas are possible.

4. FUTURE APPLICATIONS

Satellite-borne radars have wide application to both military and civilian requirements. These include location of military targets, bomb damage assessment, and general surveillance over land and water. Radar data can be used to improve present maps of the Earth, particularly for polar or other remote areas. Detailed mapping of the moon and the planets by orbital satellites using doppler radar is a next logical step.

This page intentionally left blank.

APPENDIX I

CHRONOLOGY OF DEVELOPMENT HISTORY

This page intentionally left blank.

1964

January

Design approval tests completed on first radar system. Resolution specifications met using system tester. Qualification model Recorder, RF-If, Reference Computer and Control units shipped to LMSC.
Peak of fabrication manpower reached.

February and March

Qualification model Transmitter-Modulator shipped to LMSC.
Potting problem encountered in Transmitter-Modulator pulse transformer.
Hydrogen thyratron containers ruptured by expansion of potting compound.
Frequency multiplier in R-F/I-F unit failed during vibration tests.
Radar System No. 2 acceptance tests completed.

April

Transmitter-Modulator failed during qualification tests.
Transmitter-Modulator trigger circuit found to be sensitive to power supply input voltage.
Qualification testing of radar System No. 1 started in temperature-altitude chamber.
Manuals completed for all units and testers.
Frequency multiplier redesigned using bonding and foam potting and successfully tested under vibration and low pressure.
Voltage breakdown occurred in traveling wave tube at low pressure. Vendor directed to incorporate vacuum potting of high voltage leads.
Light level change occurred in cathode ray tube during vibration tests.

May

Remaining testers shipped to LMSC.
Ground-based equipment shipped to New Boston and Vandenberg AFB.
Three pulse transformers failed during low-pressure testing.
Problem of cathode ray tube light intensity change isolated to electron gun structure. Vendor directed to change design.

June

Pulse-forming network experienced voltage breakdown during qualification testing in temperature-altitude chamber.
Compatibility tests with Agena vehicle successfully concluded in anechoic chamber.
New bellows-type, oil-filled pulse transformer received from vendor.
Two new cathode ray tubes with modified gun structure tested with satisfactory results.

July

Qualification radar system sent to LMSC Santa Cruz, California, test facility for combined radar and antenna tests.

August

Santa Cruz tests completed with resolution within specifications.
Transmitter-Modulator failed because of charging choke.

September

Qualification tests repeated on radar system in temperature-altitude chamber.
Power factor change encountered as a function of pressure.
Charging choke problem isolated to vibration. New design started using epoxy sand filler.
Clutterlock loop problem recognized.

October

Data film drive problem isolated to nose capsule film take-up spool.
Take-up film tension increased.
Pulse transformers failed because of internal voltage breakdown.
Clutterlock problems isolated. Coaxial connector shields and filter added.

November

Voltage breakdown problem in pulse transformer isolated to tuning inductor and design change incorporated.

Power factor change problem isolated to radio frequency interference filters and corrective action taken.

December

Radar system tests successfully completed in temperature-altitude chamber. Vehicle launched on December 21. Film capsule recovered on December 24.

1965

January

Analysis of radar map data indicated excellent results.

This page intentionally left blank.

APPENDIX II

ESTIMATE OF RADAR BACK-SCATTERING COEFFICIENTS

This page intentionally left blank.

APPENDIX II - ESTIMATE OF RADAR BACK-SCATTERING COEFFICIENTS

1. GENERAL

Telemetry data of returned radar power were used to determine the back-scattering coefficient, σ_o, for various types of terrain. The results presented here are based upon a particular set of assumptions; it is recognized that another study, using the same flight data, might yield somewhat different results. As only a small portion of the telemetry data were reduced in this study, it can be expected that a more complete study would yield a wider spread of values for the various terrain types. The results presented here are believed to be representative.

2. CALIBRATION OF RADAR RECEIVER

Prior to the orbital test, a calibration curve was obtained for the flight radar receiver relating the gain control monitor voltage, F53, to received power. This calibration curve was previously given in Section IX (see Figure 38(b), page 118).

The calibration was made by reference to the thermal noise at the receiver input. The noise level was calculated from the relation

$$S = KTB(NF) \quad , \qquad \text{(A-1)}$$

where

S = receiver noise power

K = Boltzmann's constant

T = temperature degrees K

B = receiver band width

NF = receiver noise figure.

An X-band traveling wave tube in series with a calibrated attenuator was used as a random noise power signal source. With the agc loop open and the stc

functioning, the signal source was injected at the receiver input. The series attenuator was varied to double the receiver output (signal equal to receiver noise). Using this level as a point of reference, the curve of Figure 38(b) in Section IX was then obtained by varying the series attenuator and recording the voltage output at F53. (For the following calculations of σ_o, the curve was moved to the right by 0.1 volt to compensate for an in-flight shift of the F53 voltage from 0.75 volt to 0.85 volt for no signal input to the receiver.)

3. METHOD OF CALIBRATION AND ASSUMPTIONS

The equation used in the calculation of σ_o was obtained by re-arranging Equation (32) (Volume I, page 29). This yields

$$\sigma_o = \frac{P_r (4\pi)^3 R^3}{P_t G^2 \lambda^2 \phi \cdot 5\, C \Delta t \sec \theta} \quad . \qquad \text{(A-2)}$$

The quantity P_r was determined from the telemetered value of F53 voltage for each particular terrain using the calibration curve. The range R was a mid-range value obtained from flight data. P_t was determined from telemetered information. The remaining quantities other than antenna gain G were assumed constant (λ = 0.102 ft, ϕ = 0.0064 rad, C = 9.85×10^8 ft/sec, $\Delta t = 10^{-6}$ sec, and $\theta = 53^o$).

Although the peak gain of the physical antenna was known, normalizing factors were required to account for the variation of gain across the ground area which contributed radar returns to the receiver. These normalizing factors were determined in the following manner.

In the azimuth plane a rectangular beam pattern was assumed which had a width equal to the 3 db width of the actual pattern and a constant gain equal to the maximum gain of the actual pattern. This approximation is valid from a total received energy standpoint for antennas (such as the one being used) with uniform illumination.

In the range direction, the received power P_r is sampled at the agc circuit input by a gate 68 microseconds long, occurring 21.6 microseconds after reset (clock zero). An average antenna gain during this interval was calculated. The variations in gain from prf step errors and altitude changes were also taken into account.

The resulting normalized gain values versus prf step error and altitude are shown in Figure A-1. Only two altitudes, one for northbound and one for southbound passes, were used since the altitude variations were small for the passes used.

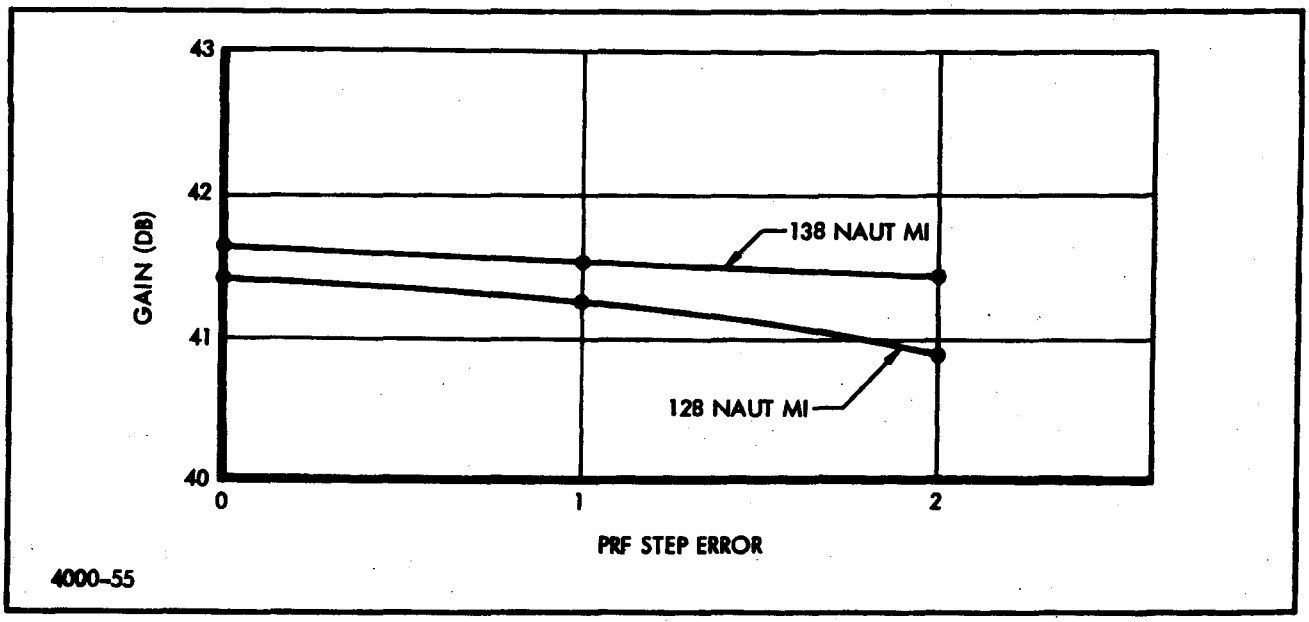

Figure A-1 - Antenna Gain versus Step Error and Altitude

4. EXAMPLE OF σ_o CALCULATION

For the calculation for pass number 9, system time 29543, broken desert north of Phoenix, Arizona,

$\theta = 53^o$, R = 171.3 mi, P_r = 85.5 dbm, P_t = 25.3 kw

G = 41.5 db, λ = 0.102 ft, C = 9.85×10^8 ft/sec, ϕ = 0.0064 radian

$$\sigma_o = \frac{2.82 \times 10^{-2} (4\pi)^3 \times (171.3 \times 6080)^3}{25.3 \times 10^3 (1.42 \times 10^4)^2 (0.102)^2 (0.0064)(9.85 \times 10^8)(10^{-6}) 0.5 (1.66)}$$

$$\sigma_o = 0.0228$$

$$\sigma_o = -16.4 \text{ db.}$$

5. COMPARISON BETWEEN KP-II RESULTS AND PREVIOUS EXPERIMENTAL DATA

Figure A-2 shows experimental curves* relating σ_o to types of terrain and aspect angle. (This figure is identical to Figure 10 in Volume I and is repeated here for reference.)

The results of calculations for σ_o as obtained in the satellite doppler radar test are shown in Table A-1. The table is divided into two sections: the first section shows the comparison of KP-II measurements with the data of Figure A-2; the second section shows the values of the various quantities used in the calculation of KP-II results.

6. CONCLUSIONS DRAWN FROM KP-II RESULTS

The results show good correlation with the previous results of Figure A-2. All comparisons must, of course, be made at an aspect angle of 53 degrees.

---

*Data on sea return are from Grant and Yaplee (refer to Proceedings of the I.R.E., July, 1957). Balance of data was experimentally obtained as a result of Goodyear Aerospace Corporation flight tests in a P2V aircraft.

a. Sea Returns

For sea returns, the results agree quite well with the Figure A-2 data. The Pacific Ocean calculation falls close to the value for the illustrated 15 to 20 knot point of the Grant and Yaplee data. A weather map for the day of the test showed a 20 to 25 knot wind.

The return from Lake Huron and Lake Superior is considerably higher than for the sea returns above. From the appearance of these lakes on the radar maps, they were assumed to be frozen.

b. Broken Desert

These figures agree very well with the previously obtained data.

c. Heavy Vegetation

The results given for a forested area of Northern Michigan and a coastal swamp area in North Carolina agree quite well with the data of Figure 10.

d. Cultural Areas

The results for cities showed a return averaging around that for the residential area data of Figure A-2. This is to be expected, however, because of the large area which is covered by the KP-II beam. The KP-II result is obtained by integration over an area approximately ten miles by one mile.

The σ_o result is therefore a composite of many terrain types as a large city can contain many different terrain samples: open fields, water, heavy vegetation, and residential, commercial and industrial areas.

The sampling rate of the telemetry system (one sample per four miles) is much too low for accurate determination of σ_o over such areas. For future flight tests a continuous channel should be used for recording the agc voltage.

7. ACCURACY

These results are subject to the measurement errors inherent in measurements taken from a complex electronic system during operation. However, the relative accuracy should be better than the absolute accuracy.

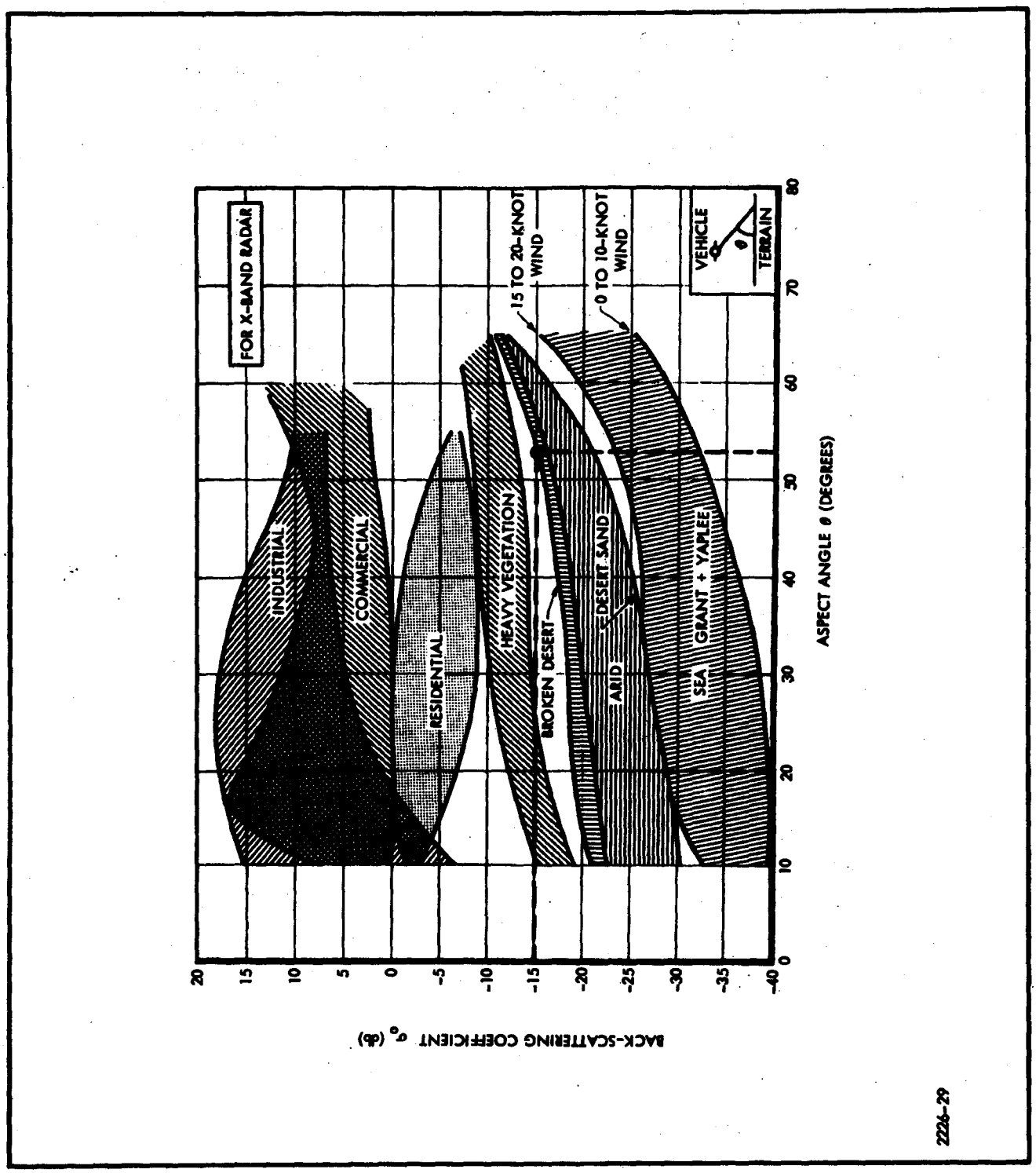

Figure A-2 - Back-Scattering Coefficients versus Aspect Angle

TABLE A-1 - BACK-SCATTERING COEFFICIENTS

Comparison data				Reference data						
Terrain type	Location	Back-scattering coefficient, σ_o (db)		Pass	System time	R(mid) (naut mi)	P_r (dbm)	P_t (kw peak)	Prf error steps	Antenna gain (db)
		KP-II	Figure 10							
Sea	Atlantic Ocean	-24.2	-23 to -32	14	58007	157.6	-92.0	25.7	0	41.4
	Pacific Ocean	-23.2		16	68725	157.8	-92.0	25.7	2	40.9
Lakes	Lake Erie	-23.0	Not given	30	57466	157.5	-91.0	26.3	1	41.3
	Lake Michigan	-19.7		24	23899	169.0	-88.0	26.4	0	41.6
Lakes (frozen)	Lake Huron	-15.9	Not given	8	24362	170.0	-84.0	26.7	0	41.8
	Lake Superior	-15.8		30	57385	157.5	-84.0	26.3	1	41.3
Broken desert	North of Phoenix	-16.4	-15 to -17	9	29543	171.3	-85.5	25.3	1	41.5
	Southern Utah	-14.7		25	29257	169.2	-83.0	27.1	1	41.5
Farm land	South of Chicago	-11.1	Not given	24	23847	169.0	-79.5	26.4	0	41.6
	Michigan	-11.3		30	57540	157.5	-79.5	26.3	1	41.3
Heavy vegetation	Coastal swamp, N. Carolina	-11.2	-8 to -13	14	57997	157.6	-79.0	25.7	0	41.4
	Forest, Michigan	-11.2		24	23912	169.0	-79.5	26.4	0	41.6
Mountains	West Virginia	-11.5	Not given	30	57535	157.5	-79.5	26.3	1	41.3
	Arizona	-11.5		9	29547	171.3	-80.5	25.3	1	41.5
	Utah	-11.8		25	29222	169.2	-80.5	27.1	1	41.5
Cultural areas	Cleveland	-6.7	Not specifically given. See discussion.	30	57470	157.5	-75.0	26.3	1	41.3
	Chicago	-7.6		24	23870	169.0	-76.0	26.4	0	41.6
	Phoenix	-10.5		9	29537	171.3	-79.5	25.3	1	41.5

Consideration of the calibration curve shows that a two percent change in telemetry could cause an error of 4 to 5 db in σ_o for low signal levels. For high level signals this error is reduced to approximately 1 db. The F53 monitor circuit should be redesigned to reduce low level signal errors.